Organelle-associated innate immune responses to self-DNA in mammals

HARVARD UNIVERSITY
Graduate School of Arts and Sciences

DISSERTATION ACCEPTANCE CERTIFICATE

The undersigned, appointed by the

Division of Medical Sciences

Committee on Immunology

have examined a dissertation entitled

Organelle-associated innate immune responses to self-DNA in mammals

presented by Kenta Mosallanejad

candidate for the degree of Doctor of Philosophy and hereby certify that it is worthy of acceptance.

Signature: Wendy S. Garrett
Wendy S. Garrett (Jun 13, 2022 14:10 EDT)

Typed Name: Dr. Wendy Garrett

Signature: Roni Nowarski
Roni Nowarski (Jun 13, 2022 14:11 EDT)

Typed Name: Dr. Roni Nowarski

Signature: Ivan Zanoni
Ivan Zanoni (Jun 13, 2022 14:27 EDT)

Typed Name: Dr. Ivan Zanoni

Signature: Igor Brodsky
Igor Brodsky (Jun 14, 2022 14:51 EDT)

Typed Name: Dr. Igor Brodsky

Date: June 02, 2022

Organelle-associated innate immune responses to self-DNA in mammals

A dissertation presented

by

Kenta Mosallanejad

to

The Division of Medical Sciences

in partial fulfillment of the requirements

for the degree of

Doctor of Philosophy

in the subject of

Immunology

Harvard University

Cambridge, Massachusetts

June 2022

Dissertation Advisor: Jonathan Kagan Kenta Mosallanejad

Organelle-associated innate immune responses to self-DNA in mammals

Abstract

Since early in evolution, mammalian cells have been equipped with pattern recognition receptors (PRRs) that detect the presence of pathogen-associated molecular pattern (PAMPs) or damage-associated molecular pattern (DAMPs) to elicit innate immune responses. Despite recent advances in the understanding of PRR signaling and its regulation, structurally homologous PRRs are often considered to operate similarly, and therefore the functional diversity of PRRs among mammals has not been explored. Also, in contrast to the increasing knowledge about the roles of mitochondria in innate immunity, the roles of peroxisomes, the other dynamic and metabolic organelles, remain elusive.

Our first study in this thesis addresses the evolutionary diversity of cyclic GMP-AMP synthase (cGAS) activity. cGAS is the enzyme PRR that detects DNA in the cytosol. As opposed to the assumption that cGAS is similarly regulated in mammals, we identify three distinct classes of regulation of cGAS self-DNA reactivity. Class 1 cGAS, which includes human, contains N-terminal domain which restricts otherwise intrinsically self-DNA-reactive C-terminal catalytic domain. N-terminus of Class 2 cGAS (mouse) rather promotes self-DNA reactivity, and Class 3 cGAS (including chimpanzee) is not reactive to self-DNA. The self-DNA reactivity of Class 1 cGAS is linked to mitochondrial localization, while other cGAS classes do not follow this rule. These findings provide new insights to the field that demand the careful consideration into species-specific functions when studying cGAS and other PRRs.

The second study in this thesis examines the roles of peroxisomes in PRR signaling. We found that peroxisomal matrix proteins are generally required for PRR responses in macrophages, including TLRs, RLRs, and NLRP3 inflammasomes. We further discover that pristanic acid, a

branched-chain fatty acid that is the substrate for peroxisomal α-oxidation, reprograms macrophages from an inflammatory state to an antiviral state through self-DNA-mediated cGAS activation. This cGAS activation by pristanic acid results not only in the induction of type I interferon (IFN) responses but also the proliferation of peroxisomes. Pristanic acid promotes histone deacetylase (HDAC) activity, which is required for cytokine responses. These results altogether demonstrate the important roles of peroxisomes in innate immune responses.

Overall, our thesis work identifies organelle-associated cGAS responses to self-DNA from two perspectives: Class 1 cGAS catalytic domain reacts with self-DNA in mitochondria; and an intermediate product of peroxisomal metabolism induces self-DNA-mediated cGAS activation.

Table of Contents

Title page i

Copyright page ii

Abstract iii

List of Figures and Tables ix

Acknowledgment x

Chapter 1: Introduction 1

1.1. Innate immune responses and pattern recognition receptors 2

1.1.1. Toll-like receptors (TLRs) 2

1.1.2. RIG-I-like receptors (RLRs) 3

1.1.3. Inflammasomes 4

1.1.4. cGAS 6

1.2. Control of innate immunity by the cGAS-STING pathway 8

1.2.1. Transcriptional and non-transcriptional host defensive responses induced by cGAS-STING 8

1.2.2. cGAS-STING activities that impact cell viability and mitosis 10

1.2.3. Sources of substrate DNA that activate cGAS-STING signaling 13

1.2.4. The biophysical mechanisms of cGAS activation and cGAMP synthesis 17

1.2.5. Regulation of DNA sensing and cGAS activation within cells 18

1.2.6. Viral targeting of cGAS as an immune evasion strategy 25

1.2.7. cGAS-STING pathway: Conclusion 26

1.3. Metabolic organelles and innate immune signaling 26

1.3.1. Mitochondria and innate immune responses 26

1.3.2. Peroxisomes and innate immune responses 30

1.3.3. Conclusion: Organelles and innate immune responses 33

Chapter 2: Three functionally distinct classes of cGAS proteins in nature revealed by self-DNA-induced interferon responses 34

2.1. Abstract 35

2.2. Introduction 35

2.3. Materials and Methods 37

2.3.1. Study design 37

2.3.2. Cell culture 37

2.3.3. Generating cells with stable or doxycycline-inducible gene expression 38

2.3.4. Real-Time quantitative reverse transcription (qRT-) PCR 40

2.3.5. Cell viability assay 40

2.3.6. Subcellular fractionation and membrane flotation assay 40

2.3.7. Immunoblotting and ELISA analysis 41

2.3.8. *In vitro* 2′3′-cGAMP assay 42

2.3.9. Live imaging confocal microscopy 43

2.3.10. Quantification and statistical analysis 43

2.4. Results 44

2.4.1. Human cGAS∆N induces type I IFN responses to self-DNA in human and mouse cells 44

2.4.2. Specific amino acids at the N-terminus of hcGAS∆N determine self-DNA reactivity 47

2.4.3. Species-specific self-DNA reactivity by mammalian cGAS proteins 50

2.4.4. Mitochondrial localization of Class 1 cGAS∆N correlates with signaling activity 54

2.4.5. Viral protease-mediated release of Class 1 cGAS∆N induces type I IFN responses 61

2.5. Discussion 65

Chapter 3: Regulation of Innate Immune Responses by Peroxisomes 68

3.1. Abstract 69

3.2. Introduction 69

3.3. Materials and Methods 71

3.3.1. Study design 71

3.3.2. Cell culture 72

3.3.3. Generation of CRISPR-Cas9-mediated knockout (KO) cells 72

3.3.4. Generating cells with stable gene expression 73

3.3.4. Real-Time quantitative reverse transcription (qRT-) PCR 74

3.3.5. Immunoblotting analysis 75

3.3.6. Microscopic analysis of peroxisomes 75

3.3.7. HDAC assay 76

3.3.8. Quantification and statistical analysis 76

3.4. Results 76

3.4.1. Peroxisomes are required for PRR-mediated cytokine production 76

3.4.2. Pristanic acid rewires innate immune responses 80

3.4.3. Pristanic acid induces IFN responses in a cGAS-dependent manner 82

3.4.4. Pristanic acid activates HDAC to stimulate cGAS-STING signaling 86

3.5. Discussion 87

Chapter 4: Discussion 90

4.1. Overview 91

4.2. cGAS 91

4.2.1. Self-DNA reactivity in human cGAS revealed by the C-terminal epitope tags 91

4.2.2. Mitochondrial localization of cGASΔN 93

4.2.3. Diversity of self-DNA reactivity of cGAS in evolution 94
4.2.4. Synthetic biology-based induction of self-DNA-mediated type I IFN responses 97
4.2.5. Future Perspectives 98
4.3. Peroxisomes 99
4.3.1. The roles of peroxisomal metabolisms in PRR responses 99
4.3.2. Pristanic acid-induced rewiring of innate immune responses 100
4.3.3. Future Perspectives 102
4.4. Conclusion 103
Appendices – Supplementary Figures and References 105
Supplementary Figures 106
References 114

List of Figures and Tables

Figure 1.1. Overview of cGAS activation and cGAS-STING signaling. 7

Figure 1.2. Regulation of cGAS activity in cells 19

Figure 2.1. Human cGAS∆N induces aberrant type I IFN responses 47

Figure 2.2. Specific amino acids at the N-terminus of hcGAS∆N determines self-DNA reactivity 50

Figure 2.3. cGAS∆N activities are diverse in mammalian species 54

Figure 2.4. Mitochondrial localization and signaling activities of cGAS 60

Figure 2.5. Design of synthetic cGAS as a PRR-guard hybrid that responds to a viral protease 65

Figure 3.1. Peroxisomes are required for innate immune responses to PAMPs 79

Figure 3.2. Pristanic acid promotes IFN responses and inhibits inflammatory responses 81

Figure 3.3. cGAS-STING signaling is required for IFN responses to pristanic acid 83

Figure 3.4. Pristanic acid proliferates peroxisomes through cGAS activation 85

Figure 3.5. Pristanic acid activates HDAC to stimulate cGAS 87

Figure S1. Human cGAS∆N induces type I IFN responses in a STING-dependent manner 106

Figure S2. cGAS∆N activities vary across mammalian species 109

Figure S3. cGAS-DNA condensates interfere biochemical analysis of cGAS subcellular localization 111

Figure S4. Peroxisomal matrix proteins are required for PRR responses 112

Figure S5. Pristanic acid induces cGAS-STING-dependent IFN responses 113

Table 1.1. cGAS-STING-dependent cell death 13

Acknowledgment

First, I would like to thank my thesis advisor Dr. Jonathan Kagan, who provided me with the opportunity to study in the Kagan lab. Without his tremendous supports, none of this work would have been achieved. I truly appreciate that he always kept his door (physically or virtually) open and allow me to bring data or concern to discuss with him. Having a great mentor like Jon let me grow essential skills to be a full-fledged scientist, such as hypothesis building, critical thinking, and logical presentation skills. The solar powered figure of Albert Einstein that he gave me at the Christmas party five years ago is still on my lab desk, always reminding me of the importance of pushing my brain to think through science and everything.

I would also like to thank all the members in the Kagan lab, who shared passion for understanding innate immune responses, a lot of helpful ideas and suggestions on my thesis work, and a lot of fun time inside and outside the lab, often with beer. I would not have been able to complete my thesis work without “the Kagan family”.

Outside the lab, I thank my collaborators, my committee, and Harvard Immunology Program. My thesis works would have never been possibly done without the collaboration with Dr. Wen Zhou, Dr. Apurva A. Govande, Dr. Philip J. Kranzusch, and Dr. Dustin C. Hancks, who provided me with research materials, expertise, and excellent advice. My dissertation advisory committee (DAC), Dr. Wendy Garrett, Dr. Jatin Vyas, and Dr. Sun Hur gave me a lot of positive and helpful comments during DAC meetings, which has accelerated my thesis project and therefore I truly appreciate. I would also like to thank my dissertation defense committee, Dr. Wendy Garrett, Dr. Ivan Zanoni, Dr. Roni Nowarski, and Dr. Igor Brodsky for providing me with the opportunity to present my thesis work. Furthermore, I am grateful for Harvard Immunology program, which allowed me to be a part of the great community of scientists and connected me with the best classmates that I could have wished for – Alec Walker, Alexandra Schnell, Marie Siwicki, Jefte Drijvers, Jeroen Tas, John Mindur, and Tianli Xiao.

I would like to thank Dr. Hidenori Ichijo, my supervisor throughout the undergraduate and the master's program in the University of Tokyo. I would have never thought of applying to graduate schools in the United States if he had not suggested it when we were having Japanese sake together. I appreciate that he changed my career and life in a positive way.

This acknowledgment section is never complete without thanking my family. I would like to thank my family back in Japan for their physical and mental support in my decision to come to the United States and to pursue the doctoral degree. With that, I would like to thank my parents, Jamal and Junko, and my grandparents, Jiro and Makiko.

Lastly, my girlfriend Hanae. She has always shared her time, interests, support, love, and life even 6,707 miles away from Boston. Without hearing her voice on the phone every day, I would have never been able to survive the hard times that I had in tackling difficulties during this thesis work. Thank you, Hanae, for always being there for me.

Chapter 1: Introduction

Kenta Mosallanejad[1] and Jonathan C. Kagan[1]

[1]Division of Gastroenterology, Boston Children's Hospital, Harvard Medical School, 300 Longwood Avenue, Boston, MA 02115, USA.

Sections of this chapter are adapted from:

Mosallanejad, K., & Kagan, J. C. (2022). Control of innate immunity by the cGAS-STING pathway. *Immunol Cell Biol*, doi:10.1111/imcb.12555 (2022).

Author Contribution

K.M. and J.C.K. conceptualized, investigated, wrote, and edited this review article. K.M. designed and generated all illustrations.

1.1. Innate immune responses and pattern recognition receptors

Cells are equipped with protein-based machineries that link the detection of microorganisms to innate immune responses that fight against pathogen infections[1]. Central to the function of these host-defensive molecular machines are members of the pattern recognition receptor (PRR) superfamily. PRRs recognize conserved microbial molecules that are known as pathogen-associated molecular patterns (PAMPs), with the most common being nucleic acids and microbial cell-wall components[1]. Recent evidence suggests that PRRs also respond to damage-associated molecular patterns (DAMPs)[2]. Upon binding to ligands, these receptors activate adaptor molecules and downstream signaling cascades to induce the transcription of inflammatory cytokines and/or antiviral cytokine type I interferon (IFN)[2]. Comprehensive review of PRRs is the scope of other review articles[3], and a few examples related to this thesis are described herein.

1.1.1. Toll-like receptors (TLRs)

TLR family is the first to be identified and therefore one of the best-characterized PRR families[1]. TLRs are found on either the plasma membrane or within endosomes, mostly of phagocytes such as macrophages and dendritic cells (DCs)[1]. TLRs are type I integral membrane glycoproteins consisting of extracellular leucine-rich repeat (LRR) motifs, which recognize PAMPs and DAMPs, and cytoplasmic Toll/interleukin-1 (IL-1) receptor (TIR) domains, which interact with downstream signaling proteins[4]. Upon ligand binding, TLR interacts with TIR domain-containing adaptor molecules such as MyD88 (myeloid differentiation primary response protein 88) and TRIF (TIR domain-containing adaptor protein inducing IFN-β) to activate downstream signaling pathways that induce cytokine transcription and other immune responses[4].

Among TLR superfamily is TLR4, the first identified as the mammalian homologue of Drosophila Toll[5]. TLR4 is responsible for the cell surface detection of lipopolysaccharide (LPS), the major cell wall component of Gram-negative bacteria[6-8]. TLR4 forms a complex with MD-2 in the extracellular space[9], and recognizes LPS with the help of GPI-linked membrane protein

CD14[10]. TLR4 homodimerizes through TIR domain upon LPS binding, resulting in the conformational changes that initially recruit MyD88 via the sorting adaptor TIRAP (also known as Mal)[11-14]. MyD88 engagement promotes the assembly of higher order complexed called Myddosome, containing MyD88, IL-1R-associated kinase 4 (IRAK4), and IRAK2, and it activates the transcription factor nuclear factor kappa B (NF-κB) to induce the transcription of proinflammatory cytokine such as IL-1β[15-17]. In addition to MyD88 pathway activation, LPS binding triggers the internalization of TLR4 to the endosomes in a CD14-dependent manner, where it activates TRIF-dependent signaling[18]. Activation of TRIF pathway downstream of TLR4 is analogous to MyD88 pathway – the sorting adaptor TRIF-related adaptor molecule (TRAM, also known as TICAM) bridges TRIF and TLR4 on the endosomes[19,20], which triggers the formation of higher order complexed called Triffosome[17]. TRIF complex in turn activates TANK-binding kinase 1 (TBK1) and IκB kinase-ε (IKKε), which promotes interferon regulatory factor 3 (IRF3)- and IRF7-dependent transcription of type I IFN[21,22]. While TLR4 activates both MyD88- and TRIF-dependent pathways, other TLRs activate either one of them. For example, while TLR2/TLR1 or TLR2/TLR6 heterodimers on the plasma membrane recognize bacterial PAMPs (such as peptidoglycans, lipoteichoic acids on Gram-positive bacteria, lipoproteins, and the yeast cell wall component zymosan) and induce MyD88-dependent gene expression[23-28], TLR3 senses viral double-stranded (ds) RNA within endosomes and triggers TRIF-dependent signal activation[22,29-32].

1.1.2. RIG-I-like receptors (RLRs)

Although some TLRs are responsible for extracellular RNA detection, the presence of RNA in the cytosol is recognized by other PRRs. Among intracellular RNA sensors are RLRs, which belong to a family of ubiquitously expressed DExD/H-box RNA helicases[33]. RLR family includes retinoic acid-inducible gene I (RIG-I), melanoma differentiation-associated protein 5 (MDA5), and laboratory of genetics and physiology 2 (LGP2)[33-35]. While RIG-I and MDA5 consist of helicase domain, carboxy-terminal domain (CTD), and two amino-terminal caspase activation and recruiting domains (CARDs), LGP2 lacks CARDs and subsequent signal-inducing ability that

RIG-I and MDA5 harbor[34,35]. Although RIG-I and MDA5 recognize both microbe- and host-derived RNA[33,36,37], they have different specificities for their ligands: while RIG-I senses short (30 - 300 base pairs (bp)) 5'-triphosphate (ppp) or 5'-diphosphate (pp) dsRNA with a blunt end, MDA5 is the sensor of longer dsRNA (up to 2 kb) or higher-order RNA structures[38-43]. RNA binding to the helicase domain and CTD of RIG-I releases CARDs from an autoinhibited conformation[44], leading to not only K63-linked polyubiquitination by E3 ligase Riplet/RNF135[45] but also binding to unanchored K63-linked polyubiquitination[46], which induces ATP hydrolysis-dependent tetramerization of RIG-I on RNA[47,48]. In contrast, RNA-unbound MDA5 has an open conformation, and RNA binding to helicase domain forms ATP-sensitive MDA5 polymers as helical filaments on RNA[49,50]. These RNA-induced RLR oligomers allow the binding of RLR CARD and CARD of adaptor protein mitochondrial antiviral signaling (MAVS, also known as IPS-1, VISA, and Cardif)[51-54], a transmembrane protein on mitochondria, mitochondrial-associated membrane (MAM) on endoplasmic reticulum (ER), and peroxisomes[55,56]. This CARD-CARD interaction induces prion-like aggregation of MAVS, which recruits ubiquitin E3 ligase tumor necrosis factor (TNF) receptor-associated factor (TRAF) family proteins that activates TBK1 and IKKε to induce IRF3- and NF-κB-dependent gene transcription such as type IFN and proinflammatory cytokines[57].

1.1.3. Inflammasomes

As described above, inflammatory cytokines such as IL-1β are produced by NF-κB downstream of PRRs such as TLRs and RLRs. However, IL-1β and IL-18, another IL-1 family member also known as IFN-γ-inducing factor (IGIF), are primarily translated as inactive precursor proteins that require proteolytic processing by caspase-1, also known as IL-1β-converting enzyme (ICE), to be activated and released into the extracellular space[58-61]. Works in recent years have identified several PRRs that initiate the secondary signal that is responsible for IL-1β and IL-18 maturation[62-69]. These PRRs include nucleotide-binding domain, leucine-rich repeat containing (or NOD-like receptor, NLR) proteins, absent in melanoma 2 (AIM2)-like receptors (ALRs), and

the protein pyrin[62-69]. NLRs, ALRs, and pyrin detect a wide variety of intracellular PAMPs and DAMPs, and upon recognition of ligands, these sensors form large multimeric structures called inflammasomes, leading to caspase-1 activation and subsequent IL-1β/IL-18 cleavage[70-72]. Inflammasomes are comprehensively reviewed elsewhere[70-72], and we herein describe NLRP3 and AIM2 inflammasomes, which are the best-studied inflammasomes and related to this thesis.

NLR family pyrin domain-containing 3 (NLRP3, also known as NALP3, CIAS, PYPAF, and cryopyrin), responds to a wide range of PAMPs such as bacterial toxin and microbial nucleic acids, and DAMPs such as extracellular ATP, silica, uric acid crystals, and cholesterol crystals[73-81]. NLRP3 contains an amino (N) -terminal pyrin domain (PYD), a central domain present in NAIP, CIITA, HET-E, and TP1 (NACHT), and a carboxy (C) -terminal LRR[82-84]. During inflammation, priming stimuli such as TLR ligands upregulate NLRP3 and IL1B gene expression mostly in immune cells[85], and the secondary stimuli above causes the disruption of cellular homeostasis such as potassium ion (K^+) efflux, reactive oxygen species (ROS), and mitochondrial damage, which trigger NLRP3 oligomerization through NACHT domain[86]. NLRP3 oligomer recruits apoptosis-associated speck-like protein containing a CARD (ASC, also known as Pycard) through PYD-PYD interaction[63] and induces ASC filament formation that further coalesces into an ASC aggregates or “speck” [87,88]. This ASC then recruits premature form of cysteine protease caspase-1 (procaspase-1) through CARD-CARD interaction, where procaspase-1 undergoes auto-processing to release active form of caspase-1[63]. Mature caspase-1 not only cleaves precursor IL-1β (proIL-1β) and proIL-18 into mature forms as described above[58-61], but also cleaves the protein gasdermin D (GSDMD) to release its N-terminal death domain ($GSDMD^{Nterm}$) from the C-terminal autoinhibitory domain[89,90]. Consequently, $GSDMD^{Nterm}$ binds to phosphatidylinositol phosphates and phosphatidylserine in the inner leaflet of the plasma membrane, forming a pore-forming oligomer which secretes mature IL-1β and IL-18 with or without pyroptosis, a lytic form of inflammatory programmed cell death[91-95].

AIM2, a family member of ALRs also known as HIN-200, is a cytosolic sensor of dsDNA that assembles inflammasome upon ligand recognition as NLRP3 does[65-68,70-72]. AIM2 contains N-terminal PYD and C-terminal hematopoietic interferon-inducible nuclear protein (HIN) domain[65-68]. Electrostatic binding of dsDNA to HIN domain of AIM2 releases PYD, which leads to polymerization of AIM2 into filaments through PYD and subsequently recruits ASC via PYD-PYD interaction[96-99]. ASC in AIM2 inflammasome recruits and activates caspase-1 to induce IL-1β maturation and pyroptosis in a similar manner to NLRP3 inflammasomes[65-68].

1.1.4. cGAS

Besides AIM2 and other ALR members that induce inflammasome-mediated IL-1β release and cell death, several PRRs survey dsDNA in the intracellular space and trigger type I IFN responses[100]. Among IFN-inducing dsDNA sensors is the enzyme cyclic GMP-AMP synthase (cGAS), which recognizes B-form DNA independent of its sequence through contacts with the sugar-phosphate backbone[101,102]. Upon dsDNA binding, cGAS produces 2'3'-cyclic-GMP-AMP (2'3'-cGAMP, hereafter cGAMP), a second messenger molecule that binds to the protein stimulator of interferon genes (STING, also known as MITA, MPYS, and ERIS) to induce innate immune responses[103-105]. cGAS is an enzyme that contains latent nucleotidyltransferase (NTase) activity. *In vitro* studies have demonstrated that binding to dsDNA or RNA-DNA hybrids stimulates cGAS enzymatic activity, resulting in the synthesis of 2'3'-cyclic-GMP-AMP (2'3'-cGAMP, hereafter cGAMP) from ATP and GTP[101] (Figure 1.1). Within cells, cGAMP serves as a second messenger that binds to the endoplasmic reticulum (ER)-resident protein STING[103-105]. STING also has the ability to detect bacteria-derived cyclic dinucleotides (e.g. cyclic di-AMP, cyclic di-GMP, and 3'3'-cGAMP)[106-109]. Binding to cGAMP or bacterial cyclic dinucleotides triggers conformational changes in STING, followed by its trafficking from the ER to the ER-Golgi intermediate compartment (ERGIC) and the Golgi apparatus[110-112]. As in the case of many other ER proteins, STING trafficking is mediated by vesicles formed by the GTPase SAR1 and the COPII complex[112]. Upon reaching at the ERGIC and Golgi, STING is palmitoylated and

oligomerizes into a signaling platform that recruits downstream kinases and other molecular complexes to initiate cytokine transcription and other innate immune responses[113,114].

Because cGAS is the main focus of this thesis work, the next section will describe the various innate immune responses caused by cGAS-STING signaling, as well as the mechanisms in which this pathway is regulated.

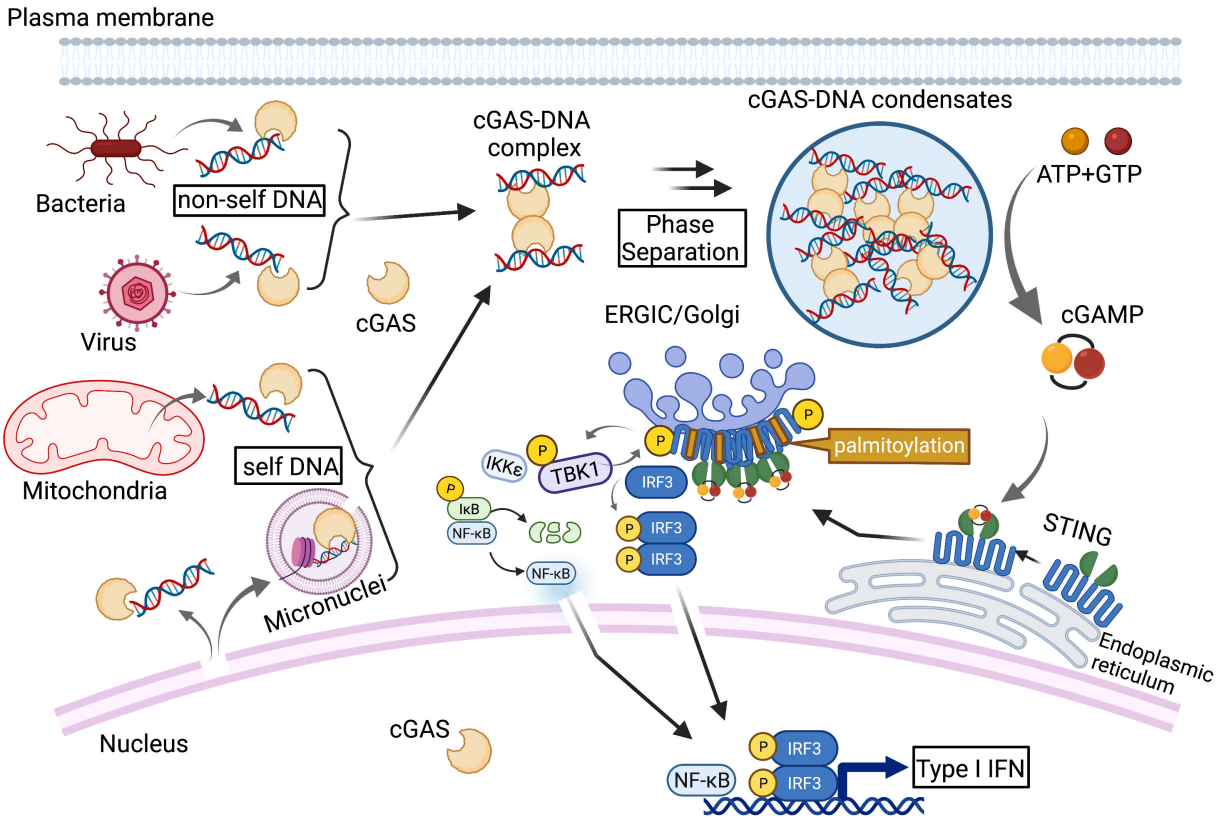

Figure 1.1. Overview of cGAS activation and cGAS-STING signaling

cGAS binds to both pathogen-derived and host organelles-derived DNA in the cytosol and micronuclei, which then forms cGAS-DNA 2:2 complexes. These complexes undergo phase separation to further assemble into larger oligomers with liquid-like biophysical properties. These cGAS-DNA condensates allow efficient catalytic action of cGAS, which turns ATP and GTP into cGAMP. cGAMP binds to STING on the ER membrane, which in turn oligomerizes and traffics to the ERGIC/Golgi. Activated STING recruits TBK1 that phosphorylates STING at its C-terminal tail (CTT). IRF3 is recruited to the pLxIS motif among the phosphorylated residues at the CTT of

Figure 1.1. (Continued)

STING, then gets phosphorylated by TBK1. Phosphorylated IRF3 dimers and translocates to the nucleus, where it induces the transcription of type I IFN and proinflammatory cytokines in collaboration with NF-κB, which is also activated by TBK1 and IKKε downstream of STING.

1.2. Control of innate immunity by the cGAS-STING pathway

1.2.1. Transcriptional and non-transcriptional host defensive responses induced by cGAS-STING

Within the Golgi apparatus, palmitoylated STING oligomers interact with the kinase TANK-binding kinase 1 (TBK1)[113]. This interaction between STING and TBK1 dimer is mediated by the PLPLRT/SD domain present in the cytoplasmic C-terminal tail (CTT) of STING, leading to TBK1 auto-phosphorylation and activation[115,116]. Activated TBK1 phosphorylates STING at Serine 366 (S366, S365 in mice) within a sequence also present in its C-terminus called a pLxIS motif (p, hydrophilic residue; x, any residue; S, phosphorylation site)[116,117]. This TBK1-mediated phosphorylation of STING is dependent on the oligomerization. Indeed, TBK1 cannot phosphorylate the STING dimer it is bound to due to the large space between the TBK1 active site and S366 of directly bound STING molecule[116]. The transcription factor interferon regulatory factor 3 (IRF3) is then recruited to the phosphorylated pLxIS motif, where is in turn phosphorylated by TBK1[116,117]. Activated IRF3 then dimerizes and translocates to the nucleus, where it induces the transcription of type I IFN genes in collaboration with NF-κB[118]. Type I IFN then elicits an antiviral state of cells in an autocrine or paracrine manner, through binding to its receptor IFN-α/β receptor (IFNAR)[119]. The IFNAR1-IFNAR2 complex activates the Janus Kinase (JAK)-signal transducer and activator of transcription (STAT) pathway, leading to the transcriptional induction of interferon-stimulated genes (ISGs) that target multiple stages in the viral life cycle[119].

As mentioned above, NF-κB is another transcription factor that is activated downstream of STING. Although the activation of NF-κB is dependent on TBK1 and its related kinase IKKε, it does not require IRF3 activation[120]. In addition to synergizing with IRF3 to induce type I IFN, NF-

κB induces the transcription of inflammatory cytokines and chemokines. Mouse STING mutants that contain a defective pLxIS motif (STING-S365A), which lack the IRF3 binding site and do not activate IRF3, revealed that STING induces IRF3- and IFN-independent antiviral responses[121-123]. These IRF3-independent factors that are upregulated during these responses include CXCL1, CXCL2, 4-BBL1, and COX2, whose expression is dependent on NF-κB[121]. Moreover, STING-mediated NF-κB activation in dendritic cells upregulates the surface expression of major histocompatibility complex II (MHC-II) and costimulatory molecules such as CD80 and CD86[121]. These events are considered hallmark activities needed to stimulate T cell-mediated inflammatory responses[124]. The IRF3-independent transcriptional responses are important for host defense, as the STING-S365A mice are resistant to herpes simplex virus 1 (HSV-1) infection[121-123]. STING-S365A mutations are associated with polyarthritis in DNA clearance-defective *DNase II*$^{-/-}$ mice even in the absence of IRF3 activation[125].

In addition to the transcription of type I IFN and cytokine genes, cGAS-STING signaling has been implicated in other innate immune responses. Autophagy is one such non-transcriptional consequences of STING activation[112]. Evolutionarily more ancient than the IFN genes, autophagy is a cellular process that was first described to maintain cell homeostasis under conditions of starvation[126]. Under these conditions, intracellular contents are encapsulated into membrane-bound structures called autophagosomes, which are delivered to lysosomes and degraded. The degraded materials can then be recycled for use by the cell as a means of self-sustenance. Autophagy also operates as a host-defense mechanisms to encapsulate cytosol-localized pathogens, leading to their eventual delivery to and destruction within lysosomes[127]. During infections with the DNA virus HSV-1 or *Mycobacterium tuberculosis* (Mtb), DNA from these pathogens can activate cGAS[128-131]. The resulting cGAMP production leads to STING-dependent autophagy of the pathogens and lysosomal degradation[129,132]. Mechanistically, the STING-containing ERGIC serves as a source of the hallmark processes in autophagosome formation—the lipidation of the protein LC3[112]. LC3 lipidation is dependent on autophagy protein 5 (ATG5) and WD repeat domain phosphoinositide-interacting protein 2 (WIPI2) but not on Unc51-like

autophagy activating kinase 1 (ULK1), ULK2, or Beclin 1, the components in the conventional autophagy[112]. A STING mutant lacking its C-terminal activation domain still triggers autophagy, suggesting that STING induces autophagy in a IRF3-independent manner[112]. STING-induced autophagy also functions as negative feedback of cGAS-STING pathway, as TBK1 activates p62/SQSTM1-dependent autophagy of STING for lysosomal degradation[133]. Because STING orthologs in *Xenopus tropicalis* and the sea anemone *Nematostella vectensis* induce autophagy without IRF3 activation or I IFN transcription[112], autophagy induction is thought to be the primordial function of cGAS-STING signaling.

Overall, cGAS-STING pathway induces IFN and other cytokine responses as well as cytokine-independent autophagy, all of which play significant roles in restricting pathogens.

1.2.2. cGAS-STING activities that impact cell viability and mitosis

In addition to the aforementioned activities that mediate host defensive type I IFN and autophagy responses, recent studies have revealed cGAS-STING activities that impact cells in unexpectedly diverse manners. For example, several instances of STING-mediated induction of programed cell death have been reported[134-143] (Table 1.1). T cells that experience intense STING activation trigger type I IFN-independent apoptosis by inducing the transcription of BH3-only proteins and other proapoptotic genes through the activities of IRF3 and p53[134]. STING also induces transcription-independent T cell apoptosis by disrupting calcium homeostasis and therefore sensitizing cells to ER stress and the unfolded protein responses (UPR), as revealed by a study using an autoinflammatory disease-associated STING mutant[135]. A gain-of-function STING mutant N154S (N153S in mouse) develops lung inflammation, myeloid cell expansion, and T cell cytopenia in IRF3-lacking mice[136], and the T cell death caused by this mutant was abrogated by ER stress inhibitors[135]. More recent data has indicated that STING signaling renders tumor cells sensitive to apoptosis induced by reactive oxygen species (ROS)[137]. This process may be mediated by the actions of ROS-metabolizing ISGs[137], which impact the extent of cellular damage that can be inflicted by oxidation.

In addition to apoptosis, cGAS-STING signaling promotes other forms of cell death. STING activation induces type I IFN and TNFα secretion. These cytokines can act synergistically to stimulate the necroptosis-inducing kinases receptor interacting kinase 1 (RIPK1)- and RIPK3 in neighboring cells[138]. STING-dependent necroptosis is not only induced by DNA viruses such as murine gammaherpesvirus 68 (MHV68), but also by mitochondrial DNA (mtDNA) that has been released into the cytosol[138,139]. Indeed, a mtDNA-STING-cell death pathway is required for the ischemia reperfusion (I/R) injury-induced intestinal barrier disruption *in vivo*[140].

Pyroptosis, the inflammatory cell death commonly caused by the actions of inflammasomes[144], is also positively regulated by cGAS-STING activation. cGAS-STING signaling promotes inflammasome assembly and activation in several experimental contexts, resulting in pyroptosis through type I IFN-dependent and -independent mechanisms. Type I IFN upregulates the expression of ISGs such as guanylate-binding proteins (GBPs) and immunity-related GTPases (IRGs)[145]. These factors can rupture cytosolic bacterial membranes to expose bacterial DNA to the protein AIM2. DNA-bound AIM2 then seeds the assembly of an inflammasome that stimulates pyroptosis[146]. Type I IFN also has been reported to induce the expression of the bacterial LPS receptor caspase-11, which can stimulate the NOD-, LRR- and pyrin domain-containing protein 3 (NLRP3) inflammasome by Gram-negative bacteria[147]. Indeed, cGAS and STING are required for cell death in murine macrophages that occurs during infections with *Chlamydia trachomatis* and *Francisella novicida*[141,142]. A study using BLaER1 human monocytes revealed that cytosolic DNA detection by cGAS causes the translocation of STING to lysosomes, where STING induces cell death via lysosomal rupture[143]. This lysosomal cell death (LCD) elicits pyroptosis by potassium (K^+) efflux-induced NLRP3 activation.

Altogether, activation of cGAS and STING leads to various forms of cell death in both pathogenic and sterile inflammation, but questions remain as to how cells determine which forms of cell death to induce in a certain context.

DNA repair machineries, including homologous recombination (HR) and non-homologous end joining (NHEJ), are crucial for genomic stability and cell viability but also must be tightly

regulated, because excessive DNA repair can lead to undesired chromosomal rearrangement[148]. cGAS has been implicated in the regulation of DNA repair, either as a positive and negative regulator[149-151]. Negative regulation of HR is mediated by chromatin-bound cGAS in the nucleus[150]. DNA-bound cGAS oligomerizes and therefore compacts DNA into higher-order state, which is resistant to RAD51 recombinase-mediated strand invasion[150]. This STING-independent role of cGAS accelerates the generation of micronuclei and cell death under severe genomic injury caused by irradiation. On the contrary, recently reported positive regulation of DNA repair is mediated by cytosolic DNA-bound cGAS[151]. Upon exposure of cells to ionizing radiation, DNA damage-induced cytosolic DNA leakage stimulates cGAS-STING signaling, leading to TBK1-mediated phosphorylation of phosphoribosyl pyrophosphate synthetases 1 and 2 (PRPS1/2)[151]. Phosphorylated PRPS1 and 2, in turn, promote DNA synthesis and repair. These opposing roles of cGAS in DNA repair indicate that cGAS functions in a context-dependent fashion, including cell types and the magnitude of DNA damages, which warrants future investigations.

Cellular senescence defines the irreversible cell cycle arrest caused by various cellular and environmental stresses, including inflammation and aging[152]. In the case of DNA damage, the cGAS-STING pathway induces a senescence-associated secretory phenotype (SASP), the hallmark phenotype of senescence in which cells secrete a variety of proteins including cytokines, chemokines, growth factors, and proteases[153-155]. SASP is not only the hallmark of senescence, but is also an amplifier of this process. The requirement for cGAS-STING in cellular senescence has been revealed by both *in vitro* and *in vivo* studies using ionizing radiation and other DNA-damaging agents[153-155]. In response to these agents, wild type cells arrest their growth rates, whereas cGAS-deficient cells continue to proliferate and do not exhibit SASP. The anti-proliferative roles of cGAS-STING may serve as anti-cancer mechanisms, as cGAS expression levels positively correlate with the survival of human lung adenocarcinoma patients[153].

In summary, cGAS-STING signaling induces not only cytokine responses but also other consequences affecting cellular homeostasis. Below, we will address the types of DNA ligands that activate cGAS and STING.

Cell Death	Cell Types	Stimulation / Model	Refs.
Apoptosis	T cells	Small molecule STING agonist	134
		STING gain-of-function mutant (N154S in human, N153AS in mice)	135, 136
	HNSCC cells	DNA-damaging agent, radiation	137
Necroptosis	L929 fibroblasts	Sendai virus (SeV), murine gammaherpesvirus-68 (MHV68)	138
	HT29 colon cancer cells	SMAC mimetic (LBW-242) + pan-caspase inhibitor (z-VAD-fmk)	139
	Mice (in vivo)	Ischemia reperfusion (I/R) injury	140
Pyroptosis	BMDMs	*Chlamydia trachomatis, Francisella novicida*	141, 142
	BLaER human monocytes	Horse testis (HT)-DNA lipofection	143

Table 1.1. cGAS-STING-dependent cell death

Summary of cGAS-STING-dependent cell death described in the main text. HNSCC: Head and neck squamous cell carcinomas, BMDM: bone marrow-derived macrophage, BLaER: tamoxifen-inducible derivative of the RCH-ACV B-cell leukemia cell line

1.2.3. Sources of substrate DNA that activate cGAS-STING signaling

1.2.3.1. Microbial DNA that activates cGAS

As expected from the role of cGAS in the innate immune responses, microbial DNA serves as an IFN-inducing cGAS ligand (Figure 1.1). Several DNA viruses carrying dsDNA activate cGAS-STING signaling in *in vitro* and *in vivo* studies. These DNA viruses include adenovirus[156], vaccinia virus (VACV)[128], African swine fever viruses (ASFV)[157], and herpesviruses such as cytomegalovirus (CMV)[158,159], MHV68[128], and HSV-1[160]. cGAS-STING pathway has also been implicated in the cellular responses to some RNA viruses. RNA retroviruses such as human immunodeficiency virus 1 (HIV-1), murine leukemia virus (MLV), Simian immunodeficiency virus (SIV), and human T lymphotropic virus type 1 (HTLV-1), activate cGAS by providing cytosolic DNA as reverse transcription intermediates (RTIs)[161]. In addition to those retroviruses, cGAS-STING signaling is involved in the responses to RNA viruses such as West Nile virus (WNV) and

dengue virus, although cGAS is thought to sense the mtDNA leaked during viral infection, not the viral nucleic acids[128,162].

DNA from bacteria also activate cGAS-STING signaling. Microbial DNA released from extracellular bacteria such as *Pseudomonas aeruginosa*, *Klebsiella pneumoniae*, and *Staphylococcus aureus*, and intracellular bacteria such as *Listeria monocytogenes*, *Francisella spp.*, *Neisseria gonorrhoeae*, Mtb, and *Rickettsia parkeri* bind to cGAS to elicit type I IFN responses[131,146,163-166]. While these DNA-induced IFN responses are beneficial to some facultative bacteria such as *Listeria* and *Francisella*, as shown *in vivo*[165,167], obligate bacteria such as *Rickettsia* are sensitive to IFN-mediated killing, and cytosolic DNA released from lysed *Rickettsia* subpopulation induces inflammasome-mediated host cell death that masks cGAS-STING-dependent IFN production to protect the remaining population[146]. Some bacteria utilize secretion systems and toxins to destabilize phagosomal membranes and release their contents, including DNA, into the cytosol. For example, Mtb uses its ESX-1 secretion system, a subtype of Type VII Secretion System (T7SS), to deliver virulence factors into macrophages[131]. These secretion systems are important for cGAS activation, as their mutations lead to weak type I IFN responses during infection[131].

In addition to DNA, some bacteria produce cyclic dinucleotides (CDNs) that directly activate STING without stimulating cGAS. c-di-GMP is synthesized from two GTP monomers by the act of bacterial diguanylate cyclase, and regulates bacterial metabolism, virulence, and biofilm formation[168]. STING recognizes c-di-GMP to restrict bacterial growth by inducing type I IFN and other cytokine responses[109]. Similarly, c-di-AMP produced by bacteria such as *Chlamydia trachomatis* stimulates STING[169]. However, during an infection, most of these bacteria also release DNA that is sensed by cGAS. The relative contribution of bacterial DNA and CDN to host inflammatory responses is largely undefined.

Lastly, cGAS has been implicated in the defense against parasites and fungi. For example, cGAS responds to the genomic DNA of *Plasmodium falciparum*, and cGAS-deficient mice permit higher parasite burden after infection than wild type mice[170]. The cGAS-STING pathway also

contributes to the type I IFN responses in *Aspergillus fumigatus* induced keratitis, although whether cGAS directly binds to fungal DNA is unclear[171].

1.2.3.2. Self-DNA as an IFN-inducing cGAS substrate

In addition to DNA from microbes, self-DNA can access the cytoplasm and activate cGAS (Figure 1.1). During mitosis within cells with genomic instability, which is a hallmark of many cancers[172], DNA may segregate from the main chromosome to form perinuclear compartments called micronuclei. Nuclear envelope (NE) rupture after mitosis makes the DNA in micronuclei accessible to the cGAS immunosurveillance, therefore leading to the production of type I IFN responses[173-175]. This DNA damage-induced exposure of nuclear DNA to cGAS in the cytosol also occurs during senescence, anti-mitotic chemotherapy, and dysregulation of epigenetic modification such as DNA hypomethylation that leads to skin inflammation[153,154]. Recently, however, Flynn *et al.* have proposed that chromatin bridges rather than micronuclei are the platforms of cGAS activation during mitotic errors, as IFN-inducing abilities of the antimitotic drugs correlated with the generation of cGAS-coated chromatin bridges, not micronuclei[176]. These findings suggest that not all DNA damages activate cGAS in a same manner, and the source of cGAS ligand depends on the context of DNA damages. Cytosolic DNA, when not optimally metabolized, stimulates the cGAS-STING pathway. Loss-of-function mutations in the genes encoding nucleases that degrade cytosolic DNA, such as three prime repair exonuclease 1 (TREX1), lead to cGAS-STING-dependent production of ISGs, which can lead to a disease called Aicardi–Goutières syndrome (AGS)[177].

As mentioned in the section above, mtDNA is also a cGAS ligand. The perturbation of mitochondrial function either by infectious or non-infectious stimuli leads to mitochondrial damages that release mtDNA into the cytosol. RNA viruses such as measles virus (MeV), which do not possess cGAS ligands, induce mtDNA-dependent cGAS activation in addition to activating RNA sensing pathways[178]. During intrinsic apoptosis, Bax/Bak-mediated mitochondrial outer membrane permeabilization (MOMP) triggers the cytosolic release of mtDNA that activates cGAS

and STING, which is inhibited by apoptotic caspases (caspase-9 and caspase-3/7) that are downstream of MOMP[179,180]. The mechanism by which these caspases inhibit cGAS-STING activation is likely via the cleavage of cGAS, as described later[181]. Recent studies have found that inflammatory cytokines such as TNFα and IL-1β treatment leads to mtDNA release into cytosol, which triggers cGAS-dependent type I IFN responses[182,183]. Also, even in the absence of exogenous stimuli, heterozygous knockout of the mtDNA-binding protein transcription factor A, mitochondrial (TFAM) in murine cells leads to the cytosolic release of mtDNA, resulting in the production of ISGs that render cells protective against HSV-1 infection[184].

Extracellular self-DNA can also stimulate cGAS. Macrophages and other myeloid cells internalize self-DNA from the extracellular space through phagocytosis. In principle, phagocytosed cargo should be degraded in lysosomes, with luminal DNA being hydrolyzed down to single nucleotides by DNases present in the intra-lysosomal environment. Early studies, prior to the discovery of cGAS or STING, revealed that mice and cells deficient in the lysosomal enzyme DNase II are prone to express high levels of IFNs and other ISGs[185]. Subsequent work revealed that STING pathway activation was responsible for these responses[186]. These results suggested that in the absence of efficient lysosomal nuclease activity, DNA can somehow leak into the cytosol and activate cGAS-STING dependent responses.

Additional instances of extracellular DNA activating cGAS-STING have been reported. For example, non-apoptotic cell death caused by tissue injury and tumor irradiation can release DNA into the extracellular space, as can the production of DNA-containing neutrophil extracellular traps (NETs). NETs are released by neutrophils during a cell death process called NETosis, and consist of chromatin and antimicrobial molecules[187]. The abundance of extracellular DNA at the sites of inflammation or tissue injury may result in a phenocopy of DNase II deficiency. In this regard, phagocytes that internalize NETs or chromosomal fragments released at sites of irradiation may contain such high amounts of lysosomal DNA that DNase II is overwhelmed, resulting in DNA leakage in the cytosol and the stimulation of cGAS[188]. Consistent with this idea, myeloid cells are the primary source of cGAS-mediated IFN responses at sites of tissue injury[188].

Overall, there are several sources of DNA that can activate the cGAS-STING pathway. This promiscuity of DNA detection raises the question of how this inflammatory network is regulated to ensure efficient distinction between self and non-self-DNA. In the next sections, we discuss our current knowledge of how DNA-induced cGAMP synthesis by cGAS is regulated.

1.2.4. The biophysical mechanisms of cGAS activation and cGAMP synthesis

cGAS is a 522 amino-acid protein that consists of a basic unstructured N-terminal domain, and a conserved C-terminal Mab21 domain with NTase activity. While cGAS monomers cannot synthesize cGAMP, cGAS dimers formed upon interactions with the sugar phosphate backbone of dsDNA display enzymatic activity. Binding of a parallel-aligned pair of dsDNA to the two DNA-binding sites (A-site and B-site) on each of two cGAS molecules stabilizes 2:2 cGAS-DNA complex, accompanied with the cGAS conformational changes that generate ATP and GTP pockets near the catalytic residues[189,190]. The cGAS dimerization and conformational changes occur independently on the sequence of dsDNA, but neither single stranded DNA (ssDNA) nor RNA induces cGAS conformational changes and subsequent cGAMP synthesis although they can bind to cGAS[102,191]. The cGAS dimers further align adjacently to form a ladder-like structure[192]. In addition, a newly discovered DNA binding site in human cGAS (C-site) allows multivalent interaction between cGAS and DNA to form the mesh-like structure[193]. The formation of these higher order cGAS-DNA complexes requires the certain length of DNA (> 45 bp), and the shorter DNA does not lead to human cGAS oligomerization and efficient cGAMP production[194]. Mouse cGAS, in contrast, can oligomerize upon binding to short DNA and produce cGAMP, as the amino acids in the DNA binding sites allow more stable interaction with DNA[194]. Indeed, when the residues at this position are substituted for those in mouse cGAS, human cGAS gains the ability to synthesize cGAMP in response to short DNA[194].

cGAS-DNA complexes further assemble into micrometer-sized condensed liquid droplets through the process called phase separation[195]. These higher-order complexes have liquid-like properties—the droplet formation is reversible, and the droplets can fuse to form larger spherical

units. These membrane-less granules consisting of cGAS and DNA provide a platform for cGAMP production, where cGAS encounters its substrates more efficiently. This liquid droplet formation is dependent on the concentration of cGAS and DNA[195], suggesting that cGAS is activated only when cytosolic DNA levels reach a certain threshold, such as in the case of infection or cellular stresses with DNA damage. Moreover, under physiological salt concentrations, the formation of cGAS liquid droplets is dependent on intracellular ion concentration, mostly zinc[195]. Indeed, addition of zinc (Zn^{2+}) to cultured cells activates cGAS to induce type I IFN responses in the presence of dsDNA treatment[196]. Zn^{2+} is not the only ion that contributes to cGAS activation. Divalent cations such as magnesium (Mg^{2+}) and manganese (Mn^{2+}) are required cofactors of cGAS that catalyze the conversion of ATP and GTP into cGAMP[108]. Mn^{2+} directly activates cGAS even in the absence of dsDNA by inducing the noncanonical conformational changes of cGAS to mimic DNA-activated cGAS, which has a unique η1 helix in the catalytic pocket allowing substrate entry and cGAMP synthesis[196].

1.2.5. Regulation of DNA sensing and cGAS activation within cells

Despite the increasing knowledge about the mechanism of cGAS activation *in vitro*, the intracellular behavior of cGAS is more complicated and remains an active area of investigation. Here, we will focus on the subcellular distribution and posttranslational modification of cGAS as the major factors that regulate DNA sensing and activation of cGAS within cells (Figure 1.2).

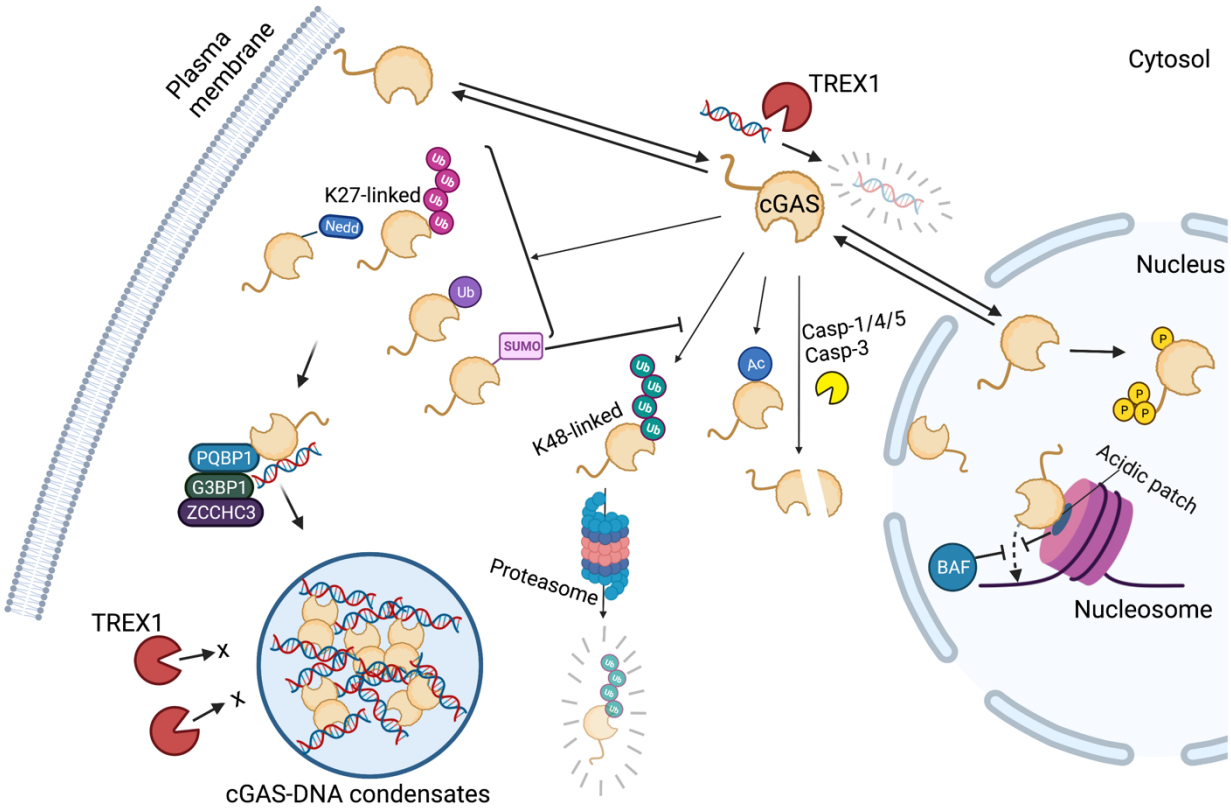

Figure 1.2. Regulation of cGAS activity in cells

cGAS activation is positively and negatively regulated by various mechanisms in cells. cGAS is localized in not only in cytosol but also in the nucleus and on the plasma membrane, which restricts the access to the cytosolic DNA. cGAS reactivity to chromosomal DNA is restricted in the nucleus. cGAS tethering to the acidic patch of nucleosomes and BAF binding to DNA prevents cGAS from binding DNA. Besides these mechanisms restricting cGAS accessibility to DNA, cGAS is hyperphosphorylated at its N-terminal region and catalytic activity is attenuated.

Post-translational modification such as K27-linked polyubiquitination, monoubiquitination, Neddylation, and SUMOylation positively regulate cGAS activity, whereas K48-linked polyubiquitination, acetylation, and Caspase-mediated cleavage of cGAS negatively regulate activity. Moreover, cofactor proteins including PQBP1, G3BP1, and ZCCHC3 promotes DNA binding, oligomerization, and phase separation of cGAS.

Figure 1.2 (Continued)

Phase separation-induced condensates restricts TREX1-mediated degradation of DNA and therefore accelerate cGAMP synthesis.

1.2.5.1. Subcellular localization of cGAS

cGAS was originally thought to reside in the cytosol to avoid nuclear self-DNA detection[101]. Despite this general idea, soon after cGAS was identified, Knipe and colleagues reported that cGAS can be detected in the nucleus of human fibroblasts and keratinocytes[197]. Other studies have reported cGAS localization in micronuclei, chromatin bridges, and the nucleus. cGAS activation in micronuclei and chromatin bridges are discussed in the section above. Yang *et al.* revealed that cGAS translocates from the cytosol to the nucleus during mitosis and relocates to the cytosol to react with DNA fragments in the presence of DNA damage[153]. Liu *et al.* found that cGAS translocates from cytosol to the nucleus upon DNA damage to suppress DNA repair[149]. More recently, Sun *et al.* identified a nuclear export signal (NES) within cGAS 169-174 a.a. (LEKLKL), which is responsible for chromosome maintenance region 1 (CRM1)-dependent cGAS translocation from the nucleus to the cytosol upon DNA stimulation[198]. Other groups reported that cGAS does not translocate to the nucleus in response to a stimulus, but is rather a nuclear resident protein[199]. Finally, work from our lab examining a tagged allele of cGAS revealed different localization patterns of this protein in different cells[200]. For example, cGAS was localized to the plasma membrane in macrophages, but was distributed in the cytosol and/or the nucleus in non-phagocytic cells[200]. It is unclear why different groups have found cGAS to be localized to distinct regions of the cell, and much more work needs to be done to understand the behavior of cGAS within cells.

The collective data described above could be used to suggest that cGAS is a nuclear protein under several experimental (and perhaps physiological) conditions. However, this conclusion would have significant functional implications for immunosurveillance, as nuclear cGAS is well-recognized to be an inactive protein. Elegant work from Gentili *et al.* has shown that

the nucleus-localized pool of cGAS is ~200-fold less responsive to DNA than extra-nuclear cGAS[201]. Within the nucleus, the protein barrier-to-autointegration factor 1 (BAF) operates as the negative regulator of cGAS sensing of chromatin DNA upon nuclear rupture[202]. BAF outcompetes cGAS for DNA binding, thereby inhibiting the formation of cGAS-DNA oligomers in the nucleus. Moreover, while cGAS is able to bind to histone-containing DNA and uncoated DNA, only the latter is able to stimulate cGAMP production efficiently[201,203,204]. Cryo-electron microscopy revealed the mechanism underlying chromatin-mediated inhibition of cGAS activity, as an acidic patch of the histone H2A-H2B contacts cGAS and inhibits cGAS oligomerization upon DNA binding[205-209]. Thus, an increasing body of evidence supports the idea that the exclusive localization of cGAS to the nucleus would result in the inactivation of its ability to drive type I IFN responses to infection. As such, it is likely that an extra-nuclear pool of cGAS exists and may be responsible for pathogen detection.

cGAS has been reported to be present on the plasma membrane of macrophages, through interactions between the basic N-terminal domain of cGAS and phosphatidylinositol-4,5-bisphosphate (PtdIns(4,5)P_2; also known as PIP_2)[200]. The deletion of the cGAS N-terminal domain released cGAS to the cytosol, resulting in the detection of self-DNA and aberrant type I IFN induction. This data suggests that the N-terminal domain of cGAS is required to prevent self-DNA recognition, perhaps by tethering this protein to the cell surface. The finding that N-terminus of cGAS is required to prevent self-DNA reactivity was recently validated by Li *et al.*, who further demonstrated that the self-DNA detected by cGAS is likely to be mtDNA[210]. Indeed, N-terminal deletion mutants of cGAS were found to be localized to the microchondria[210]. This data is interesting to consider in the context of the *in vitro* behaviors of cGAS, which suggested that DNA-induced liquid droplet formation is potentiated by the cGAS N-terminal domain. As droplet formation *in vitro* is associated with enhanced cGAMP production, one would have expected that deletion of a driver of droplet formation (the N-terminal domain) would impair IFN responses within cells. Yet the opposite results were obtained independently[200,210]. More work is needed to

understand the relative importance of the cGAS N-terminal domain in liquid droplet formation and self-DNA detection.

A recent study by Zhou *et al.* revealed that cGAS-DNA phase separation is not required for the intrinsic ability of cGAS to produce cGAMP *in vitro*[211]. Rather, phase separation may be important to restrict DNA degradation by exonuclease TREX1. Cell-free studies demonstrated that TREX1 is restricted to the outer shell of a cGAS-DNA containing liquid droplet. It is likely that the phase separation resists other negative regulators than TREX1, as the droplet-deficient cGAS mutant signals weaker than wild type cGAS even in the absence of TREX1[211]. In addition to cytosolic DNA, TREX1 can degrade micronuclear DNA to prevent cGAS activation[212]. The access to the ruptured micronuclei is achieved by ER localization of TREX1 and does not depend on DNA-binding function of TREX1. It is unclear whether cGAS-DNA phase separation occurs in micronuclei to resist TREX1-mediated DNA degradation.

Altogether, DNA sensing by cGAS is regulated not only by the physical separation of receptor and ligand within cells, but also by several safeguard mechanisms offered by DNA- or cGAS-binding proteins in the nucleus and the cytosol. These may be the main factors that underline the difference of cGAMP synthetic activity of cGAS *in vitro* and in cells. However, there is still a lack of consensus about cGAS localization, possibly due to the difference in the experimental settings such as cell types and imaging protocols used in each study. Future investigation that compares these factors will shed more light on the cell biology of cGAS.

1.2.5.2. Post-translational modifications of cGAS

In addition to regulation by subcellular localization, interaction with other molecules regulate cGAS through post-translational modifications (PTMs). Phosphorylation of cGAS has been reported to inhibit cGAS activity. Akt phosphorylates cGAS at S305 in human cGAS (S291 in mouse cGAS) within the C-terminal catalytic domain, thereby negatively regulating cGAMP synthesis in response to exogenous dsDNA[213]. Cyclin-dependent kinase 1 (CDK1)-cyclin B complex phosphorylates the same serine residues of cGAS upon mitotic entry to suppress

cGAMP synthesis upon self-DNA recognition in the nucleus[214]. These residues are dephosphorylated by type 1 phosphatase (PP1) upon mitotic exit to allow cGAS reactivity to exogenous DNA in the cytosol. Furthermore, multiple serine residues within the N terminus of cGAS are phosphorylated by Aurora kinase B (AurB) and other kinases during mitosis[210]. This hyperphosphorylation, along with chromatin tethering, blocks cGAS activation by self-DNA in the nucleus during cell cycle transition[210]. In addition to serine phosphorylation, cGAS is phosphorylated at tyrosine residues. B-lymphocyte kinase (BLK) phosphorylates cGAS at Y215, thereby preventing cGAS nuclear translocation upon DNA damage[149].

Ubiquitination and other ubiquitin-like protein conjugation events affect cGAS-STING signaling. K27-linked polyubiquitination of cGAS by ER-resident E3 ligase RNF185 positively regulates cGAS-mediated responses to HSV-1 infection[215]. Additionally, E3 ligase TRIM56-induced monoubiquitination of cGAS at K335 is necessary for cGAS oligomerization upon DNA binding[216]. Moreover, cGAS is subject to K48-linked polyubiquitination at K271 and K414, which targets cGAS for proteasomal degradation. As a positive feedback loop of cGAS-STING signaling, this K48-linked ubiquitination is inhibited by tripartite motif (TRIM) E3 ligases. TRIM38 conjugates small ubiquitin-like modifier (SUMO) to cGAS that inhibits DNA binding and K48-linked polyubiquitination of cGAS[217], while TRIM14 recruits deubiquitinating enzyme (DUB) USP14 to cleave K48-linked ubiquitin chains on cGAS[218].

Neddylation is the covalent conjugation of neural precursor cell expressed, developmentally downregulated 8 (NEDD8), another ubiquitin-like protein. cGAS is neddylated on K231 and K421 by roles of E2 enzyme Ube2m and E3 ligase Rnf111, inhibition of which abolishes type I IFN induction during HSV-1 infection[219].

Acetylation of cGAS has been reported to modulate cGAS-STING signaling. cGAS K384, K394, and K414 are acetylated in the steady state, and DNA binding of cGAS stabilizes the interaction with histone deacetylase 3 (HDAC3), which deacetylates cGAS to activate signaling[220]. Aspirin, a non-steroidal anti-inflammatory drug (NSAID), inhibits cGAS activation by directly binding and acetylation on these residues. Treatment of aspirin suppresses inflammation in AGS

patient cells and in an AGS mouse model, suggesting cGAS acetylation prevents self-DNA-induced cGAS-STING signal activation. In different experimental contexts, it was found that the cGAS acetylation in the N-terminal domain at K47, K56, K62, and K83 by the lysine acetyltransferase 5 (KAT5) potentiates cGAS-STING signaling during DNA virus infections[221].

The cleavage of cGAS also modulates is inflammatory activities in cells. The canonical and non-canonical inflammasome activation leads to caspase-1- and caspase-11-mediated cGAS cleavage, respectively, to dampen cGAS-STING signaling[222]. Similarly, activated caspase-3 cleaves cGAS during apoptosis to suppress DNA-induced cytokine responses, keeping apoptotic cells immunologically silent[181].

Besides post-translational modification, several proteins enhance cGAS-DNA complex formation by physically interacting either the enzyme or the substrate. GTPase-activating protein SH3-binding protein 1 (G3BP1) was identified as a protein that interacts with cGAS in the cytosol to promote DNA binding and subsequent activation[223]. Recently, the interaction with G3BP1 has been found to promote primary condensation of cGAS even in the resting cells, which primes cGAS for its rapid response to DNA[224]. Although G3BP1 is required for stress granule (SG) assembly and therefore plays an important role in RNA-sensing innate immune signaling, cGAS activation by G3BP1 is independent of SG assembly[223].

In addition, polyglutamine binding protein 1 (PQBP1) and CCHC-type zinc-finger (ZF) protein ZCCHC3 are co-sensors of cGAS, which bind to both DNA and cGAS to promote cGAS recognition of DNA[225,226]. While PQBP1 is specific receptor for the reverse-transcribed retroviral DNA such as HIV-1, ZCCHC3 binds DNA from HSV-1 and synthetic dsDNA in the cytosol. Because the affinity of cGAS alone for DNA is low and the recognition is promiscuous[189,194], these co-receptors are essential for optimal cGAS-DNA complex formation. Absence of these co-receptors in the nucleus may explain the low reactivity of cGAS to the self-DNA in the nucleus in addition to the presence of BAF as mentioned above, which needs further examination. Moreover, PQBP1 interacts with extrinsic tau, transmissible neurodegenerative disease protein, and then triggers cGAS-STING-dependent NF-κB activation[227]. As this finding bridges cGAS-STING

signaling to tau-related neurodegenerative disorders, identification of cGAS-STING signaling regulators that are known to play important roles in a disease pathogenesis will indicate the unexpected involvement of cGAS and STING in that disease.

Altogether, cGAS-STING signaling is regulated by various mechanisms in cells including subcellular localization and post-translational modifications. In the next section, we will discuss how cGAS-STING pathway is targeted by pathogens.

1.2.6. Viral targeting of cGAS as an immune evasion strategy

Viruses and bacteria utilize several strategies to inhibit cGAS-STING. Here we focus on virus-mediated modifications of cGAS. Some DNA and RNA viruses target cGAS for degradation. The NS2B protease complex of dengue virus (DENV) cleaves cGAS to block its activation by mtDNA released from stressed mitochondria during infection[228]. Other viruses take indirect strategies to degrade cGAS. NS1 protein of Zika virus (ZIKV) stabilizes caspase-1, which cleaves cGAS as described above[229]. F17 protein in poxviruses binds to Raptor and Rictor, regulators of mammalian target of rapamycin complexes mTORC1 and mTORC2, to hyperactivate mTOR leading to the proteasomal degradation of cGAS[230].

Other viral proteins physically perturb DNA sensing and activation of cGAS. VP22 and UL37 from HSV-1[231,232], UL31, UL42, and UL83 from human cytomegalovirus (HCMV)[233-235], and ORF52 and LANA from Kaposi's sarcoma-associated herpesvirus (KSHV)[236,237], ORF9 from Varicella-Zoster virus (VZV) are known examples of cGAS-inhibiting viral proteins[238]. Among these viral proteins, VP22, ORF52, and other structurally similar tegument proteins have been found to compete DNA binding and phase separation with cGAS, thereby inhibiting cGAS-DNA phase separation[239]. In contrast, the HSV-1 UL37 tegument protein inhibits cGAS through PTM. UL37 deamidates N210 within the activation loop of human cGAS, which blocks cGAMP synthesis by impinging on the catalytic site[232]. This deamidation residue of cGAS is conserved in mice but not in many other non-human primates, which accounts for the species-specific permissiveness of HSV-1.

1.2.7. cGAS-STING pathway: Conclusion

cGAS function has been implicated as a driver of inflammation in a variety of cellular processes. Studies from diverse laboratories have unified our understanding of the intrinsic enzymatics that govern DNA-induced cGAS activities. However, much less unanimity exists regarding the regulation of these intrinsic activities within cells. The cell biology of the cGAS-STING pathway will therefore likely remain at the forefront of research in this area. The open questions in this regard include how the regulation of cGAS activation is in different cell types and different species. Also, the mechanisms of cGAS activation by non-self- and self-DNA in cells are regarded to be the same, but there is still a possibility that they are different, which warrants further investigation. Since the dysregulation of cGAS binding of self-DNA and subsequent aberrant cytokine production underlies a variety of diseases, future studies will likely be focused on filling the gap between our knowledge of cGAS activities *in vitro* and those within cells.

1.3. Metabolic organelles and innate immune signaling

Organelles are the functional compartments within the cells, and most of them harbor some PRRs on their membrane structures[240]. Among these organelles are mitochondria and peroxisomes, which play major roles in cell metabolism, especially in fatty acid and ROS metabolism[241]. Not only these metabolic organelles serve as the platform of PRR signaling, but also their metabolism effectively regulates innate immune responses[242,243]. This chapter will overview the roles of mitochondria and peroxisomes in the regulation of PRR signaling.

1.3.1. Mitochondria and innate immune responses

Mitochondria are the dynamic double-membrane organelles specialized in adenosine triphosphate (ATP) production as well as fatty acid and ROS metabolism, and therefore are the powerhouse of the eukaryotic cells[244]. As described in the previous section, MAVS is the adaptor protein in RLR signaling that is tail-anchored on the outer mitochondrial membrane (OMM) surface[51-54]. Mitochondria are the platform of MAVS oligomerization, which is required for RLR-mediated antiviral responses[245]. The importance of MAVS mitochondrial localization is

underscored by the fact that an RNA virus hepatitis C virus (HCV) blocks RLR signaling by the proteolytic activity of the NS3/4A protein that cleaves MAVS off the mitochondria[246]. Mitochondria are the platform for not only MAVS oligomerization but also the interaction between MAVS and mitochondrial resident proteins that regulate RLR signaling[247-252]. For example, NLR family protein NLRX1 was identified as the OMM protein that negatively regulates MAVS by binding CARD that interferes RIG-I-MAVS interaction[248], although the localization and the roles of NLRX1 in RLR regulation is now controversial[248,253,254]. Other examples include mitofusin 1 (MFN1) and MFN2, the OMM proteins responsible for mitochondrial fusion, which have been reported to interact with MAVS to promote and inhibit its oligomerization, respectively[249,250]. Although these direct roles of MFN1 and MFN2 in the regulation of MAVS is independent of their functions in mitochondrial fusion[249,250], mitochondrial dynamics are tightly linked to RLR signaling, as the silencing of mitofusins and other genes involved in mitochondrial elongation abolishes RLR signal activity[255,256]. These results suggest that mitochondria not only provide MAVS with a signaling platform but also regulate RLR signaling by their metabolic functions. Indeed, MAVS oligomerization induces mitochondrial ROS (mtROS) that triggers further aggregation of MAVS, which is required for RLR-induced cytokine responses[257].

In addition to RLR signaling, mitochondria also serve as the platform of NLRP3 inflammasome assembly[242,258-261]. Cytosolic receptor NLRP3 is recruited to mitochondria upon activation[258], which is mediated by the interaction between the N-terminal domain of NLRP3 and MAVS[259,262]. Association with MAVS on the OMM facilitates NLRP3 oligomerization, which assembles the inflammasome and subsequent responses[262]. Indeed, cells deficient in MAVS show reduced NLRP3 inflammasome responses to non-crystalline ligands such as ATP and a potassium ionophore nigericin[259]. However, MAVS deficiency has no effect on NLRP3 inflammasome responses to crystalline substances such as alum and monosodium urate (MSU) crystals, indicating that the involvement of MAVS is context-dependent[259]. Either case, it is now

known that NLRP3 is bound to cardiolipin, the non-bilayer forming inner mitochondrial membrane phospholipid exposed to the cytosol upon mitochondrial ROS or other damages[258,260,263].

Mitochondria contain small circular DNA called mitochondrial DNA (mtDNA) inside the organelle, and like nuclear DNA, its presence in the cytosol is sensed by PRRs as the disruption of cellular homeostasis[242,264]. Not only mtDNA stimulates cGAS-STING pathway as described in section 1.2.3.[184], but also oxidized mtDNA released into the cytosol during apoptosis signal activates NLRP3[265] and other inflammasomes such as NLRC4 inflammasome[266]. Moreover, mtDNA activates TLR9, a member of TLR family that detects hypomethylated CpG motif in DNA[100]. Although recent studies have indicated CpG methylation is rarely found in mtDNA in contrast to nuclear DNA[267,268], TLR9 has been reported to recognize mtDNA and activate p38 MAPK in polymorphonuclear neutrophiles (PMNs)[269,270].

Glucose metabolism that produces ATP includes glycolysis in the cytosol and Krebs cycle and oxidative phosphorylation (OXPHOS) in the mitochondria. Inflammatory macrophages and DCs stimulated with LPS induce core metabolic switch from OXPHOS to glycolysis[271,272]. In addition to the rapid production of ATP by glycolysis, this metabolic switch accumulates the Krebs cycle intermediates that regulate inflammatory and anti-inflammatory gene expression[273]. For example, succinate, one of the Krebs cycle intermediates that accumulates upon LPS stimulation, is transported from the mitochondria to the cytosol, where it stabilizes and activates hypoxia-inducible factor 1a (HIF-1a) that directly binds *IL1B* promoter and induces gene expression[274,275]. Moreover, succinate is oxidized in the mitochondria by succinate dehydrogenase (SDH) following the metabolic switch, and this leads to succinate-induced mitochondrial membrane potential elevation and mtROS production, which upregulate proinflammatory gene expression and downregulates anti-inflammatory gene expression[276]. LPS-induced increase in the glycolytic flux also accumulates itaconate by upregulating the expression of immune-responsive gene 1 (IRG1), which synthesizes itaconate, and by downregulating the expression of itaconate dehydrogenase

1 (IDH1), which metabolizes itaconate[273,277,278]. Itaconate limits mtROS and subsequent IL-1β production by inhibiting succinate oxidization by SDH to negatively regulate succinate-mediated inflammatory responses[279]. A recent study has found another mechanism of itaconate-mediated inhibition of cytokine responses, in which itaconate directly binds to TET2 enzyme to inhibit the induction of NF-κB and STAT1 signaling target genes to dampen inflammatory responses[280].

Fatty acid oxidation (FAO) is another major mitochondrial metabolism. Mitochondrial FAO catabolizes short-chain fatty acids (SCFAs, 2-6 carbons), medium-chain fatty acids (MCFAs, 6-12 carbons), and long-chain fatty acids (LCFAs, 13-21 carbons) to acyl-CoA, NADH and $FADH_2$, which promote the Krebs cycle and following OXPHOS[242]. In addition to IL-4-stimulated alternatively activated (M2) macrophages[281,282], plasmacytoid DCs (pDCs) stimulated with TLR9 agonist or type I IFN increase FAO[283]. These core metabolic shifts are important in the further induction of type I IFN, as the treatment with a FAO inhibitor etomoxir inhibits the IFN responses[283].

Although the mechanisms how FAO and OXPHOS regulate these responses are unclear[282,283], modulating the balance of fatty acids in the cells may be one of the mechanisms, because fatty acids are now known to have immunomodulatory functions as extensively reviewed elsewhere[284-287]. Butyrate, for example, is a four-carbon SCFA with both pro- and anti-inflammatory effects. Binding of butyrate to G protein-coupled receptors (GPCRs) on the cell surface, such as GPR41 and GPR43, induces proinflammatory responses in the epithelial cells[288], while binding to GPR109A induces anti-inflammatory effects[289-291]. Moreover, butyrate incorporated in cells inhibits histone deacetylase (HDAC) independent on GPCRs, which negatively regulates the transcription of proinflammatory genes[292]. Therefore, butyrate and its structurally similar ketone β-hydroxybutyrate (BHB) have been reported to inhibit TLR4 and NLRP3 responses[290,292-294]. Another example of immunomodulatory fatty acid is a LCFA palmitate[287,295]. Palmitate mediates the inflammation in LPS-primed macrophages by activating c-Jun N-terminal kinase (JNK)[295,296]. In this context, palmitate has also been reported to attenuate

glycolysis to exacerbate the inflammatory responses, marked by the upregulation of proinflammatory cytokines such as IL-23, IL-6, and IL-12[297]. Moreover, palmitate mediates NLRP3 inflammasome-dependent IL-1β secretion[298-300]. As the mechanism, palmitate undergoes intracellular crystallization in macrophages, leading to the lysosomal rupture that releases proteolytic enzyme cathepsin B, which cleaves proIL-1β, as well as calcium that stabilizes Il1b mRNA [298,300]. Furthermore, palmitate is directly conjugated to proteins as a post-translational modification called palmitoylation[295]. Among PRR signaling, STING is known to be palmitoylated at the Golgi apparatus, which is required for the assembly that recruits downstream signaling proteins[113]. Altogether, mitochondrial fatty acid metabolism plays important roles in regulating innate immune responses, not only by metabolic reprogramming but also by balancing immunoregulatory fatty acids.

Overall, mitochondria not only serve as the platform of multiple PRR signaling pathways but also regulate pro- and anti-inflammatory cytokine responses through the metabolism and its intermediate products.

1.3.2. Peroxisomes and innate immune responses

Peroxisomes are the single-membrane organelles with highly dynamic properties, and like mitochondria, they are involved in various metabolism[301-303]. Although many substances including fatty acids and ROS are metabolized in both peroxisomes and mitochondria, ether lipid synthesis, β-oxidation of very long-chain fatty acids (VLCFAs, 22 or longer carbons), and α-oxidation of branched-chain fatty acids (BCFAs) take place only in peroxisomes[241,303]. These peroxisomal FAO is essential for cell homeostasis, as VLCFAs such as hexacosanoic acid (also known as cerotic acid) and BCFAs such as phytanic acid and pristanic acid accumulate and demonstrate severe lipotoxicity in peroxisomal disorders[301,304]. However, the effects of these fatty acids on the innate immune responses are unknown.

Peroxisomes are either self-divided or newly generated, and the peroxin (PEX) family proteins play roles in both forms of peroxisome assembly[302,305]. For example, PEX11β initiates the elongation of peroxisomes, which is followed by mitochondrial fission factor (MFF)- and FIS1-mediated constriction and dynamin-related protein 1 (DRP1)-mediated fission[305,306]. Also, peroxisomal matrix and membrane proteins contain peroxisomal targeting signals (PTSs) and membrane PTSs (mPTSs), respectively, and they are incorporated into the peroxisomes by the function of PEX proteins[305]. C-terminal PTS1-containing proteins and N-terminal PTS2-containing proteins are bound to PTS receptors PEX5 and PEX7, respectively[307,308]. These cargo-receptor complexes are then transported into the peroxisomal lumen by interacting with the docking complexes and really interesting gene (RING) complexes on the peroxisomal membranes that are composed of other PEX family proteins such as PEX14[305,309,310]. The functional loss of these PEX genes cause peroxisomal biogenesis disorders (PBDs) including Zellweger syndrome spectrum (ZSS) disorders, whose patients usually die in the first few years of life[311,312]. Therefore, peroxisomes and their functions are essential in the cell viability, while the contribution of peroxisomes in innate immune signaling is still unclear[243].

A breakthrough in the understanding of the interaction between peroxisomes and PRR signaling is the discovery of MAVS on peroxisomal membrane[56]. Peroxisomal biogenesis includes not only self-division but also *de novo* synthesis, and which is the hybrid of the pre-peroxisomes derived from both mitochondria and ER[313]. Along with this model, several mitochondrial membrane proteins such as MFF and FIS1 have been found on peroxisomes[314,315], which further led to the identification of MAVS on peroxisomes[56]. By using synthetic MAVS mutant named MAVS-Pex, which contains the transmembrane domain of peroxisomal membrane protein PEX13, Dixit *et al.* have discovered peroxisomal MAVS is functional to induce ISGs upon infections with RNA viruses[56]. This MAVS-Pex-mediated induction of ISGs are more rapid than mitochondrial MAVS (MAVS-mito)-mediated signals and independent of type I IFN, suggesting that MAVS

functions differently from peroxisomes and mitochondria[56]. Later study described IRF1-dependent type III IFN production as the specific mechanisms of peroxisomal MAVS-mediated ISGs induction upon infection with RNA viruses and bacterium Listeria monocytogenes[316]. Although peroxisomal localization of MAVS and type III IFN induction is confirmed by a study from another group, the difference between peroxisomal MAVS and mitochondrial MAVS was not observed in this study, leaving controversy over the signaling specificities of MAVS on each organelle[317].

The roles of peroxisomes in the innate immune responses, which are suggested by the presence of MAVS, have been further validated by the modulation of peroxisomal biogenesis. While overexpression of the peroxisome elongation factor peroxin 11b (PEX11β) specifically increases type III IFN responses, the deficiency of PEX19, the cargo protein required for peroxisomal assembly, leads in the increase in the overall cytokine responses against reovirus infection[316]. Although the results of PEX19 deficiency can be viewed as the possible accumulation of all MAVS proteins on the mitochondrial membrane, these also may be the consequences of the loss of peroxisomal functions in metabolism. However, the roles of peroxisomal metabolism in the innate immune responses are largely unknown other than a few recent findings. Vijayan *et al.* has reported that, in murine macrophages, peroxisomes negatively regulate LPS-induced inflammation[318]. In this study, the treatment with 4-phenyl butyric acid (4-PBA), a nonclassical peroxisome proliferator, reduced the abundance of cyclooxygenase-2 (COX-2) and inflammatory cytokines, while the knockdown of PEX14 gene increase these proteins[318]. In contrast, Di Cara *et al.* has found that peroxisomes support phagocytosis and antimicrobial peptide production upon bacterial infection in Drosophila melanogaster and murine macrophages[319]. The proinflammatory roles of peroxisomes in this study are thought to be mediated by the turnover of ROS and production of reactive nitrogen species (RNS), as well as the production of lipids such as PtdIns(4,5)P_2 and docosahexaenoic acid (DHA)[319]. Therefore, as these seemingly conflicting

reports suggest, the roles of peroxisomes in innate immune responses are still unclear and controversial, probably due to the complex roles of peroxisomes in cell metabolism.

1.3.3. Conclusion: Organelles and innate immune responses

In summary, mitochondria and peroxisomes have emerged as the regulators of PRR signaling not only by providing the platforms for the adaptor protein oligomerization but also by metabolizing lipids and ROS that directly interact with these PRR pathways. In contrast to the recent advances in the understanding of the roles of mitochondrial metabolisms in innate immune responses, much less is known about those of peroxisomal metabolisms. Because the loss of peroxisomes and their metabolic functions lead to fatal disorders, it is possible that the dysfunction of these metabolisms results in the imbalanced inflammation in response to PAMPs or DAMPs. However, the immunoregulatory roles of peroxisomal FAO substrates, including VLCFAs and BCFAs, are largely unknown and therefore require further investigations.

Chapter 2: Three functionally distinct classes of cGAS proteins in nature revealed by self-DNA-induced interferon responses

Kenta Mosallanejad[1], Wen Zhou[2,3,6], Apurva A. Govande[2,3], Dustin C. Hancks[4], Philip J. Kranzusch[2,3,5], Jonathan C. Kagan[1]

[1]Division of Gastroenterology, Boston Children's Hospital, Harvard Medical School, 300 Longwood Avenue, Boston, MA 02115, USA.

[2]Department of Microbiology, Harvard Medical School, Boston, MA 02115, USA

[3]Department of Cancer Immunology and Virology, Dana-Farber Cancer Institute, Boston, MA 02115, USA

[4]Department of Immunology, University of Texas Southwestern Medical Center, Dallas, Texas, 75235 USA

[5]Parker Institute for Cancer Immunotherapy at Dana-Farber Cancer Institute, Boston, MA 02115, USA

[6]Present address: School of Life Sciences, Southern University of Science and Technology, Shenzhen, Guangdong 518055, China.

This chapter is adapted from:

Mosallanejad, K., Zhou, W., Govande, A. A., Hancks, D. C., Kranzusch, P. J., & Kagan, J.C. (2022). Three functionally distinct classes of cGAS proteins in nature revealed by self-DNA-induced interferon responses. *bioRxiv*, doi:10.1101/2022.03.09.483681.

Author Contribution

K.M. designed the study, performed experiments, and wrote the manuscript. W.Z. and A.A.G. performed *in vitro* cGAMP analysis under the supervision of P.J.K. J.C.K. conceived the idea, supervised the research, and wrote the manuscript. D.C.H. provided critical reagents that supported these studies. All authors discussed the results and commented on the manuscript.

2.1. Abstract

Innate immune pattern recognition receptors (PRRs) emerged early in evolution. It is generally assumed that structurally homologous proteins in distinct species will operate via similar mechanisms. We tested this prediction through the study of interferon responses to self-DNA by the enzymatic PRR cyclic GMP-AMP synthase (cGAS). Contrary to expectations, we identified three functional classes of this PRR in mammals. Class 1 proteins (including human) contained a catalytic domain that was intrinsically self-DNA reactive and stimulated interferon responses in diverse cell types. This reactivity was prevented by an upstream N-terminal domain. Class 2 and 3 proteins were either not self-DNA reactive (including chimpanzee) or included proteins whose N-terminal domain promoted self-DNA reactivity (mouse). While self-DNA reactivity of Class 1 cGAS was linked to an ability to access intra-mitochondrial DNA, mitochondrial localization was not associated with other classes. These studies reveal unexpected diversity in the mechanisms of self-DNA reactivity of a PRR.

2.2. Introduction

Mammalian cells are equipped with pattern recognition receptors (PRRs) that protect the host through their ability to detect molecular evidence of infection or tissue injury. Among these PRRs is the enzyme cyclic GMP-AMP synthase (cGAS), which synthesizes the second messenger 2′3′-cyclic GMP-AMP (cGAMP) upon binding to double-stranded DNA (dsDNA) in the cytosol [101,103]. As healthy and non-infected cells should not contain cytosolic DNA, the detection of DNA by cGAS is a high-fidelity indicator of infection or cellular dysfunction. cGAS stimulates

host defensive responses via the actions of the downstream cGAMP receptor STING (also known as MITA, MPYS, and ELIS). Upon binding cGAMP, STING traffics from the endoplasmic reticulum (ER) to the Golgi apparatus and oligomerizes into a scaffold that serves to activate the kinase tank-binding kinase 1 (TBK1) and the transcription factor IFN regulatory factor 3 (IRF3) [320]. IRF3 then coordinates the expression of numerous type I interferons (IFNs) and IFN-stimulated genes (ISGs) that promote inflammation and host defense. Although cGAS was initially discovered in the cytosol and therefore regarded as a cytosolic DNA sensor [101], recent studies have discovered cGAS in additional subcellular compartments such as the nucleus and the plasma membrane [197,199-201,204]. While nuclear cGAS is tightly regulated by proteins in this organelle to prevent chromosomal DNA-induced inflammation [202,205-209], DNA in the cytosol binds cGAS and induces conformational changes that drive cGAMP-mediated IFN responses [191]. Diverse sources of DNA can activate cGAS, including those from infectious agents and host-derived nuclear and mitochondrial DNA (mtDNA) that have reached the cytosol [155,174,184]. With the exception of subtle difference in the length of DNA detected [192,194,321], it is thought that the studies of human cGAS reflect the function of this protein in other mammalian species. However, the symmetry of cGAS functions in nature have largely been explored *in vitro*, where cGAS access to DNA is not an experimental variable. Based on the common *in vitro* behaviors of cGAS, it is somewhat surprising that disparate findings have been made regarding the activities of cGAS within cells—even when studying human cGAS exclusively [195,199,200,322].

Human cGAS is a 522 amino acid protein consisting of a basic, unstructured N-terminal domain (1–159 a.a.), and a C-terminal domain (160–522 a.a.) that possesses DNA binding and nucleotidyltransferase (NTase) activities[101]. Although the N-terminal domain was initially regarded as dispensable for DNA binding and IFN induction[101], recent studies have rather reported that the N-terminal domain is required for cGAS functions. For example, several reports indicate that within cells, deletion of the N-terminus of cGAS renders this protein inactive and defective for DNA-induced IFN responses [195,199,322]. However, our group found that the deletion of the N-

terminus of cGAS leads to IFN responses to self-DNA [200]. The reason for these disparate datasets is unclear and was explored in detail herein.

In this study, we develop a small molecule activatable genetic system of cGAS-induced self-DNA reactivity. Using this system, we found that the N-terminus of human cGAS prevents the catalytic domain from inducing type I IFN responses against self-DNA in human and mouse cells. We explain previously disparate results on this topic, based on the use of epitope tags that obstruct self-DNA reactivity, and identify amino acids within human cGAS that determine these responses. Evolutionary analysis of self-DNA reactivity revealed three functionally distinct classes of cGAS proteins in nature, with notable differences in self-DNA reactivity being observed in Class 1 (which includes human), Class 2 (mouse), and Class 3 (which includes chimpanzee) cGAS. Leveraging the mechanisms of Class 1 cGAS self-DNA reactivity, we redesigned this PRR to operate as an IFN-inducing sensor of the viral protease activity that is functionally analogous to the naturally occurring guard protein NLRP1 [323-326]. These findings reveal unexpectedly diverse functions of a single PRR in nature, and a means to use synthetic biology to redesign PRR activities in a user-defined manner.

2.3. Materials and Methods

2.3.1. Study design

The aim of this study was to investigate the self-DNA reactivity of cGAS and its domains in human and other mammals. We investigated the activities of these cGAS and mutants using doxycycline-mediated transient expression system in mouse and human macrophages. Sample sizes for each experiment are indicated in the figure legends.

2.3.2. Cell culture

Immortalized bone marrow-derived macrophages (iBMDMs), HEK293Ts, and Plat-GP cells were cultured in DMEM (Gibco) supplemented with 10% FBS (Gibco), referred to as complete DMEM, at 37ºC in 5% CO_2. For passage, iBMDMs were lifted using PBS (Gibco) supplemented with 2.5 mM EDTA (Invitrogen) and plated at dilution 1:10. HEK293T and L929

cells were grown under the same conditions as iBMDMs but were passaged by washing with PBS and lifting with 0.25% Trypsin-EDTA (Gibco) with a 1:10 dilution. THP-1 cells were grown in suspension culture using RPMI-1640 media (Lonza) supplemented with 10% FBS, referred to as complete RPMI-1640, at 37°C in 5% CO_2. For passage, cells were split at a dilution of 1:5. For experiments examining the effects of PMA-induced differentiation of THP-1 cell lines, cells were treated for the 72 hours with PMA (MilliporeSigma) at a concentration of 50 ng/mL. Normal oral keratinocytes were cultured in keratinocyte SFM (Gibco) supplemented with Human Keratinocyte Growth Supplement (Gibco) and passaged by washing with PBS and lifting with 0.25% Trypsin-EDTA with a 1:10 dilution.

2.3.3. Generating cells with stable or doxycycline-inducible gene expression

cDNAs of wild type and truncation mutant cGAS were amplified by polymerase chain reaction (PCR) using oligonucleotide primers containing restriction enzyme digestion sites. For the amplification of non-human primate (NHP) cGAS, cDNAs in the pcDNA6 vector [327] were used as PCR templates. For Dox-induced gene expression, cGAS cDNAs were inserted in the BamHI and NotI restriction sites in pRetroX-TRE3G (TakaraBio) using In-Fusion Snap Assembly Master Mix (TakaraBio). For stable gene expression, cGAS DNAs were inserted in pLenti-CMV-GFP-Puro in replacement of GFP using XbaI and SalI. For fusion mutants and the T2A insertion mutant of cGAS cDNAs, In-Fusion Snap Assembly Master Mix was used to incorporate cGAS and the other PCR fragments together in the vectors. For CRISPR/Cas9-mediated gene knockout, the sense and antisense oligonucleotides containing guide RNA (gRNA) sequences and AfeI/SbfI restriction sites were purchased from Integrated DNA Technologies, and the equal molar ratios of sense and antisense oligonucleotides were annealed in water on PCR block (95ºC for 1 minute, then drop 5°C every minute to 10°C). Oligonucleotide duplexes were then subcloned into AfeI/SbfI-digested pRRL-Cas9-Puro vector (kindly provided by Dr. D. Stetson) using In-Fusion Snap Assembly Master Mix (TakaraBio). gRNAs targeting mouse genes used in this study are as follows: *Cgas* #1: GAGGCGCGGAAAGTCGTAAG, *Cgas* #2: GGCAGCCCAGAGCGCCGCGA,

Sting #1: GGCCAGCCTGATGATCCTTT, *Sting* #2: GCTGGCCACCAGAAAGATGA. All constructs generated here were sequence-confirmed by Sanger sequencing.

To generate lentiviral particles for the stable expression of transgenes, HEK293T cells were transfected with the packaging plasmids psPAX2 and pCMV-VSV-G along with the transgene in pLenti-CMV-GFP-Puro or gRNAs-containing pRRL-Cas9-Puro vector using Lipofectamine 2000 (Invitrogen). pCMV-VSV-G was a gift from Bob Weinberg (Addgene plasmid # 8454 ; http://n2t.net/addgene:8454 ; RRID:Addgene_8454) [328]. psPAX2 was a gift from Didier Trono (Addgene plasmid # 12260; http://n2t.net/addgene:12260; RRID: Addgene_12260). pLenti CMV GFP Puro (658-5) was a gift from Eric Campeau & Paul Kaufman (Addgene plasmid # 17448; http://n2t.net/addgene:17448; RRID: Addgene 17448) [329]. All genes of interest were subcloned into the GFP site. Plasmids were transfected into 10 cm^2 dishes of HEK293Ts at 50–80% confluency using Lipofectamine 2000 by mixing DNA and Lipofectamine 2000 ratio at 1:2. Media was changed on transfected HEK293Ts 16–24 hours after transfection, and virus-containing supernatants were harvested 24 hours following the media change. Viral supernatants were passed through a 0.45 μm filter to remove any cellular debris. Filtered viral supernatants were mixed with 5 μg/mL polybrene (MilliporeSigma) and placed directly onto target cells, followed by the spinfection (centrifugation at 1,250 × g, 30°C for 1 hour). Cell culture media were replaced with the appropriate complete media and cells were incubated for 24 hours. Spinfection with the viral supernatants was repeated on the following day, and cells were used for indicated assays.

Doxycycline (Dox)-inducible gene-expressing cell lines were generated using Retro-X™ Tet-On 3G Inducible Expression System (Takara Bio). Plat-GP cells were transfected with the pRetroX-Tet3G plasmid together with the packaging plasmid pCMV-VSV-G using Lipofectamine 2000. Using viral supernatant of Plat-GP cells, iBMDMs or THP-1 cells were subjected to spinfection in a similar manner as above. After consecutive spinfections for two days, Tet3G-transduced cells were selected using G418 (Invivogen) and single cell clones were isolated. Tet3G-containing cell clones were transduced with TRE3G virus prepared from Plat-GP cells

transfected with pRetroX-TRE3G containing genes of interest and packaging plasmid pCMV-VSV-G. TRE3G-transduced cells were selected using puromycin (Gibco) and pooled cell culture was used in each assay. Cells were treated with 1 μg/mL Dox (MilliporeSigma) were subjected to each analysis at the indicated time points in each figure legend.

2.3.4. Real-Time quantitative reverse transcription (qRT-) PCR

RNA was isolated from cells using Qiashredder (QIAGEN) homogenizers and the PureLink Mini RNA Kit (Life Technologies) and treated with subsequently DNase I (Invitrogen) to remove genomic DNA. Relative mRNA expression was analyzed using the TaqMan RNA-to-Ct 1-Step Kit (Thermo Fisher Scientific) with indicated Taqman probes (Thermo Fisher Scientific) on a CFX384 Real-Time Cycler (Bio-Rad Laboratories). Each C_T value was normalized with the mRNA expression of the control genes (RPS18 for human and Rps18 for human) and the relative mRNA abundance was calculated by the $\Delta\Delta C_T$ method. Taqman probes used in this study are as follows: *Ifnb* (mouse): Mm00439552_s1, *Rsad2* (mouse): Mm00491265_m1, *Rps18* (mouse): Mm02601777_g1, *IFNB* (human): Hs01077958_s1, *RSAD2* (human): Hs00369813_m1, *RPS18* (human): Hs01375212_g1.

2.3.5. Cell viability assay

Cell viability was measured using CellTiter-Glo (Promega Corporation), a luminescent assay for ATP in living cells. Untreated cells were used as a positive control for 100% cell viability and subjected to serial dilution for the standard curve. Luminescent outputs were read on a Tecan plate reader and viability was calculated using the standard curve.

2.3.6. Subcellular fractionation and membrane flotation assay

Cells were washed once with PBS and then washed with hypotonic buffer (10 mM Tris-HCl pH 7.4, 10 mM KCl, and 1.5 mM $MgCl_2$) supplemented with a protease inhibitor cocktail (Roche) and 10 U/mL Benzonase (MilliporeSigma). After wash, cells were incubated in hypotonic buffer on ice for 30 minutes, and then lysed by 7 strokes of Dounce homogenization. Lysates

were centrifuged at 4°C for 5 minutes at 2,500 × g to remove nuclei and cellular debris. This nuclear pellet was then washed three times in hypotonic buffer supplemented with 0.3% IPEGAL (MilliporeSigma) to remove any contaminating organelles and obtain the nuclear fraction (P2.5). Supernatants were centrifuged at 16,000 × g for 10 minutes to separate pellets (P16) containing membrane fractions and supernatants. While washing P16 pellets three times with hypotonic buffer, these supernatants were further centrifuged at 100,000 × g for 1 hour at 4°C. The resultant pellets (P100) were resuspended in RIPA buffer (50 mM Tris-HCl, pH7.5, 150 mM NaCl, 1% TritonX-100, 0.5% Sodium Deoxycholate, 0.1% sodium dodecyl sulfate (SDS), which was supplemented with Benzonase and cOmplete, Mini, EDTA-free Protease Inhibitor Cocktail [Roche] before use). Each fraction was analyzed by immunoblotting as described below.

For membrane flotation assay, post-nuclear supernatants (PNS) were obtained in the aforementioned method and mixed with Optiprep™-supplemented hypotonic buffer to yield a final concentration of 45% Optiprep. These PNS were placed at the bottom and overlaid by a step gradient of Optiprep ranging from 10% (top) to 45% (bottom), and then centrifuged at 100,000 × g for 90 minutes. Gradient was then equally divided to fractions and analyzed by immunoblotting. For cell-free analysis of recombinant cGAS protein, 400 nM cGAS protein obtained (as described in section 2.3.8.) was incubated with 400 nM of 100 bp interferon stimulatory DNA (ISD) in hypotonic buffer for 15 minutes in the room temperature, and then subjected to flotation assay in the presence or absence of 1% TritonX-100, 2% SDS, 10 U/mL Benzonase, or 0.75 M sodium chloride (NaCl). ISD duplex was prepared by annealing the equal molar ratios of sense and antisense oligonucleotides[195] in water on PCR block (95ºC for 1 minute, then drop 5°C every minute to 10°C).

2.3.7. Immunoblotting and ELISA analysis

Cells were lysed with RIPA buffer and the lysates were centrifuged at 4°C, 16,000 × g for 10 minutes. Supernatants were mixed with 6 × SDS sample buffer supplemented with Tris(2-carboxyethyl)phosphine hydrochloride (TCEP, Thermo Fisher Scientific) and boiled at 100°C for

5 minutes. Samples were separated by SDS-PAGE and transcribed to PVDF membrane by Immunoblotting. PVDF was blocked with 5% skim milk for 1 hour and probed with indicated primary antibodies over night at 4°C, followed by secondary antibodies (1:2000 dilution) for 1 hour. Primary antibodies used in this study include viperin (1:1000 dilution, MilliporeSigma), FLAG (1:1000 dilution, MilliporeSigma), HA (1:1000 dilution, MilliporeSigma), β-Actin (1:1000 dilution, Cell Signaling Technology), cGAS (1:1000 dilution, MilliporeSigma for cGASΔN and Cell Signaling Technologies for cGAS N detection), phospho-STING (Ser365) (1:200 dilution, Cell Signaling Technology), STING (1:1000 dilution, Cell Signaling Technology), and NS3 (1:1000, GeneTex). Secondary antibodies for human, mouse, and rat immunoglobulins (IgGs) were purchased from Rockland Immunochemicals. Culture supernatant from treated cells were collected and applied to the IP-10 antibody-coated plate for ELISA analysis (R&D Systems) following the manufacture's instruction.

2.3.8. *In vitro* 2′3′-cGAMP assay

FL cGAS and cGASΔN recombinant proteins were prepared as previously described [194,330]. Briefly, cGAS mutants were cloned into a custom pET vector for expression of an N-terminal 6 x His-SUMO2 fusion protein in *E. coli*. *E. coli* BL21-RIL DE3 (Agilent) bacteria harboring a pRARE2 tRNA plasmid were transformed with a pET cGAS plasmid, and 6 × His-SUMO2-cGAS recombinant proteins were purified from clarified *E. coli* lysate by binding to Ni-NTA (QIAGEN) and gravity chromatography. The His-SUMO2 tags were removed by dialyzed overnight at 4°C in dialysis buffer (20 mM HEPES-KOH pH 7.5, 300 mM NaCl, 1 mM DTT) after supplementing ~250 μg of human SENP2 protease (fragment D364–L589 with M497A mutation).

Nucleosomal DNA was isolated from untreated iBMDMs using EpiScope Nucleosome Preparation Kit (TakaraBio) and the counterpart naked double-stranded DNA (dsDNA) was obtained by removing histones using Proteinase K following manufacture's instruction.

cGAS activation and cGAMP synthesis was performed *in vitro* using purified components and measured with thin-layer chromatography as previously described [330]. Briefly, 5 μM cGAS

recombinant proteins were incubated with the DNA above or 45 bp interferon stimulatory DNA (ISD) [331] in a reaction buffer containing 10 mM Tris-HCl pH 7.5, 62.5 mM KCl, 10 mM $MgCl_2$, 1 mM DTT, 6.25 μM ATP, 6.25 μM GTP, and [α-^{32}P] ATP (~1 μCi) at 37ºC for 2 hours. Reactions were terminated by heating at 95ºC for 3 min, and subsequently incubated with 4 U of alkaline phosphatase (New England Biolabs) at 37ºC for 30 min to hydrolyze unreacted NTPs. 1 μL of each reaction was spotted on a PEI-Cellulose F thin-layer chromatography plate (EMD Biosciences) developed with 1.5 M KH_2PO_4 (pH 3.8) as a running buffer.

2.3.9. Live imaging confocal microscopy

GFP-tagged cGAS-expressing iBMDMs were plated on uncoated 35 mm dishes (MatTek Corporation). Cells were treated with MitoTracker Deep Red (Invitrogen) in Opti-MEM (Gibco) and incubated at 37°C, 5% CO_2 for 60 minutes. Cells were washed with PBS and imaged using a 63× oil immersion objective on the LSM 880 with Airyscan (Zeiss). Images were processed using ZEN software (Zeiss) and ImageJ (NIH). Dox-untreated cells or non-GFP-expressing cells were used for the negative controls of GFP signaling, and negative signals were subtracted from GFP signals of cGAS. For counting, at least 100 cGAS-expressing cells were examined under the microscope and the percentile of nuclear, cytosolic, or mitochondrial cGAS-expressing cells was determined.

2.3.10. Quantification and statistical analysis

Statistical significance was determined by two-way analysis of variance (ANOVA) with Tukey's multiple comparison test. $P < 0.05$ was seen as statistically significant. All statistical analyses were performed using GraphPad Prism data analysis software. All experiments were performed at least three times, and the graph data with error bars indicate the means with the standard error of the mean (SEM) of all repeated experiments.

2.4. Results

2.4.1. Human cGASΔN induces type I IFN responses to self-DNA in human and mouse cells

The functions of the C-terminal DNA binding and catalytic domain of cGAS within cells are debatable. We have reported that within THP-1 monocytes, a human cGAS mutant lacking its N-terminal domain (hcGAS 160–522 a.a., hereafter hcGASΔN) promotes type I IFN expression in the absence of exogenous dsDNA treatment [200], whereas others have concluded that hcGASΔN is functionally defective within cells [195,199]. Our prior work relied on the stable expression of hcGASΔN, which drives IFN responses constitutively and may cause aberrant cellular behaviors. To bypass this concern, we devised a distinct genetic system that enables inducible kinetic analysis of cGAS activities. We established a doxycycline (Dox)-inducible expression system for hcGAS full-length (FL) and hcGASΔN in immortalized bone marrow-derived macrophages (iBMDMs). Using this system, we found that Dox-mediated hcGASΔN expression induced the rapid expression of the gene *Ifnb*, which encodes IFN-β (Figure 2.1A). In contrast, Dox-induced FL hcGAS expression did not trigger *Ifnb* expression (Figure 2.1A). Near-coincident with *Ifnb* expression was the induced transcription of mRNA encoded by the ISG *Rsad2* (radical SAM domain-containing 2) and its product viperin (virus inhibitory protein, endoplasmic reticulum-associated, interferon-inducible) (Figure 2.1B and C). Interferon-γ-inducible protein 10 (IP-10), another ISG, was also induced by hcGASΔN (Figure 2.1D). The IFN-stimulatory activities of hcGASΔN occurred despite its lower abundance than FL hcGAS within cells (Figure 2.1C).

To validate our results, we applied our Dox-inducible system to THP-1 monocytes. Dox treatment of THP-1 cells containing the hcGASΔN transgene led to the induction of *IFNB* and *RSAD2* mRNAs, whereas cells containing the FL cGAS were poorly immunostimulatory after Dox treatment (Figure 2.1E and F). Previously, we found that the treatment of THP-1 cells with phorbol 12-myristate 13-acetate (PMA) potentiated hcGASΔN induced *IFNB* mRNA expression and ultimately caused cell death [200]. In our Dox system, we observed that PMA enhanced the IFN-

inducing ability of hcGASΔN (Figure 2.1G-I), with IP-10 production by hcGASΔN increasing over 70-fold after PMA+Dox treatment, as compared to Dox alone (Figure 2.1I). This increase in IFN stimulatory activity by PMA correlated with lethality, specifically in cells expressing hcGASΔN (Figure 2.1J). The weak immunostimulatory activities of FL cGAS-expressing cells were marginally affected by PMA treatment (Figure 2.1G-I). Finally, we applied the same system to normal oral keratinocytes. As a result, keratinocytes treated with Dox induced the expression of *IFNB* and *RSAD2* mRNAs followed by viperin and IP-10 production (Figure S1A-D). Overall, these studies in diverse mouse and human cell types indicate that hcGASΔN triggers type I IFNs that are not induced by FL cGAS.

To determine if hcGASΔN requires DNA binding to induce IFN responses upon expression, we inserted alanine substitutions (C366A/C367A) in hcGAS that abolish DNA binding [102]. Dox-mediated expression of hcGASΔN C366A/C367A did not induce viperin expression in iBMDMs (Figure 2.1K). These data indicate that the C-terminal catalytic domain of cGAS is intrinsically self-DNA reactive, and that this activity is prevented by its upstream N-terminal domain. Because DNA-bound cGAS induces IFN responses through STING activation, we examined the activation and requirement for STING in cGASΔN-induced response. As a result, Dox-induced expression of hcGASΔN led to the phosphorylation of STING at S365 (S366 in human)[116,117] and STING degradation[133], which are the hallmark readouts of STING activation (Figure S1E). Further genetic analysis revealed that hcGASΔN did not induce *Rsad2* mRNA or viperin in *Sting*$^{-/-}$ iBMDMs (Figure 2.1L, Figure S1F), indicating that, as expected, STING is required for hcGASΔN signaling. In contrast, iBMDMs derived from *Cgas*$^{-/-}$ mice induced comparable amounts of *Rsad2* mRNA and viperin protein (Figure 2.1L, Figure S1F), indicating that endogenous cGAS is not required for hcGASΔN-mediated signaling. These roles of endogenous cGAS and STING in hcGASΔN-induced IFN expression were confirmed using knockout (KO) cells generated by CRISPR-Cas9 gene editing (Figure S1G-I). Altogether, these data indicated that the N-terminal deletion of human cGAS triggers self-DNA-induced type I IFN responses in a STING-dependent manner.

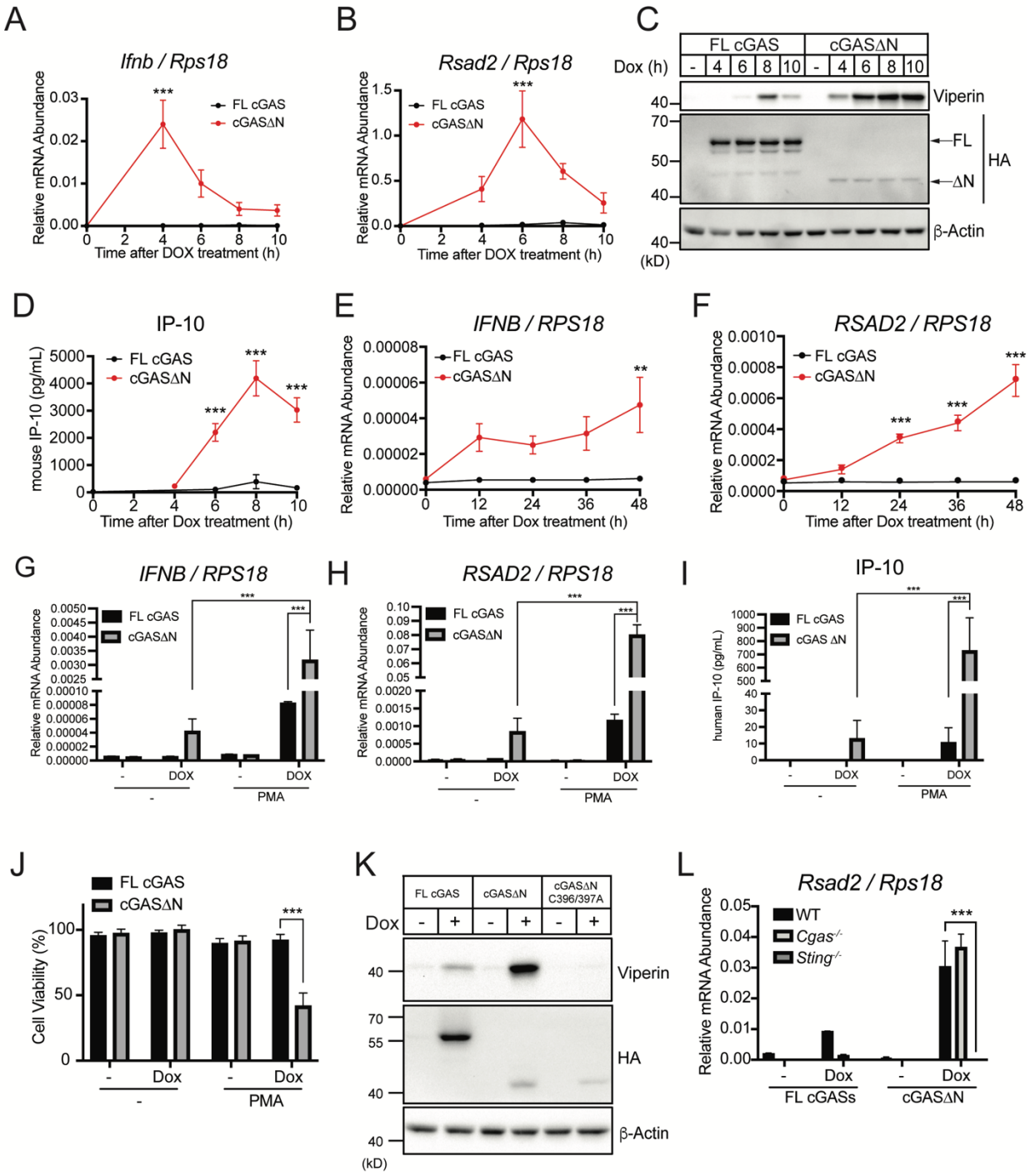
A
Ifnb / Rps18
Relative mRNA Abundance
FL cGAS
cGASΔN
Time after DOX treatment (h)
B
Rsad2 / Rps18
Relative mRNA Abundance
FL cGAS
cGASΔN
Time after DOX treatment (h)
C
FL cGAS
cGASΔN
Dox (h)
- 4 6 8 10 - 4 6 8 10
Viperin
FL
ΔN
HA
β-Actin
(kD)
D
IP-10
mouse IP-10 (pg/mL)
FL cGAS
cGASΔN
Time after Dox treatment (h)
E
IFNB / RPS18
Relative mRNA Abundance
FL cGAS
cGASΔN
Time after Dox treatment (h)
F
RSAD2 / RPS18
Relative mRNA Abundance
FL cGAS
cGASΔN
Time after Dox treatment (h)
G
IFNB / RPS18
Relative mRNA Abundance
FL cGAS
cGASΔN
DOX
PMA
H
RSAD2 / RPS18
Relative mRNA Abundance
FL cGAS
cGASΔN
DOX
PMA
I
IP-10
human IP-10 (pg/mL)
FL cGAS
cGAS ΔN
DOX
PMA
J
FL cGAS
cGASΔN
Cell Viability (%)
Dox
PMA
K
FL cGAS
cGASΔN
cGASΔN C396/397A
Dox
Viperin
HA
β-Actin
(kD)
L
Rsad2 / Rps18
Relative mRNA Abundance
WT
Cgas-/-
Sting-/-
Dox
FL cGASs
cGASΔN

Figure 2.1. Human cGASΔN induces aberrant type I IFN responses

(A and B) Real-time quantitative reverse transcription (qRT-) PCR analysis of *Ifnb* (A) and *Rsad2* (B) mRNAs in iBMDMs. Dox was treated to cells for the induction of FL human cGAS or human cGASΔN, and mRNA expression levels were analyzed at the indicated time points. (C) Immunoblot analysis of iBMDM lysates after the same treatment as in (A) and (B). Arrows in the HA panel indicate FL human cGAS and human cGASΔN. (D) IP-10 ELISA analysis of iBMDM cell culture supernatant of the cells in (A) and (B). (E and F) Real-time qRT-PCR analysis of *IFNB* (E) and *RSAD2* (F) mRNAs in THP-1 monocytes treated with Dox for indicated time points to induce FL human cGAS or human cGASΔN. (G and H) Real-Time qRT-PCR analysis of *IFNB* and *RSAD2* mRNAs in THP-1 monocytes treated with Dox together with PMA for 48 hours. (I) IP-10 ELISA analysis of THP-1 cell culture supernatant in (G and H). (J) Cell viability analysis of THP-1 cells treated as in (G) and (H). (K) Immunoblot analysis of lysates from iBMDMs treated with Dox for 8 hours to express FL hcGAS, hcGASΔN, or hcGASΔN with DNA-binding mutation (cGASΔN C396A/397A). (L) Real-Time qRT-PCR analysis of *Rsad2* mRNA in WT, *Cgas*$^{-/-}$, or *Sting*$^{-/-}$ iBMDMs treated with Dox for 8 hours to induce expression of FL human cGAS or human cGASΔN. Immunoblot data are the representative from three independent experiments. Graph data are means ± SEM of three (A, B, D, G, H, I, J, and L) or four (E and F) independent experiments. Statistical significance was determined by two-way ANOVA and Tukey's multicomparison test. Asterisks indicate the statistical significance between FL hcGAS and hcGASΔN at each time point (A, B, D, E, and F) or connected two bars (G, H, I, J, and L). **P* < 0.05; ***P* < 0.01; ****P* < 0.001.

2.4.2. Specific amino acids at the N-terminus of hcGASΔN determine self-DNA reactivity

Whereas our data have confirmed that hcGASΔN induces aberrant type I IFN responses, other studies have concluded that N-terminal deletion mutants of cGAS do not elicit IFN expression, even in the presence of exogenous dsDNA[195,199,322]. To understand these discrepancies, we noticed that each study has employed different epitope tag positions on their

respective hcGASΔN constructs. We have used C-terminally tagged hcGASΔN constructs[200], while others have used N-terminally tagged alleles[195,199,322]. Therefore, we hypothesized that the different tag positions led to the disparate results regarding hcGASΔN signaling activities. To test this hypothesis, we engineered iBMDMs to express N-terminally or C-terminally hemagglutinin (HA)-tagged hcGASΔN, as well as tag-free hcGASΔN in a Dox-dependent manner. While tag-free hcGASΔN and hcGASΔN-HA induced *Ifnb* mRNA transcripts and ISG expression, HA-hcGASΔN did not induce those responses (Figure 2.2A-D). To validate these results, we compared N-terminal or C-terminal green fluorescence protein (GFP)-tagged constructs and found that hcGASΔN-GFP but not GFP-hcGASΔN induced viperin expression (Figure 2.2E). Moreover, the addition of an N-terminal FLAG tag to an otherwise active allele (hcGASΔN-HA) inhibited the type I IFN responses induced by this protein (Figure 2.2F, G). These results therefore explain reported differences in cGAS function, as the position of the epitope tag determines self-DNA reactivity.

To further understand the effect of N-terminal tags on hcGASΔN activity, we generated differently truncated hcGAS-HA constructs and expressed each in a Dox-inducible manner in iBMDMs. Among all the hcGAS constructs tested, only hcGASΔN (160–522 a.a.) and hcGAS 158–522 a.a. induced *Ifnb* and *Rsad2* mRNAs, and viperin protein production (Figure 2.2H-J). Addition of 4 or more amino acids to the N-terminus of hcGASΔN abolished all signaling activities of this protein. These results indicate that hcGASΔN contains a precise requirement for the N-terminal amino acids for IFN responses to self-DNA.

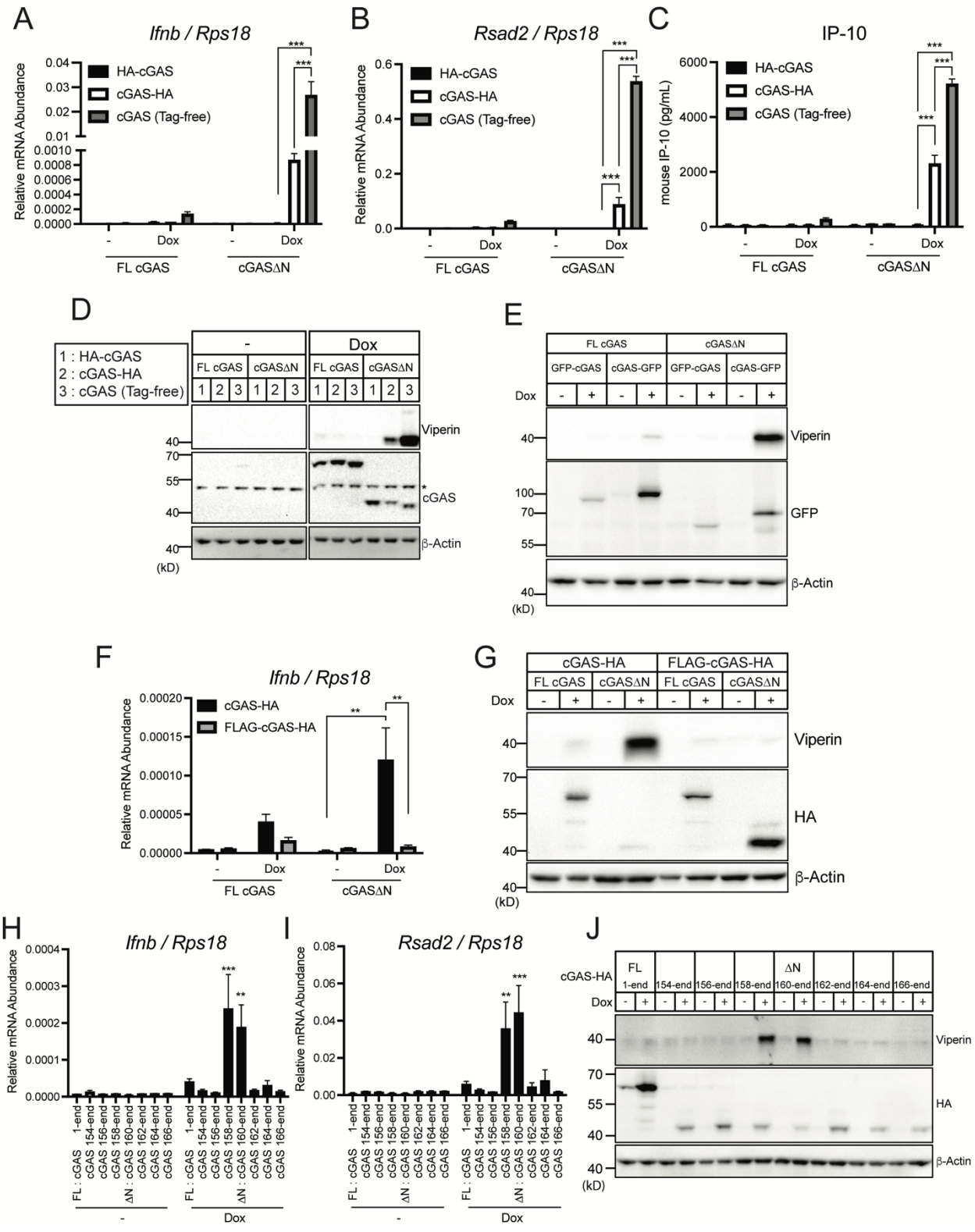
A
Ifnb / Rps18
Relative mRNA Abundance
HA-cGAS
cGAS-HA
cGAS (Tag-free)
Dox
FL cGAS
cGASΔN
B
Rsad2 / Rps18
C
IP-10
mouse IP-10 (pg/mL)
D
1 : HA-cGAS
2 : cGAS-HA
3 : cGAS (Tag-free)
Viperin
cGAS
β-Actin
(kD)
E
GFP-cGAS
cGAS-GFP
GFP
F
FLAG-cGAS-HA
G
Viperin
HA
β-Actin
H
I
J
cGAS-HA
1-end
154-end
156-end
158-end
160-end
162-end
164-end
166-end
Viperin
HA
β-Actin

Figure 2.2. Specific amino acids at the N-terminus of hcGASΔN determines self-DNA reactivity

(A and B) Real-Time qRT-PCR analysis of *Ifnb* (A) and *Rsad2* (B) mRNAs in iBMDMs treated with Dox for 8 hours to induce expression of N-terminally HA-tagged hcGAS (HA-cGAS), C-terminally HA-tagged hcGAS (cGAS-HA), or hcGAS with no tags (Tag-free). (C) IP-10 ELISA analysis of iBMDM cell culture supernatant in (A) and (B). (D) Immunoblot analysis of iBMDMs treated with Dox as in (A) and (B). The asterisk indicates non-specific bands. (E) Immunoblot analysis of iBMDMs treated with Dox for 8 hours to induce expression of N-terminally GFP-tagged hcGAS (GFP-cGAS) or C-terminally GFP-tagged hcGAS (cGAS-GFP). (F) Real-Time qRT-PCR analysis of *Ifnb* mRNAs in iBMDMs treated with Dox for 8 hours to induce expression of hcGAS-HA or N-terminally FLAG-tagged hcGAS-HA (FLAG-hcGAS -HA). (G) Immunoblot analysis of iBMDMs treated with Dox as in (F). (H and I) Real-Time qRT-PCR analysis of *Ifnb* (H) and *Rsad2* (I) mRNAs in iBMDMs treated with Dox for 8 hours to induce expression of differently truncated hcGAS. (J) Immunoblot analysis of lysates of iBMDMs treated as in (H) and (I). Immunoblot data are the representative from three independent experiments. Graph data are means ± SEM of three (A, B, and F) or five (C, H, and I) independent experiments. Statistical significance was determined by two-way ANOVA and Tukey's multicomparison test. Asterisks indicate the statistical significance between connected two bars (A, B, C, and F) or between untreated and Dox-treated conditions for indicated hcGAS mutants (H and I). $*P < 0.05$; $**P < 0.01$; $***P < 0.001$.

2.4.3. Species-specific self-DNA reactivity by mammalian cGAS proteins

The C-terminal catalytic domain of cGAS is highly conserved among mammalian species at the amino acid level, and the functional level *in vitro*[211,332]. We therefore hypothesized that the signaling activity of cGASΔN would be conserved throughout evolution. To assess whether cGASΔN signaling activity is conserved in mice, we expressed mouse cGAS (mcGAS) FL and ΔN in iBMDMs. Whereas some studies have used mcGAS (148–507 a.a.) as the ΔN mutant of mcGAS, other groups have used differently truncated versions[101,322]. Since mcGAS 145–507 a.a. is more similar to hcGASΔN, in terms of the N-terminal primary sequence (Figure 2.3A), we tested

both versions of mcGAS truncation mutants. Interestingly, both mcGASΔN versions were unresponsive to self-DNA upon Dox-mediated expression in iBMDMs, leading to no IFN activities upon Dox-induction (Figure 2.3B-D). FL mcGAS, in contrast, induced strong type I IFN responses upon expression via Dox (Figure 2.3B-D). Thus, in contrast to our findings with hcGAS and its ΔN counterpart, mouse FL cGAS is self-DNA-reactive whereas both versions of mouse ΔN are weakly immunostimulatory. These findings prompted a broader evolutionary analysis of self-DNA reactivity by FL cGAS and cGASΔN. We generated iBMDMs that encoded FL and cGASΔN proteins from several non-human primates (NHPs), including orangutan, marmoset, gibbon, chimpanzee, white-handed gibbon, crab-eating macaque, and rhesus macaque (Figure 2.3E), and assessed IFN responses upon Dox-induced transgene expression. Like the behaviors of the human proteins, no self-DNA responsiveness was observed for FL cGAS proteins from any NHP examined (Figure 2.3F, G), even though they responded to exogenous DNA delivered into the cytoplasm of cGAS-deficient cells (Figure S2A). Also similar to human, cGASΔN from orangutan, marmoset, and gibbon all induced *Ifnb* mRNA and viperin protein production, to an extent even greater than what was observed for hcGASΔN (Figure 2.3F, G and Figure S2B-E). In contrast, several other NHP cGASΔN proteins, including those from chimpanzee and crab-eating macaque did not trigger type I IFN responses upon expression in iBMDMs (Figure 2.3F, G and Figure S2B-E). Most activities observed in iBMDMs were also made in PMA-treated THP-1 cells. For example, hcGASΔN and FL mcGAS induced *IFNB* transcripts, while FL hcGAS and mcGASΔN did not (Figure 2.3H). Orangutan cGASΔN was also active in iBMDMs and THP-1 cells (Figure 2.3H, I). PMA-mediated potentiation of ISG expression and cell death was also induced in THP-1 cells expressing hcGASΔN, and orangutan cGASΔN, which expressed *IFNB* transcripts (Figure 2.3J and Figure S2F-I). However, marmoset and gibbon cGAS were only active in iBMDMs, not in THP-1 cells.

When taken together, we have identified three functional classes of the cGAS proteins in nature. Class 1 proteins restrict self-DNA reactivity by the N-terminal domain in human or mouse cells (or both), and include human, orangutan, gibbon, and marmoset. Class 2 proteins use the

N-terminus to promote IFN responses to self-DNA (mouse). Class 3 proteins do not display any self-DNA reactivity (chimpanzee, crab-eating macaque, white-handed gibbon, and rhesus macaque) (Figure 2.3K).

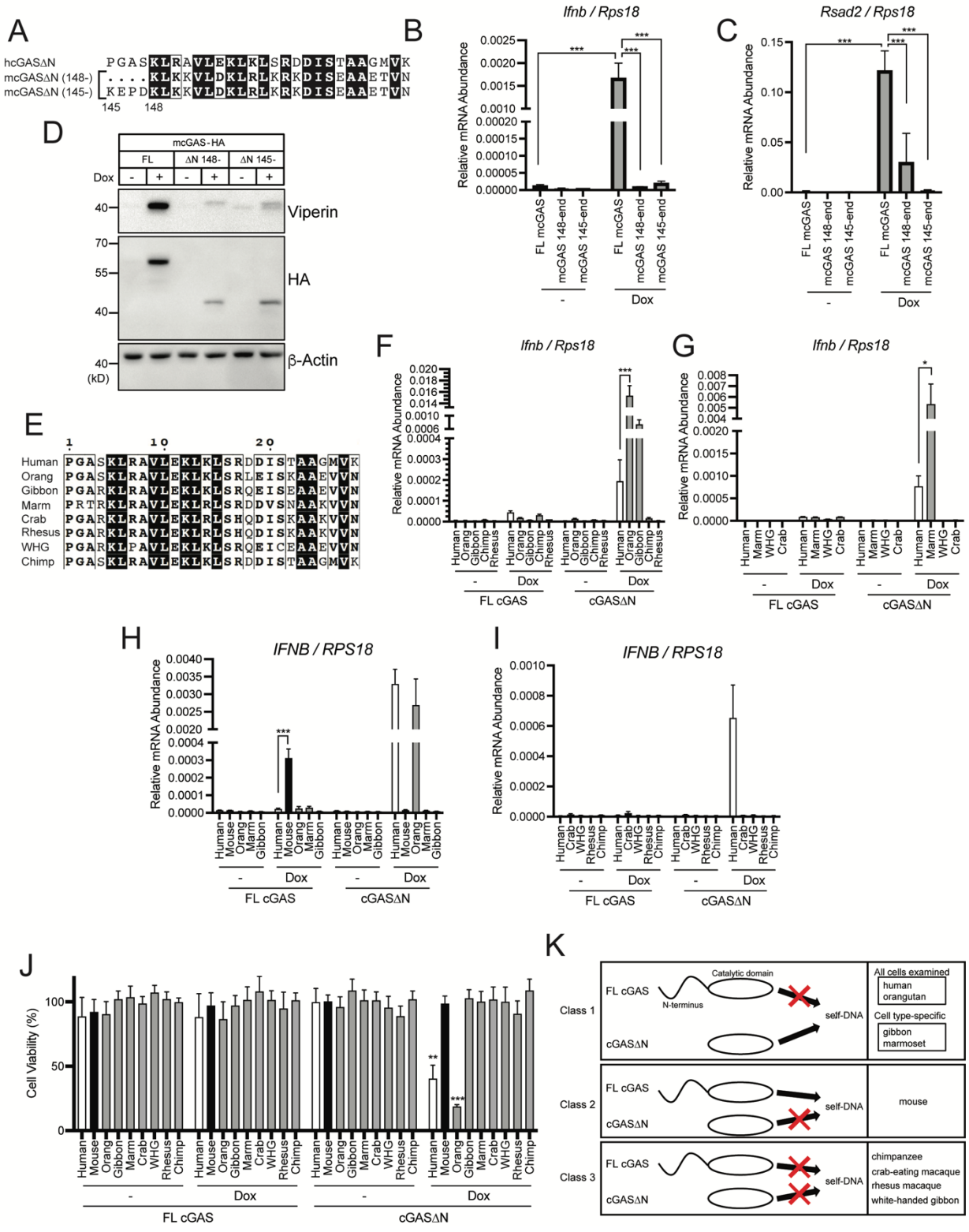
A
hcGASΔN PGASKLRAVLEKLKLSRDDISTAAGMVK
mcGASΔN (148-) ....KLKKVLDKLRLKRKDISEAAETVN
mcGASΔN (145-) KEPDKLKKVLDKLRLKRKDISEAAETVN
145 148
B
Ifnb / Rps18
Relative mRNA Abundance
FL mcGAS
mcGAS 148-end
mcGAS 145-end
Dox
C
Rsad2 / Rps18
D
mcGAS-HA
FL
ΔN 148-
ΔN 145-
Dox
Viperin
HA
β-Actin
(kD)
E
Human PGASKLRAVLEKLKLSRDDISTAAGMVK
Orang PGASKLRAVLEKLKLSRLEISKAAEVVN
Gibbon PGARKLRAVLEKLKLSRQEISEAAEVVN
Marm PRTRKLRAVLEKLRLSRDDVSNAAKVVN
Crab PGARKLRAVLEKLRLSHQDISKAAKVVN
Rhesus PGARKLRAVLEKLRLSHQDISKAAKVVN
WHG PGARKLPAVLEKLKLSRQEICEAAEVVN
Chimp PGASKLRAVLEKLKLSRDDISTAAGMVK
F
Ifnb / Rps18
FL cGAS
cGASΔN
G
Ifnb / Rps18
H
IFNB / RPS18
I
IFNB / RPS18
J
Cell Viability (%)
K
Class 1
Class 2
Class 3
FL cGAS
cGASΔN
Catalytic domain
N-terminus
self-DNA
All cells examined
human
orangutan
Cell type-specific
gibbon
marmoset
mouse
chimpanzee
crab-eating macaque
rhesus macaque
white-handed gibbon

Figure 2.3. cGASΔN activities are diverse in mammalian species

(A) N-terminal amino acid sequences of human cGASΔN, mouse cGAS 145-, and mouse cGAS 148-. (B and C) Real-Time qRT-PCR analysis of *Ifnb* (B) and *Rsad2* (C) mRNAs in iBMDMs treated with Dox for 8 hours to induce expression of indicated cGAS mutants. (D) Immunoblot analysis of iBMDM lysates treated as in (B) and (C). (E) N-terminal amino acid sequences of human cGASΔN and non-human primate (NHP) cGAS truncation mutants. Orang: orangutan, Marm: marmoset, Crab: crab-eating macaque, Rhesus: rhesus macaque, WHG: white-handed gibbon, Chimp: chimpanzee. (F and G) Real-Time qRT-PCR analysis of *Ifnb* (F) and *Rsad2* (G) mRNAs in iBMDMs treated with Dox for 8 hours to induce expression of indicated cGAS mutants. (H and I) Real-Time qRT-PCR analysis of *IFNB* (H) and *RSAD2* (I) mRNAs in THP-1 monocytes treated with PMA and Dox for 48 hours to induce expression of indicated cGAS mutants. (J) Cell Viability of THP-1 cells treated with PMA and Dox as in (H) and (I). (K) Model of three classes of cGAS in mammals. In Class 1 cGAS, the N-terminal domain (NTD) inhibits otherwise self-DNA-reactive catalytic domain. In Class 2 cGAS, the NTD promotes and is required for the reactivity to self-DNA. Class 3 cGAS does not react to self-DNA regardless of the presence of the NTD. Immunoblot data are the representative from three independent experiments. Graph data are means ± SEM of three independent experiments. Statistical significance was determined by two-way ANOVA and Tukey's multicomparison test. Asterisks indicate the statistical significance between connected two bars (B, C, F, G, and H) or between untreated and Dox-treated conditions for indicated cGAS (J). *$P < 0.05$; **$P < 0.01$; ***$P < 0.001$

2.4.4. Mitochondrial localization of Class 1 cGASΔN correlates with signaling activity

The different classes of cGAS proteins identified raise questions about the underlying mechanisms of these observations. We considered the possibility that each class of cGAS proteins may display intrinsic differences in DNA-induced cGAMP production. To address this possibility, we incubated recombinant cGAS with DNA *in vitro* and measured cGAMP synthesis. We examined Class 1 human and orangutan cGASΔN, Class 2 mouse FL cGAS, and Class 3

chimpanzee cGAS. The Class 1 and 2 proteins chosen were all active as IFN inducers within cells, whereas Class 3 chimpanzee cGAS was not (Figure 2.3F-I). We also included N-terminally FLAG-tagged hcGASΔN and mouse and chimpanzee cGASΔN, all of which were inactive at self-DNA-induced IFN expression within cells. Despite notable differences in self-DNA reactivity associated with each class of proteins within cells, all the cGAS proteins examined behaved similarly in these *in vitro* assays (Figure 2.4A). All cGAS proteins were able to synthesize cGAMP in response to synthetic dsDNA, but not to nucleosomal DNA that was isolated from iBMDMs (Figure 2.4A). Protease treatment of nucleosomes rendered the resulting DNA capable of stimulating cGAMP production by all classes of cGAS examined (Figure 2.4A). The inability of cGAS to produce cGAMP in response to nucleosomal DNA was reported for human cGAS [203-209], but our findings suggest that this inability extends across all three classes of cGAS we have examined. Therefore, the diversity in cGASΔN signaling activities is not due to protein intrinsic activities, but rather by cellular factors that regulate its activation.

We considered the possibility that access to intracellular DNA may underlie the phenotypes associated with each class of cGAS proteins. To test this idea, we examined the subcellular localization of cGAS. Previously, by biochemical analysis and immunofluorescence microscopy, we have reported that cGAS is localized on the plasma membrane through the association with PIP_2 in the lipid raft[200]. In the previous study, we centrifuged cell homogenates at 2,500 x g and 100,000 x g to obtain nuclear (P2.5) and membrane (P100) fractions, respectively[200]. In this procedure, we discovered cGAS co-sedimentation in the P100 fraction, which we regarded as the membrane fraction. However, by adding a single centrifugation step at 16,000 x g between these two centrifugations, we detected a membrane protein Na^+/K^+ ATPase in P16 rather than P100 fraction of THP-1 cells (Figure S3A) and iBMDMs (Figure S3B) which contained cGAS. Therefore, these data indicate that cGAS does not co-sediment with membrane proteins. Similarly, although cGAS migration from dense to light fractions in the membrane flotation assay using Optiprep density gradient led us to hypothesize the membrane localization

of cGAS in the previous report[200], we found that cGAS migrated to the different fractions from those of membrane proteins such as Na^+/K^+ ATPase and STING (Figure S3C and D). cGAS flotation was indeed resistant to the detergent TritonX-100 as we previously reported, and only sensitive to the strong detergent sodium dodecyl sulfate (SDS) (Figure S3E). However, although we therefore concluded in the past that cGAS associates with the lipid raft as a Triton-resistant structure, TIRAP, a PIP2-associated protein[12], did not float in the presence of TritionX-100, which contradicts to this conclusion. Altogether, these results indicate that cGAS is found in cytosolic insoluble fractions rather than membrane fractions in the biochemical analysis.

In this and our previous study, we added the endonuclease Benzonase in cell lysates during the biochemical analysis to exclude the effects of post-lysis DNA binding of cGAS on the results[200]. However, it is still possible that post-lysis binding of cGAS to the cellular structures that cannot be eliminated merely by Benzonase treatment led to cGAS detection in cytoplasmic insoluble fractions. To test whether any post-lysis binding of cGAS protein to the cellular structures is reflected on the membrane flotation assay, we added recombinant human cGAS protein to post-nuclear supernatant (PNS) of iBMDMs and performed the assay. As a result, surprisingly, the presence of cell homogenates allowed cGAS recombinant protein to migrate to the light fractions, to which endogenous mouse cGAS also migrated (Figure S3F). The flotation of recombinant cGAS protein was independent of endogenous cGAS protein, as the use of PNS from cGAS-deficient macrophages led to the same results (Figure S3G). Therefore, these results indicate that post-lysis binding of cGAS to cellular structures is reflected in the biochemical analysis, which prevents the biological interpretation of the results.

To understand which cellular structure induces the flotation of recombinant cGAS protein, we used recombinant cGAS N-terminal domain (cGAS N) and C-terminal domain (cGASΔN) instead of full-length protein. Intriguingly, while cGAS ΔN protein migrated to light density fractions, cGAS N did not (Figure S3H). Because cGASΔN contains DNA binding domain[101], we

hypothesized that binding of DNA that remains in PNS induces cGAS protein flotation. To test whether DNA induces recombinant cGAS protein flotation, we incubated cGAS protein and 100 bp interferon stimulatory DNA (ISD) and then performed the assay. As a result, the presence of ISD induced cGAS flotation even in the absence of PNS (Figure S3I). Moreover, this flotation of cGAS-DNA complex was resistant to 1% TritonX-100 but sensitive to 2% SDS (Figure S3J), which was consistent to the results in Figure S3E. cGAS has been reported to undergo phase separation to form liquid-like large oligomers with DNA, which is inhibited by the high concentration of sodium chloride (NaCl)[195]. To test whether cGAS-DNA complex that migrates to the light density fractions is liquid-like condensates, we incubated recombinant cGAS protein and ISD in the presence of high concentration of NaCl. As a result, NaCl prevented recombinant cGAS protein from floating even in the presence of ISD, suggesting that the cGAS-DNA complex harbors the property of liquid-like droplets (Figure S3K). Surprisingly, this cGAS-DNA oligomer was resistant to Benzonase even at the concentration that degrades free DNA (Figure S3L and M).

Therefore, these data altogether suggested that cGAS-DNA condensation formed after cell homogenization even in the presence of Benzonase is reflected in the biochemical analysis, which disturbs the understanding of subcellular localization of cGAS.

These results led us to study cGAS localization by live cell confocal imaging as an alternative approach. Live cell confocal imaging of C-terminally GFP-tagged hcGAS in iBMDMs revealed that hcGASΔN localized in the mitochondria, while FL hcGAS-GFP was distributed in either the cytosol or the nucleus (Figure 2.4B and C). Interestingly, when an N-terminal GFP or HA tag was placed onto hcGASΔN, mitochondrial localization was abolished (Figure 2.4D). Similarly, N-terminally tagging hcGASΔN abolished IFN activities, as described in Figure 2.2E. These findings are consistent with a recent study by Chen and colleagues in human cells [210]. We reasoned that if mitochondrial localization was important for hcGASΔN signaling, forcing its localization to distinct subcellular locations should prevent IFN activities. We therefore engineered

hcGASΔN to contain C-terminal membrane localization sequences that direct this protein to the outer mitochondrial membrane (OMM), the peroxisomes, or the ER. This was accomplished by appending onto hcGASΔN transmembrane domains from MAVS (OMM), Pex13 (peroxisomes) or VAMP2 (ER). When expressed via Dox in iBMDMs, none of the membrane-targeted hcGASΔN proteins induced type I IFN responses (Figure 2.4E-G). These data indicate that restricting hcGASΔN from access to mitochondria prevents self-DNA reactivity.

To determine if mitochondrial localization was also linked to self-DNA responses induced by other classes of cGAS in nature, we examined the localization of orangutan cGASΔN (Class 1) and FL mcGAS (Class 2), both of which are self-DNA reactive, and the inactive chimpanzee cGASΔN protein (Class 3). Like its human counterpart, orangutan cGASΔN localized to mitochondria, suggesting that IFN activities and mitochondrial localization are a common feature of class 1 cGAS proteins (Figure 2.4H). Interestingly, we found that mouse FL cGAS, which is self-DNA reactive, was not localized to mitochondria (Figure 2.4I and J) and chimpanzee cGASΔN, which is not self-DNA reactive, was localized to mitochondria (Figure 2.4K). Therefore, the correlation of mitochondrial localization and signaling activity of cGASΔN perfectly explains the activities of Class 1 cGAS proteins, but not those of Class 2 or 3. These results suggest that the regulation of self-DNA reactivity for each class of cGAS proteins may differ from each other.

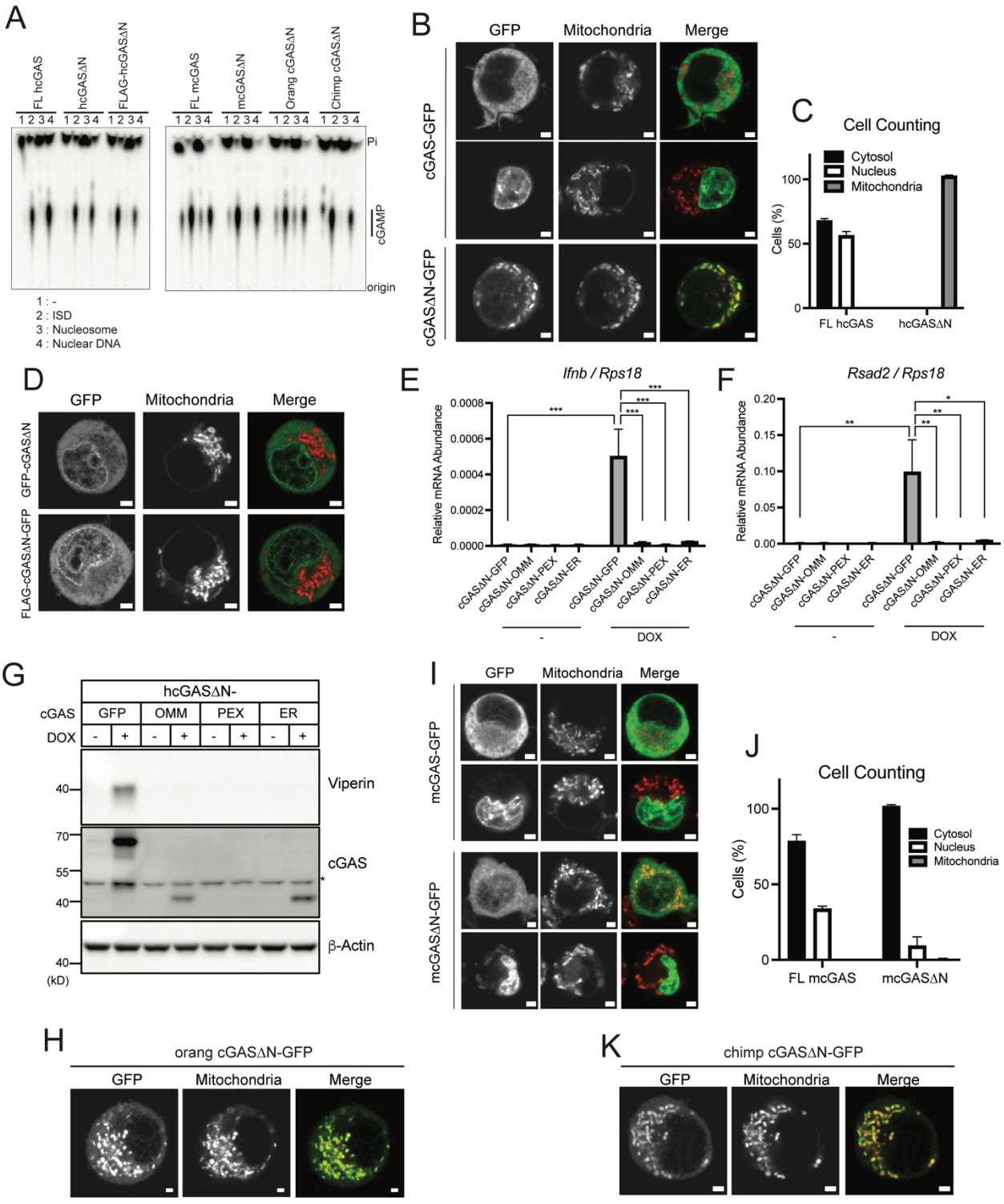
A
FL hcGAS
hcGASΔN
FLAG-hcGASΔN
FL mcGAS
mcGASΔN
Orang cGASΔN
Chimp cGASΔN
1 2 3 4
Pi
cGAMP
origin
1 : -
2 : ISD
3 : Nucleosome
4 : Nuclear DNA
B
GFP
Mitochondria
Merge
cGAS-GFP
cGASΔN-GFP
C
Cell Counting
Cytosol
Nucleus
Mitochondria
Cells (%)
FL hcGAS
hcGASΔN
D
GFP-cGASΔN
FLAG-cGASΔN-GFP
E
Ifnb / Rps18
Relative mRNA Abundance
cGASΔN-GFP
cGASΔN-OMM
cGASΔN-PEX
cGASΔN-ER
DOX
F
Rsad2 / Rps18
G
hcGASΔN-
cGAS
OMM
PEX
ER
DOX
Viperin
cGAS
β-Actin
(kD)
I
mcGAS-GFP
mcGASΔN-GFP
J
FL mcGAS
mcGASΔN
H
orang cGASΔN-GFP
K
chimp cGASΔN-GFP

Figure 2.4. Mitochondrial localization and signaling activities of cGAS

(A) cGAS production of cGAMP *in vitro* with purified components. Recombinant cGAS proteins, including FL hcGAS, hcGASΔN (160-522 a.a.), FLAG-hcGASΔN, FL mcGAS, mcGASΔN (148-507 a.a.), orang cGASΔN, and chimp cGASΔN, were activated with indicated double-stranded DNA. cGAMP formation was monitored by incorporation of [α-^{32}P] ATP. Reactions were visualized by treating with alkaline phosphatase and separating by thin-layer chromatography. (B) Live confocal micrographs of C-terminally GFP-tagged human FL cGAS or cGASΔN. Representative cell images are shown. (C) Cell counting in (B). Cells with nuclear, cytosolic, and mitochondrial cGAS localization were counted and the ratio was calculated. (D) Live confocal micrographs of human cGASΔN with indicated tags. Representative cell images are shown. (E and F) Real-Time qRT-PCR analysis of *Ifnb* (E) and *Rsad2* (F) mRNAs in iBMDMs treated with Dox to induce expression of hcGASΔN with indicated localization tags. (G) Immunoblot analysis of iBMDM lysates treated as in (E) and (F). The asterisk indicates non-specific bands. (H) Live confocal micrographs of C-terminally GFP-tagged orangutan (orang) FL cGAS or cGASΔN. Representative cell images are shown. (I) Live confocal micrographs of C-terminally GFP-tagged mouse FL cGAS or cGASΔN. Representative cell images are shown. (J) Cell counting in (I). Cells with nuclear, cytosolic, and mitochondrial cGAS localization were counted and the percentages of each localization pattern were calculated. (K) Live confocal micrographs of C-terminally GFP-tagged chimpanzee (chimp) FL cGAS or cGASΔN. Representative cell images are shown. Scale bars in all the images indicate 2 μm. Green signals indicate GFP, and red signals indicate mitochondria in all the merged images. Images and immunoblot data are representative from three independent experiments. Graph data are means ± SEM of three independent experiments. Statistical significance was determined by two-way ANOVA and Tukey's multicomparison test. Asterisks indicate the statistical significance between connected two bars. **P* < 0.05; ***P* < 0.01; ****P* < 0.001.

2.4.5. Viral protease-mediated release of Class 1 cGASΔN induces type I IFN responses

The N-terminal domains of human and mouse cGAS display DNA binding and liquid droplet-forming activities, which are thought to synergize with similar activities in the C-terminal catalytic domain to maximize cGAS responses to DNA[195]. Studies of Class 2 (mouse) cGAS support this model, as deletion of the N-terminal domain renders cGAS less reactive to DNA *in vitro*[195,322] and less inflammatory in cells, as compared to FL mcGAS (Figure 2.3B-D). However, this theme displays inconsistencies when considering Class 1 human cGAS. cGASΔN from humans is less DNA reactive than FL hcGAS *in vitro*[195,322], but hcGASΔN is more inflammatory within cells (Figure 2.1A-C). The relative contributions of the N- and C-termini to cGAS functions within cells have only been studied in isolation, where cells were engineered to express either of these domains (not both).

We reasoned that if the primary function of the N-terminal domain of cGAS was to promote DNA binding, then the C-terminal catalytic domain would be less functional in the presence of a separate polypeptide encoding its N-terminal domain, as these domains would compete for the same DNA ligands. Alternatively, the mitochondrial localization model would predict that the N-terminal domain could only prevent DNA-induced IFN responses if it was physically attached to the catalytic domain. To test these predictions, we generated a hcGAS transgene that contains a T2A ribosome skip sequence[333,334] between the N-terminal domain (hcGAS N) and hcGASΔN (Figure 2.5A). Thus, a single mRNA would operate as a bicistronic message that produces hcGAS N and hcGASΔN upon translation. We found that Dox-mediated expression of this engineered cGAS within iBMDMs produced hcGASΔN, indicating T2A functionality, and also led to the production of the ISG viperin (Figure 2.5B). These results suggest that the N-terminal domain cannot inhibit cGASΔN signaling activity when these domains are separate polypeptides. These data therefore support the idea that the activities present in the C-terminal catalytic domain are sufficient to stimulate IFN responses, and that a central function of the N-terminal domain may be to prevent localization of the C-terminus to self-DNA.

Our ability to induce self-DNA reactivity by hcGASΔN, even within cells that contain cGAS N, raised the possibility that other means of dissociating these domains would stimulate IFN production. In this regard, we considered the protein NLRP1, which has emerged as a cytoplasmic sensor of viral and bacterial proteases [323-326]. Cleavage of NLRP1 by pathogen proteases leads to the induction of inflammasome-mediated cell death. In this regard, NLRP1 is considered a guard protein, as opposed to a PRR, with the latter detecting conserved microbial products and the former detecting virulence factor activities [335,336]. No examples of an IFN-inducing sensor of viral protease activity exists. Given that the T2A-mediated separation of the cGAS N- and C-termini was sufficient to trigger IFN responses, it was possible that cGAS can be engineered to operate as an IFN-inducing sensor of viral protease activity. Hepatitis C virus (HCV) is a hepatotropic virus that possesses the protease NS3/4A. This protease is immune-evasive, based on its ability to cleave the RIG-I like receptor (RLR) signaling adaptor MAVS off membranes [246]. In Figures 2.4E-G, we anchored hcGASΔN to the outer mitochondrial membrane (OMM) using the transmembrane domain of MAVS, which contains the NS3/4A cleavage site. Therefore, we hypothesized that this hcGASΔN-OMM protein would be cleaved by NS3/4A, leading to the release of hcGASΔN to the cytoplasm and subsequent IFN induction. To test this hypothesis, hcGASΔN-OMM was stably expressed in iBMDMs that encoded a Dox-inducible NS3/4A transgene (Figure 2.5C). Expression of hcGASΔN-OMM in the absence of NS3/4A did not lead to any IFN activities, but Dox-mediated induction of NS3/4A stimulated some expression of *Ifnb* and *Rsad2* mRNAs (Figure 2.5D, E). Endogenous MAVS in these cells was cleaved upon Dox treatment, confirming the proteolytic function of NS3/4A protein (Figure 2.5F). Notably, the induction of *Ifnb* and *Rsad2* mRNAs was enhanced substantially when orangutan cGAS was used instead of hcGAS in these assays (Figure 2.5D, E). Orangutan cGASΔN-OMM enabled the detection of viperin production and IP-10 secretion upon expression of NS3/4A, which hcGASΔN-OMM barely induced (Figure 2.5F, G). Furthermore, and consistent with the importance of mitochondrial localization of Class 1 cGASΔN for self-DNA reactivity, the addition of FLAG-tag to these cGAS constructs abolished IFN responses upon NS3/4A expression (Figure 2.5D-G). All

Dox-inducible activities were mediated by the protease activity of NS3/4A, as no changes in IFN activities were observed in cells that produced catalytically dead NS3/4A mutant (Figure 2.5D-G). These collective data validate the model that the N-terminal domain of Class 1 cGAS proteins prevents self-DNA reactivity and reveal a synthetic biology-based strategy to redesign this PRR into a PRR-guard hybrid, which operates as an IFN-inducing sensor of viral protease activities.

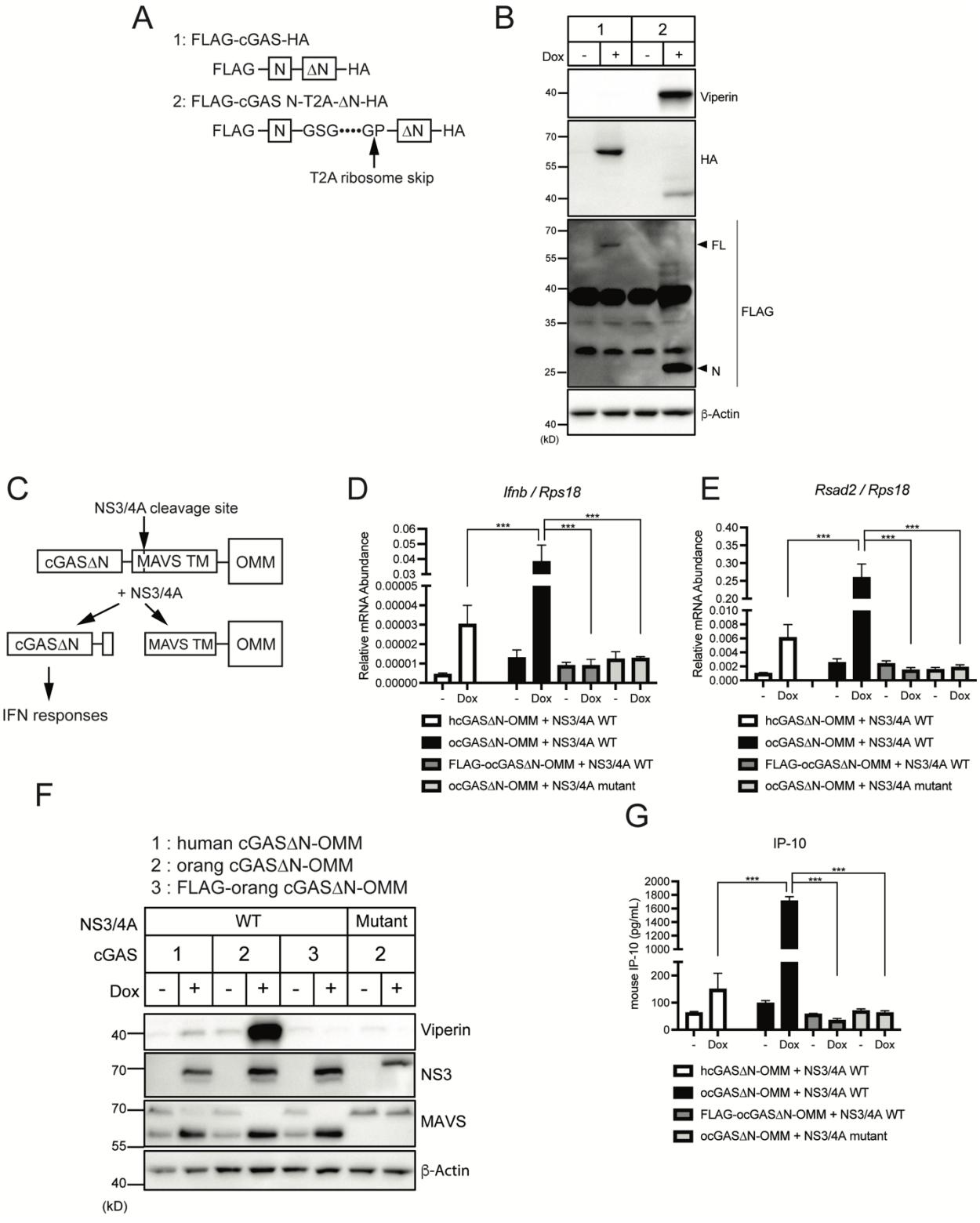
A
1: FLAG-cGAS-HA
FLAG N ΔN HA
2: FLAG-cGAS N-T2A-ΔN-HA
FLAG N GSG••••GP ΔN HA
T2A ribosome skip
B
1
2
Dox
Viperin
HA
FL
FLAG
N
β-Actin
(kD)
C
NS3/4A cleavage site
cGASΔN
MAVS TM
OMM
+ NS3/4A
IFN responses
D
Ifnb / Rps18
Relative mRNA Abundance
hcGASΔN-OMM + NS3/4A WT
ocGASΔN-OMM + NS3/4A WT
FLAG-ocGASΔN-OMM + NS3/4A WT
ocGASΔN-OMM + NS3/4A mutant
E
Rsad2 / Rps18
F
1 : human cGASΔN-OMM
2 : orang cGASΔN-OMM
3 : FLAG-orang cGASΔN-OMM
NS3/4A
WT
Mutant
cGAS
Viperin
NS3
MAVS
β-Actin
G
IP-10
mouse IP-10 (pg/mL)

Figure 2.5. Design of synthetic cGAS as a PRR-guard hybrid that responds to a viral protease

(A) Schematic designs of cGAS constructs with T2A ribosome skip consensus sequences. FLAG-cGAS N-T2A-ΔN-HA is separated upon translation at the indicated arrow. (B) Immunoblot analysis of lysates of iBMDMs treated with Dox for 8 hours to induce expression of cGAS constructs shown in (A). (C) Schematic design of cGAS-outer mitochondrial membrane (OMM) construct and the cleavage by NS3/4A protease. (D and E) Real-Time qRT-PCR analysis of *Ifnb* (D) and *Rsad2* (E) mRNAs in cGAS-expressing iBMDMs treated with Dox for 24 hours to induce expression of WT or mutant NS3/4A proteases. Cells stably expressed indicated human cGAS (hcGAS) or orangutan cGAS (ocGAS) constructs. (F) Immunoblot analysis of iBMDMs treated as in (D) and (E). (G) IP-10 ELISA analysis of iBMDM cell culture supernatant in (D) and (E). Immunoblot data are representative from three independent experiments. Graph data are means ± SEM of three independent experiments. Statistical significance was determined by two-way ANOVA and Tukey's multicomparison test. Asterisks indicate the statistical significance between connected two bars. $*P < 0.05$; $**P < 0.01$; $***P < 0.001$.

2.5. Discussion

Because the amino acid sequence of cGAS is highly conserved throughout evolution, studies have been largely based on the assumption that the regulatory mechanisms of cGAS in one species hold true for another. In this study, while we confirmed the self-DNA reactivity of the human cGAS catalytic domain, we also identified the evolutionary diversity of cGAS regulation. These results allowed us to stratify the regulation of self-DNA reactivity of mammalian cGAS into three classes (Figure 2.3K). Class 1 cGAS in human and the NHPs orangutan, gibbon, and marmoset contains an N-terminal domain that restricts the otherwise self-DNA-reactive catalytic domain. Class 2 cGAS in mouse is the opposite – the N-terminus is required to promote self-DNA reactivity. Class 3 cGAS in other NHPs (chimpanzee, white-handed gibbon, crab-eating macaque, and rhesus macaque) displayed no evidence of an ability to react to self-DNA. This diversity may have derived from unique host-pathogen conflicts in each mammalian species throughout

evolution, resulting in differential means of DNA detection and consequently, self-DNA reactivity. Moreover, these observations are intriguing from a clinical perspective, as animal models including mouse, chimpanzee, and rhesus macaque are often components of therapeutic development pipelines.

Our mechanistic analysis revealed an exquisite sensitivity of the N-terminus of human cGASΔN for self-DNA responsiveness, as adding greater than two amino acids onto the N-terminus was sufficient to abolish IFN activities. These findings may be considered from the perspective of the common use of N-terminal epitope tags to study FL and cGASΔN functions, which we now consider to be the cause of much conflicting literature. Future studies should consider the position of the epitope tags to be as important an experimental variable as the species of the cGAS protein under investigation.

Our finding of hcGASΔN localization to mitochondria is consistent with a recent study reporting that human cGASΔN triggers IFN responses upon localization to these organelles [210]. While these findings explain the operation of human cGAS and other Class 1 cGAS proteins, we found that cGAS proteins in other classes do not follow this rule of self-DNA reactivity. Indeed, FL mcGAS (Class 2) induces IFN responses without localizing to mitochondria and chimpanzee cGASΔN (Class 3) does not trigger these responses even though it localizes to mitochondria. Given that cGAS proteins in all three classes react with DNA and synthesize cGAMP *in vitro*, these findings emphasize the diversity of cGAS regulation that is best revealed from studies within cells. The rules that govern cGAS in Class 2 and Class 3 activities were not revealed in this study and warrant future investigation.

Finally, our redesign of two Class 1 cGAS proteins into PRR-guards that can use self-DNA reactivity as a functional output of viral protease detection is noteworthy. Viral proteases, particularly NS3/4A, are naturally immune-evasive because they cleave host signaling proteins to inactivate PRR-induced responses to infection. Classic therapeutic strategies to target viral proteases involve inhibition, which results in selective pressure for viral escape mutants. Rather than inhibiting viral proteases, our redesigned cGAS has forced the normally immune-evasive

NS3/4A protease to operate as an immunostimulant, which offers several opportunities for further study in the context of infection. These findings provide a mandate to consider synthetic biology-based strategies to alter the host-pathogen conflicts that determine infectious outcome.

Chapter 3: Regulation of Innate Immune Responses by Peroxisomes

Kenta Mosallanejad[1], Jonathan C. Kagan[1]

[1]Division of Gastroenterology, Boston Children's Hospital, Harvard Medical School, 300 Longwood Avenue, Boston, MA 02115, USA.

Author Contribution

K.M. designed the study, performed experiments, and wrote the manuscript. J.C.K. conceived the idea and supervised the research.

3.1. Abstract

Peroxisomes are the highly dynamic organelles and, like mitochondria, play essential roles in cell metabolism such as oxidation of very long-chain fatty acids (VLCFAs) and branched-chain fatty acids (BCFAs). While mitochondria, which oxidize short-, medium-, and long-chain fatty acids (SCFAs, MCFAs, and LCFAs, respectively), have been revealed to regulate innate immune responses, the roles of peroxisomes and their metabolism remain unclear. Here, we genetically depleted peroxisomal protein components in macrophages and revealed that the peroxisomal activities are required for the innate immune responses to a wide variety of PAMPs. Moreover, we also found that pristanic acid, a BCFA substrate of peroxisomal α-oxidation, inhibits Toll-like receptor 4 (TLR4)-mediated production of interleukin-1β (IL-1β) but potentiates type I interferon (IFN) responses to Toll-like receptor (TLR) and RIG-I-like receptor (RLR) agonists. Pristanic acid activated histone deacetylase (HDAC) activity, which was required for cGAS-STING pathway-mediated type I IFN induction. Therefore, pristanic acid reprograms macrophages from an inflammatory state to an antiviral state, suggesting an immunoregulatory function of peroxisomal metabolism. The immunomodulatory effects of other substrates of peroxisomal metabolisms need to be further investigated to comprehensively understand the roles of peroxisomes in the innate immune responses.

3.2. Introduction

Peroxisomes are highly dynamic single membrane-bound organelles in eukaryotic cells. These organelles play essential roles in cell metabolisms such as reactive oxygen species (ROS) detoxification and fatty acid oxidation (FAO) in corporation with mitochondria[241]. While mitochondria are responsible for the oxidation of short-, medium-, and long-chain fatty acids (SCFAs, MCFAs, and LCFAs, respectively), very long-chain fatty acids (VLCFAs, 22 or longer carbons) and branched-chain fatty acids (BCFAs) are first oxidized in peroxisomes and then transported to the mitochondria for further oxidation[241,301].

Cells are equipped with pattern recognition receptors (PRRs) that elicits innate immune responses upon recognition of pathogen-associated molecular patterns (PAMPs) and damage-associated molecular patterns (DAMPs)[2,337]. Mitochondria have been revealed to regulate these PRR-mediated cytokine production, both by providing the signaling platforms and through cell metabolism[244]. For example, mitochondrial antiviral signaling (MAVS, also known as IPS-1, Cardif, VISA) is the adaptor protein in the RIG-I-like receptor (RLR) signaling, which forms oligomers on the mitochondrial membrane upon activation and further recruits and activate the downstream transcriptional pathways[51-54]. Also, mitochondria produce ROS upon damages, which triggers the oligomerization of adaptors in various PRR signaling pathways[242]. Moreover, mitochondrial FAO has been found to be required for and further promote type I interferon (IFN) responses[283]. Although the mechanisms in which mitochondrial FAO supports innate immune responses have not been fully uncovered, these mechanisms include not only through adenosine triphosphate (ATP) production but also by modulating the balance of immunomodulatory fatty acids. Indeed, many mitochondrial FAO substrate fatty acids have been reported to regulate innate immune responses, such as SCFA butyrate and LCFA palmitate, which inhibits and promotes proinflammatory cytokine expression, respectively[290-292,295]. Despite the consensus that the mitochondria play essential roles in innate immune responses, the roles of peroxisomes, the counterpart of mitochondria in cell metabolism, are largely unexplored.

Recently, our group has identified the peroxisomal localization of MAVS, which was functional in the IFN responses against RNA viruses[56]. Peroxisomal MAVS induces the expression of interferon-stimulated genes (ISGs) faster than mitochondrial MAVS does, and this induction is dependent on type III IFN rather than type I IFN[56,316]. Although the differentiation between type I and III IFN by peroxisomal and mitochondrial MAVS is controversial as another group has shown both type I and III IFN are induced by MAVS on both organelles[317], the view of peroxisomes as the platform of PRR responses is now widely accepted[243]. Also, although studies

have investigated into the roles of peroxisomal metabolism in innate immunity by genetically or pharmacologically modulating peroxisomal biogenesis, these studies have shown conflicting results[318,319]. While Di Cara *et al.* showed that peroxisomal ROS detoxification is required for bacterial phagocytosis and antimicrobial peptide production[319], Vijayan *et al.* found that peroxisomes negatively regulate TLR4 responses in macrophages[318]. Therefore, the roles of peroxisomes and their metabolisms in the innate immune responses are totally unclear.

In this study, by genetically depleting peroxisomes or their lumen proteins, we reveal that peroxisomal metabolisms are required for TLR, RLR, and NLRP3 inflammasome-mediated cytokine responses. Moreover, we identified pristanic acid, a BCFA that is substrate of peroxisomal FAO, as the inhibitor of TLR4-induced inflammatory cytokine production and the promoter of TLR- and RLR-mediated type I IFN responses. Pristanic acid-induced IFN responses was mediated by the activation of histone deacetylase (HDAC). These findings shed light on the novel roles of BCFA in immune reprogramming of macrophages and indicate the immunomodulatory roles of peroxisomes as the organelles that metabolizes BCFAs. Because peroxisomes metabolize a wide variety of molecules, further investigations are warranted for the comprehensive understanding of the immune regulation by peroxisomes.

3.3. Materials and Methods

3.3.1. Study design

The aim of this study was to investigate the roles of peroxisomes in the innate immune responses. We investigated the cytokine responses in mouse macrophages which are genetically depleted peroxisomes or their matrix proteins, as well as cells treated with pristanic acid. Sample sizes for each experiment are indicated in the figure legends.

3.3.2. Cell culture

Immortalized bone marrow-derived macrophages (iBMDMs) and human embryonic kidney (HEK) 293T cells were cultured in Dulbecco's Modified Eagle Medium (DMEM, Gibco) supplemented with 10% fetal bovine serum (FBS, Gibco), referred to as complete DMEM, at 37ºC in 5% CO_2. For passage, iBMDMs were lifted using phosphate buffered saline (PBS, Gibco) supplemented with 2.5 mM ethylenediaminetetraacetic acid (EDTA, Invitrogen) and plated at dilution 1:10. HEK293T cells were grown under the same conditions as iBMDMs but were passaged by washing with PBS and lifting with 0.25% Trypsin-EDTA (Gibco) with a 1:10 dilution. THP-1 cells were grown in suspension culture using RPMI-1640 media (Lonza) supplemented with 10% FBS, referred to as complete RPMI-1640, at 37°C in 5% CO_2. For passage, cells were split at a dilution of 1:5.

For treatment of cells with phytanic acid (MilliporeSigma), pristanic acid (MilliporeSigma), GW6471 (MilliporeSigma), and trichostatin A (TSA, MilliporeSigma) was added in the cell culture media for 24 hours unless indicated otherwise. Ethanol (MilliporeSigma) was used as the negative control for pristanic acid and phytanic acid, and dimethyl sulfoxide (DMSO, MilliporeSigma) was used as the negative control for GW6471 and TSA.

For treatment of cells with PAMPs, lipopolysaccharide (LPS, Invivogen) and nigericin (Invivogen) were added to the cell culture media. Calf thymus DNA (CT-DNA) (Invivogen) was mixed with Lipofectamine 2000 (Invitrogen) at 1:2 ratio in Opti-MEM (Gibco) and incubated for 5 minutes before addition to the cell culture media.

3.3.3. Generation of CRISPR-Cas9-mediated knockout (KO) cells

For cloning, the sense and antisense oligonucleotides containing guide RNA (gRNA) sequences and AfeI/SbfI restriction sites were purchased from Integrated DNA Technologies, and the equal molar ratios of sense and antisense oligonucleotides were annealed in water on PCR block (95ºC for 1 minute, then drop 5°C every minute to 10°C). Oligonucleotide duplexes were then subcloned into AfeI/SbfI-digested pRRL-Cas9-Puro vector (kindly provided by Dr. D.

Stetson) using In-Fusion Snap Assembly Master Mix (TakaraBio). gRNAs targeting mouse genes used in this study are as follows: *Pex19* #1: GCGGCTGCTGAGGAAGGTTG, *Pex19* #2: GCTGAGGAAGGTTGCGGTGT, *Pex19* #3: GCCCGAGTTCTGCAGCTCAG, *Pex14* #1: GGCACCACATTTTCACTTCC, *Pex14* #2: GCCGGACCCGAGAATTCTGT, *Pex14* #3: GGCAGAGCCCACTTGCGACC, *Pex5*: GACAAGGCCCTTCGGCAGGA, *Pex7*: GCCGCATAGCCGTGGCGGCC

To generate lentiviral particles for the stable expression of Cas9 and gRNAs, HEK293T cells were transfected with the packaging plasmids psPAX2 and pCMV-VSV-G along with the gRNAs-containing pRRL-Cas9-Puro vector using Lipofectamine 2000 (Invitrogen). Plasmids were transfected into 10 cm^2 dishes of HEK293Ts at 50%–80% confluency using Lipofectamine 2000 by mixing DNA and Lipofectamine 2000 ratio at 1:2. Media was changed on transfected HEK293Ts 16-24 hours after transfection, and virus-containing supernatants were harvested 24 hours following the media change. Viral supernatants were passed through a 0.45 μm filter to remove any cellular debris. Filtered viral supernatants were mixed with polybrene (Millipore) and placed directly onto target cells, followed by the spinfection (centrifugation at 1,250 x g for 1 hour). Cell culture media were replaced with the appropriate complete media and cells were incubated for 24 hours. Spinfection with the viral supernatants was repeated on the following day. Cells with successful Cas9 and gRNA insertion were selected using puromycin (Gibco) and pooled cell culture was used in each assay.

3.3.4. Generating cells with stable gene expression

cDNAs of Pex11β and GFP-PTS1 were amplified by polymerase chain reaction (PCR) using oligonucleotide primers containing restriction enzyme digestion sites. Amplified cDNAs were inserted in pLenti-CMV-GFP-Puro, gifted by Eric Campeau & Paul Kaufman (Addgene plasmid # 17448; http://n2t.net/addgene:17448; RRID: Addgene 17448) [329], in replacement of

GFP using XbaI and SalI. All constructs generated here were sequence-confirmed by Sanger sequencing.

To generate lentiviral particles for the stable expression of transgenes, HEK293T cells were transfected with the packaging plasmids psPAX2 and pCMV-VSV-G along with the transgene in pLenti-CMV-GFP-Puro using Lipofectamine 2000 (Invitrogen). pCMV-VSV-G was a gift from Bob Weinberg (Addgene plasmid # 8454 ; http://n2t.net/addgene:8454 ; RRID:Addgene_8454) [328]. psPAX2 was a gift from Didier Trono (Addgene plasmid # 12260; http://n2t.net/addgene:12260; RRID: Addgene_12260). Plasmids were transfected into 10 cm^2 dishes of HEK293Ts at 50–80% confluency using Lipofectamine 2000 by mixing DNA and Lipofectamine 2000 at 1:2 ratio. Media was changed on transfected HEK293Ts 16–24 hours after transfection, and virus-containing supernatants were harvested 24 hours following the media change. Viral supernatants were passed through a 0.45 μm filter to remove any cellular debris. Filtered viral supernatants were mixed with 5 μg/mL polybrene (MilliporeSigma) and placed directly onto target cells, followed by the spinfection (centrifugation at 1,250 × g, 30°C for 1 hour). Cell culture media were replaced with the appropriate complete media and cells were incubated for 24 hours. Spinfection with the viral supernatants was repeated on the following day. Cells with successful transgene incorporation were selected using puromycin (Gibco) and pooled cell culture was used in each assay.

3.3.4. Real-Time quantitative reverse transcription (qRT-) PCR

RNA was isolated from cells using Qiashredder (QIAGEN) homogenizers and the PureLink Mini RNA Kit (Life Technologies) and treated with subsequently DNase I (Invitrogen) to remove genomic DNA. Relative mRNA expression was analyzed using the TaqMan RNA-to-Ct 1-Step Kit (Thermo Fisher Scientific) with indicated Taqman probes (Thermo Fisher Scientific) on a CFX384 Real-Time Cycler (Bio-Rad Laboratories). Each C_T value was normalized with the mRNA expression of the control genes (RPS18 for human and Rps18 for human) and the relative mRNA abundance was calculated by the $\Delta\Delta C_T$ method. Taqman probes used in this study are as

follows: *Ifnb* (mouse): Mm00439552_s1, *Rsad2* (mouse): Mm00491265_m1, *Rps18* (mouse): Mm02601777_g1, *IFNB* (human): Hs01077958_s1, *RSAD2* (human): Hs00369813_m1, *RPS18* (human): Hs01375212_g1.

3.3.5. Immunoblotting analysis

Cells were lysed with RIPA buffer (50 mM Tris-HCl, pH7.5, 150 mM NaCl, 1% TritonX-100, 0.5% sodium deoxycholate, 0.1% sodium dodecyl sulfate (SDS), which was supplemented with cOmplete, Mini, EDTA-free Protease Inhibitor Cocktail [Roche] before use) and the lysates were centrifuged at 4°C, 16,000 × g for 10 minutes. Supernatants were mixed with 6X SDS sample buffer supplemented with Tris(2-carboxyethyl)phosphine hydrochloride (TCEP, Thermo Fisher Scientific) and boiled at 100°C for 5 minutes. Samples were separated by SDS-PAGE and transcribed to PVDF membrane by Immunoblotting. PVDF was blocked with 5% skim milk for 1 hour and probed with indicated primary antibodies over night at 4°C, followed by secondary antibodies (1:2000 dilution) for 1 hour. Primary antibodies used in this study include viperin (1:1000 dilution, MilliporeSigma), β-Actin (1:1000 dilution, Cell Signaling Technology), cGAS (1:1000 dilution, MilliporeSigma), STING (1:1000 dilution, Cell Signaling Technology), PEX14 (1:1000 dilution, GeneTex), and catalase (1:200, Santa Cruz). Secondary antibodies for human, mouse, and rat immunoglobulins (IgGs) were purchased from Rockland Immunochemicals.

3.3.6. Microscopic analysis of peroxisomes

For immunofluorescence analysis, cells were fixed with 2% paraformaldehyde (PFA, Electron Microscopy Sciences) in PBS for 15 minutes at room temperature. Then, cells were permeabilized with 0.1% Triton X-100 in PBS for 10 minutes, followed by the incubation overnight in the blocking buffer (2% goat serum, 50mM ammonium chloride in PBS) at 4°C. The primary antibodies against Pex14 (GeneTex) were diluted in the blocking buffer and incubated with the cells overnight at 4°C. Antibody binding was detected by secondary antibodies conjugated to AlexaFluor 488 or 594 (Life Technologies). Nuclei were stained with DAPI (Thermo Scientific). Confocal images were acquired using a spinning disk confocal head (CSU-X1, Perkin Elmer Co.,

Boston, MA) coupled to inverted Zeiss Axiovert 200M microscope equipped with a 63X lens (Pan Apochromat, 1.4 NA). The imaging system operates under control of SlideBook 6 (Intelligent Imaging Innovations Inc, Denver, CO).

For imaging of GFP-PTS1 expression, live cells cultured on 12-well plates were examined by Eclipse TS100 (Nikon) and images were captured using NIS-Elements F software.

3.3.7. HDAC assay

HDAC activity was measured using HDAC Activity Colorimetric Assay Kit (BioVision) following manufacture's instruction. Briefly, pristanic acid, phytanic acid, or TSA were incubated at 37°C for 1 hour with HeLa nuclear extract and HDAC substrate provided in the kit. After stopping the reaction by adding Lysine developer, absorbance at 400 nm was measured.

3.3.8. Quantification and statistical analysis

Statistical significance was determined by one-way analysis of variance (ANOVA) with Tukey's multiple comparison test. $P < 0.05$ was seen as statistically significant. All statistical analyses were performed using GraphPad Prism data analysis software. All experiments were performed at least three times, and the graph data with error bars indicate the means with the standard error of the mean (SEM) of all repeated experiments.

3.4. Results

3.4.1. Peroxisomes are required for PRR-mediated cytokine production

The biogenesis of peroxisomes is mediated by peroxin (Pex) family proteins, which transport peroxisomal membrane and matrix proteins from cytosol[301,305,311,312]. Pex19 is a chaperon that recruits peroxisomal membrane proteins, while Pex14 is responsible for the import of the matrix proteins[305,309,311,338]. To deplete peroxisomes, we silenced the expression of *Pex19* and *Pex14* genes in mouse immortalized bone marrow-derived macrophages (iBMDMs) using CRISPR/Cas9-mediated gene editing technique. Pex19 protein was not detected in the immunoblotting analysis of gRNA-delivered cells, validating the efficiency of *Pex19* gene knockout

(KO) (Figure 3.1A). To further confirm that these cells are devoid of peroxisomes, we stably expressed green fluorescence protein (GFP) fused with peroxisomal targeting signal 1 (PST1) (GFP-PTS1). Because PTS1 is recognized by Pex5 and imported into peroxisomal matrix[307,310], GFP-PTS1 localizes in peroxisomes in the control cells (Figure 3.1B). In contrast, Pex19-deficient cells showed cytosolic distribution of GFP-PTS1, indicating the lack of peroxisomes (Figure 3.1B).

To examine the roles of peroxisomes in innate immune responses, we stimulated Pex19 KO cells with lipopolysaccharide (LPS), a ligand for TLR4. As a result, the production of proIL-1β was attenuated in the absence of Pex19, while the amount of tumor necrosis factor alpha (TNFα) was not affected (Figure 3.1C and D). Consistently, the secretion of mature IL-1β upon the treatment with LPS and nigericin, a potassium ionophore that stimulates NLRP3 inflammasome, was attenuated in Pex19 KO iBMDMs (Figure 3.1E). Next, we generated Pex14 KO iBMDMs, which retain peroxisomal membranes but lack matrix proteins, to examine the roles of peroxisomal functions in these PRR responses. Pex14-deficient cells showed cytosolic diffusion of GFP-PTS1, validating the loss of peroxisomal protein import machinery (Figure 3.1B). These cells showed reduced proIL-1β synthesis and mature IL-1β release upon TLR4 and NLRP3 activation, respectively (Figure 3.1F, G), while they released comparable amount of TNFα (Figure 3.1H). Similarly, Pex14 KO cells induce attenuated proIL-1β protein synthesis upon TLR2 agonist Pam3CSK4 (Figure S3A). Moreover, we examined IFN responses to RLR agonist poly (I:C) and cGAS agonist calf thymus DNA (CT-DNA) in Pex14-deficient iBMDMs. As a result, Pex14 KO cells induced less mRNA expression of *Ifnb* (encoding IFN-β, type I IFN), *Ifnl2/3* (encoding IFN-λ, type III IFN), and *Rsad2* encoding interferon-stimulated gene (ISG) viperin (Figure S3B-D). Therefore, these results suggested that peroxisomes, particularly their matrix proteins, are required for antiviral responses and a subset of proinflammatory responses such as IL-1β production but not for other inflammatory cytokines such TNFα release.

Given the requirement for Pex14-mediated protein import in PRR responses, we further investigated into which peroxisomal matrix proteins are responsible for these responses. Peroxisomal lumen proteins are mainly categorized by PTS1-containing proteins and PTS2-containing proteins, which are recognized by PTS receptors Pex5 and Pex7, respectively[310]. Therefore, we generated Pex5- and Pex7-deficient iBMDMs to examine the requirement for peroxisomal proteins containing each PTS. As a result, while the proIL-1β production upon LPS stimulation in *Pex7* gRNA-expressing iBMDMs was unaffected, iBMDMs expressing *Pex5*-targeting gRNA produced lower amount of proIL-1β, suggesting PTS1-containing proteins are required for inflammatory responses (Figure S3E).

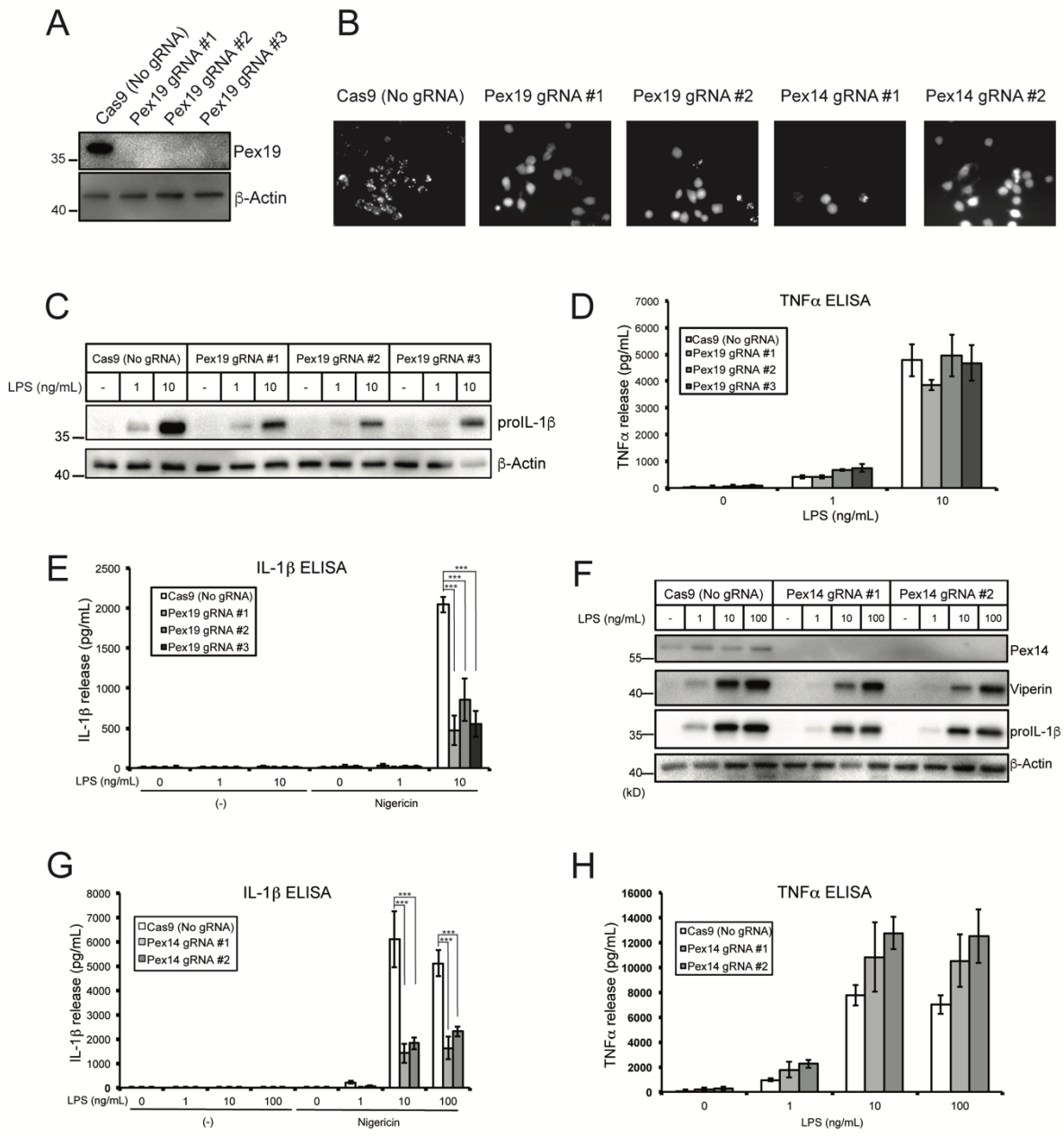

Figure 3.1. Peroxisomes are required for innate immune responses to PAMPs

(A) Immunoblot analysis of lysates from iBMDMs expressing Cas9 and gRNA targeting Pex19. (B) Microscopic images of GFP-PTS1 expressed in iBMDMs that contain indicated gRNAs. (C) Immunoblot analysis of lysates from *Pex19* gRNA-expressing iBMDMs treated with LPS for 3 hours. (D) ELISA analysis of TNFα released in the culture supernatant in (B). (E) ELISA analysis

Figure 3.1 (Continued)

of IL-1β released in the culture supernatant of iBMDMs treated with LPS for 3 hours and nigericin for 1.5 hours. (F) Immunoblot analysis of *Pex14* gRNA-expressing iBMDMs treated with LPS for 3 hours. (G) ELISA analysis of IL-1β released in the culture supernatant of *Pex14* gRNA-expressing iBMDMs treated as in (E). (H) ELISA analysis of TNFα released in the culture supernatant of iBMDMs in (F). Graph data are means ± SEM of three independent experiments. Immunoblot data and micrographs are representative of three independent experiments. Statistical significance was determined by one-way ANOVA and Tukey's multicomparison test. Asterisks indicate the statistical significance between connected two bars. ***$P < 0.001$.

3.4.2. Pristanic acid rewires innate immune responses

Peroxisomes are responsible for the α-oxidation of BCFAs such as phytanic acid and pristanic acid, and the disturbance of peroxisomal function leads to the cytosolic accumulation of these fatty acids[303,311]. Both phytanic acid and pristanic acid are derived from dietary intake, but pristanic acid is also an intermediate of α-oxidation of phytanic acid[303,339]. Given that the substrates of the mitochondrial FAO demonstrate immunomodulatory properties[290-292,295], we hypothesized that these fatty acids also could modulate PRR-mediated responses.

To examine the effect of BCFAs on innate immune responses, iBMDMs are treated with phytanic acid or pristanic acid for 24 hours. As a result, pristanic acid increased the expression of *Ifnb* and *Rsad2* but not *Il1b* mRNA, while phytanic acid did not induce expression of these cytokines (Figure 3.2A-C). Consistently, pristanic acid enhanced type I and III IFN responses during RLR activation by poly (I:C) delivered to the cytosol (Figure 3.2D and E). Similarly, treatment with pristanic acid enhanced the viperin protein synthesis upon LPS stimulation (Figure 3.2F), while proIL-1β synthesis upon LPS treatment was rather reduced in pristanic acid-primed cells (Figure 3.2G). Surprisingly, however, type I IFN responses induced by cGAS agonist calf

thymus (CT)-DNA were not affected in these cells (Figure 3.2H and I). Altogether, these results suggest that pristanic acid inhibits proinflammatory responses but promotes antiviral responses.

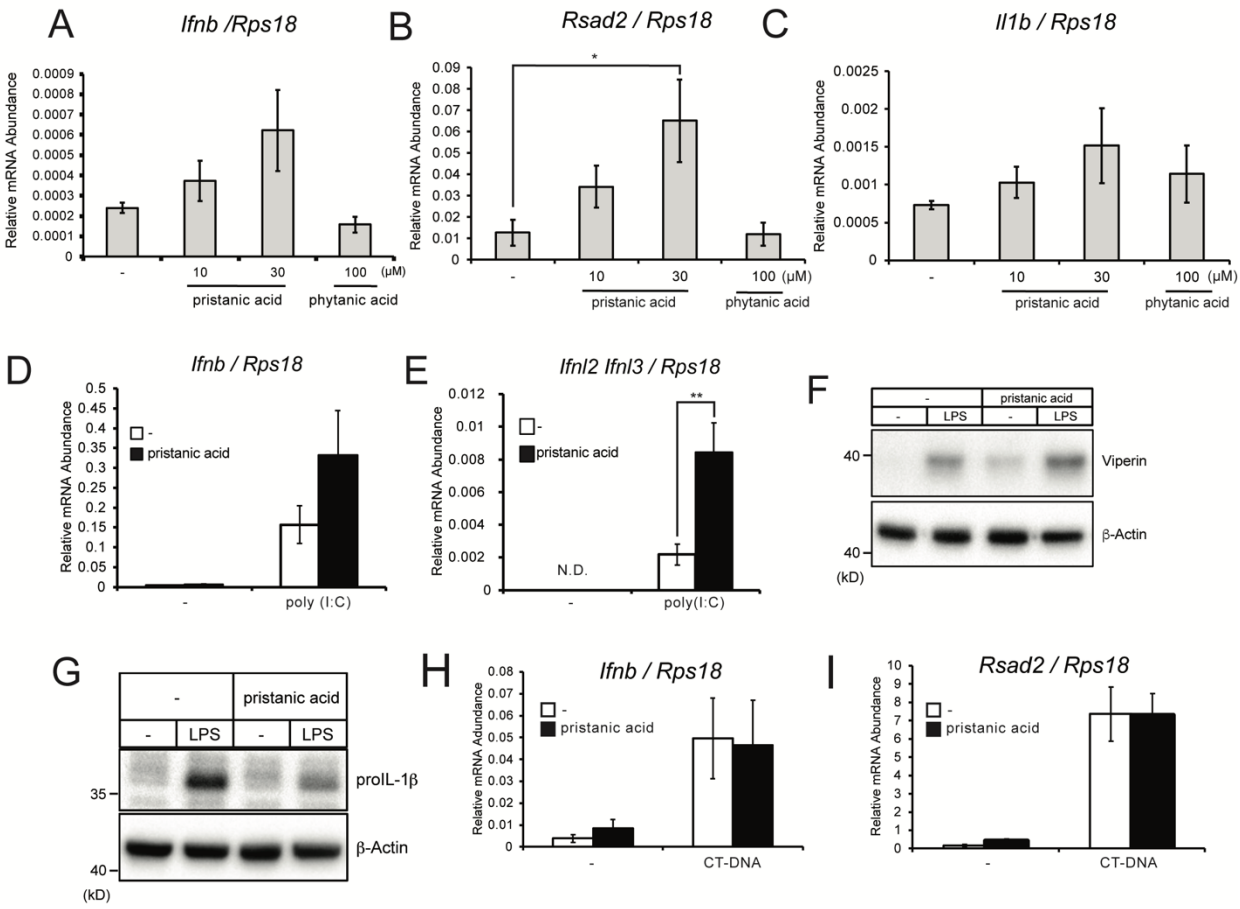

Figure 3.2. Pristanic acid promotes IFN responses and inhibits inflammatory responses

(A-C) Real-Time qRT-PCR analysis of *Ifnb* (A), *Rsad2* (B), and *Il1b* (C) mRNA in the iBMDMs treated with the indicated concentrations of pristanic acid or phytanic acid for 24 hours. (D and E) Real-Time qRT-PCR analysis of *Ifnb* (D) and *Ifnl2*/*3* (E) mRNA in the iBMDMs treated with 30 μM pristanic acid for 24 hours and then transfected with 1 μg/mL poly (I:C) for 4 hours. (F and G) Immunoblot analysis of lysates from iBMDMs treated with 30 μM pristanic acid for 24 hours and 10 ng/mL LPS for 3 hours. (H, I) Real-Time qRT-PCR analysis of *Ifnb* (H) and *Rsad2* (I) mRNA in the iBMDMs treated with 30 μM pristanic acid for 24 hours and then transfected with 1 μg/mL CT-

Figure 3.2 (Continued)

DNA for 4 hours. Graph data are means ± SEM of three independent experiments. Immunoblot data are representative of three independent experiments. Statistical significance was determined by one-way ANOVA and Tukey's multicomparison test. Asterisks indicate the statistical significance between connected two bars. $*P < 0.05$; $**P < 0.01$.

3.4.3. Pristanic acid induces IFN responses in a cGAS-dependent manner

To determine through which PRR pathway pristanic acid induces IFN expression, we used MAVS- and cGAS-deficient iBMDMs, which lack functional RLR and cGAS-STING signaling, respectively. As a result, pristanic acid induced IFN responses in MAVS KO cells but not in cGAS KO cells (Figure 3.3A and B). cGAS-deficient cells induced *Ifnb* mRNA expression upon pristanic acid when cGAS expression was reconstituted by viral vector gene delivery, validating the requirement for cGAS in pristanic acid-induced IFN responses (Figure S4A). Furthermore, pristanic acid did not inhibit LPS-induced proIL-1β synthesis in iBMDMs lacking cGAS (Figure 3.3C). Therefore, it is suggested that pristanic acid requires cGAS to rewire the innate immune profiles in macrophages. To examine whether STING, the adaptor protein in cGAS signaling, is also required, we used synthetic STING antagonist C-178[340]. Pretreatment of iBMDMs with C-178 decreased type I IFN responses upon transfection with CT-DNA, validating the STING inhibitory function of this compound (Figure S4B). As a result, C-178 attenuated the transcription of *Ifnb* or *Rsad2* mRNA upon pristanic acid treatment (Figure 3.3D and E). These data suggest that pristanic acid requires cGAS-STING pathway to rewire the innate immune responses.

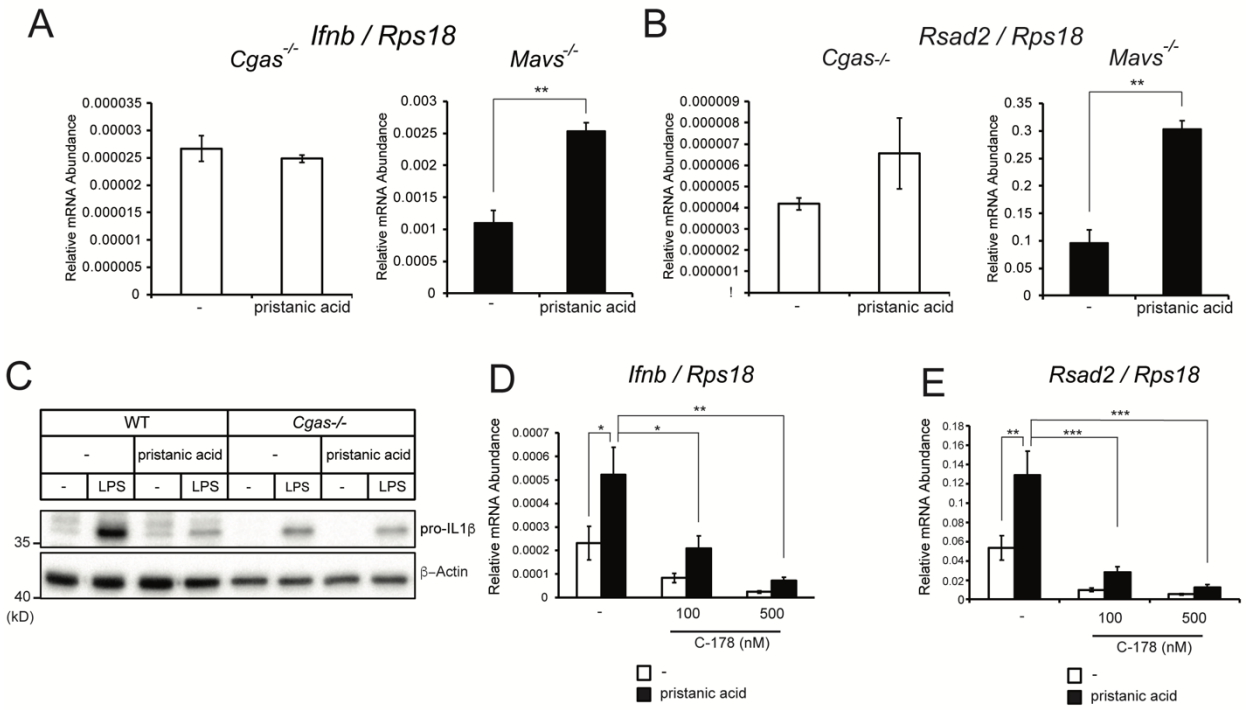

Figure 3.3. cGAS-STING signaling is required for IFN responses to pristanic acid

(A and B) Real-Time qRT-PCR analysis of *Ifnb* (A) and *Rsad2* (B) mRNA in cGAS- or MAVS-deficient iBMDMs treated with 30 μM pristanic acid for 24 hours. (C) Immunoblot analysis of lysates from wild type or cGAS-deficient iBMDMs treated with 30 μM pristanic acid for 24 hours and 10 ng/mL LPS for 3 hours. (D and E) Real-Time qRT-PCR analysis of *Ifnb* (D) and *Rsad2* (E) mRNA in iBMDMs treated with 30 μM pristanic acid for 24 hours together with indicated concentrations of C-178. Graph data are means ± SEM of three independent experiments. Immunoblot data are representative of three independent experiments. Statistical significance was determined by one-way ANOVA and Tukey's multicomparison test. Asterisks indicate the statistical significance between connected two bars. $*P < 0.05$; $**P < 0.01$; $***P < 0.001$.

To elucidate the mechanisms in which pristanic acid triggers cGAS-STING pathway activation, we examined the involvement of reported bioactivities of pristanic acid. Phytanic acid and pristanic acid have been reported to function as peroxisome proliferator-activated receptor

alpha (PPARα) agonists[341]. Therefore, we asked whether PPARα activation is required for cGAS activation by using PPARα antagonist GW6471. Co-treatment of GW6471 inhibited the induction of *Ifnb* and *Rsad2* mRNA by pristanic acid, suggesting the requirement for PPARα activity (Figure 3.4A and B). Because PPARα induces peroxisome proliferation[342,343], we examined whether the treatment with pristanic acid proliferates peroxisomes in macrophages. As expected, pristanic acid increased the abundance of Pex14-positive structures (Figure 3.4C) and the amount of catalase protein (Figure 3.4D) in iBMDMs, indicating proliferation of peroxisomes. Interestingly, the increase in catalase protein abundance was not observed in cGAS-deficient cells (Figure 3.4D). Also, LPS did not increase the abundance of catalase, suggesting that TLR activation does not proliferate peroxisomes (Figure 3.4D). Therefore, these results indicate that cGAS activity is required for pristanic acid-induced peroxisomal proliferation. To examine the effect of peroxisomal proliferation in type I IFN production, we stably induced the expression of *Pex11b* gene, which encodes Pex11β protein, in iBMDMs by lentivirus-mediated gene delivery. The overexpression of Pex11β leads to the elongation and subsequent fission of peroxisomes, therefore proliferates peroxisomes[306,344,345]. The delivery of *Pex11b* gene increased Pex14-positive structures in iBMDMs, indicating successful proliferation of peroxisomes (Figure 3.4E). However, these Pex11β-expressing iBMDMs expressed comparable levels of *Ifnb* and *Rsad2* mRNA to the cells delivered empty vector, even in the presence of PRR ligands such as cytosolic poly (I:C) and LPS (Figure 3.4F-I). Also, Pex11β expression did not alter level of *Il1b* mRNA expression upon LPS treatment (Figure 3.4J). Therefore, these data suggest that the immune reprogramming by pristanic acid is not merely due to proliferation of peroxisomes. Altogether, these data suggest that pristanic acid triggers cGAS-STING-mediated IFN responses through PPARα activation, which subsequently induces peroxisomal proliferation.

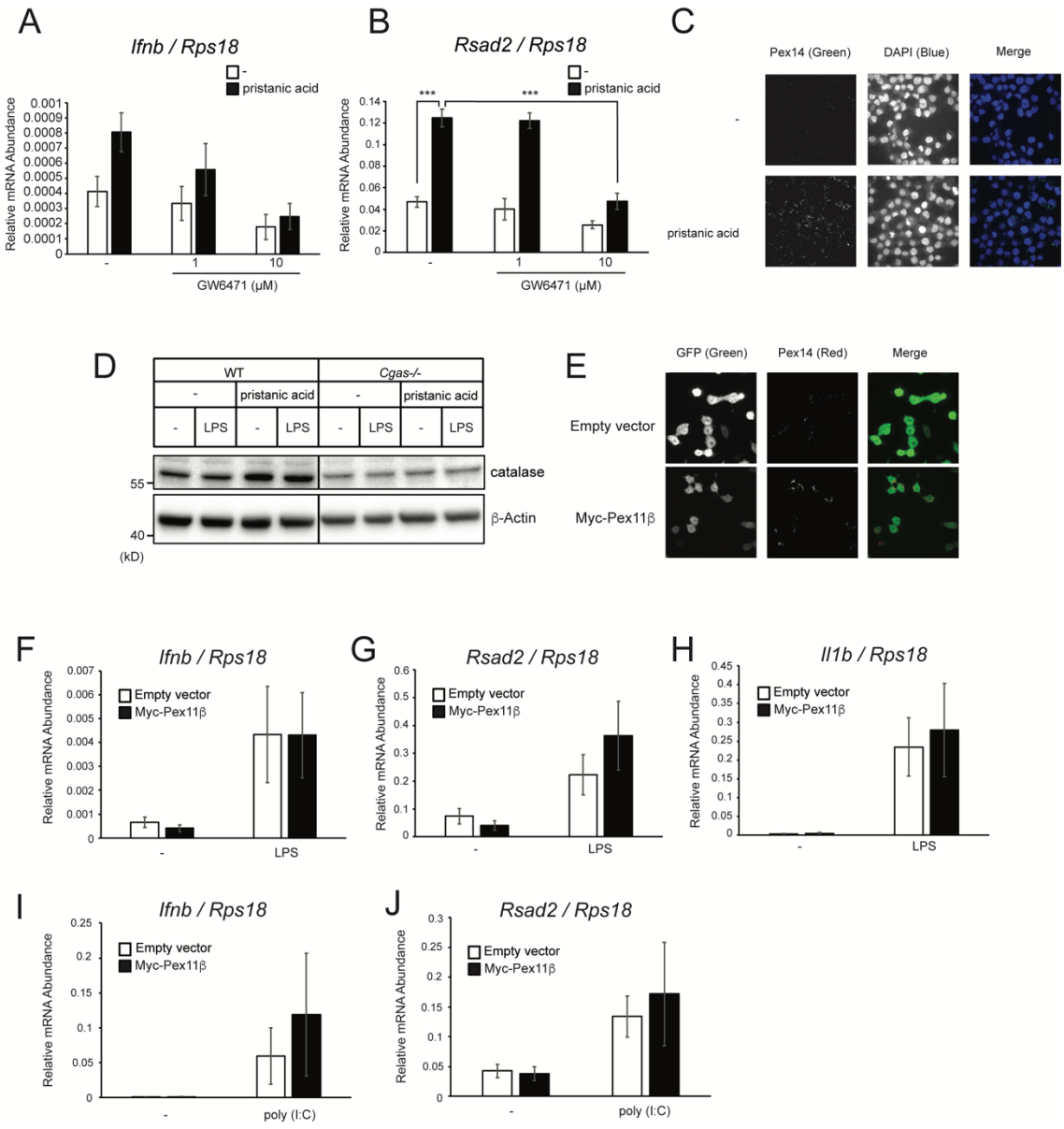

Figure 3.4. Pristanic acid proliferates peroxisomes through cGAS activation

(A and B) Real-Time qRT-PCR analysis of *Ifnb* (A) and *Rsad2* (B) mRNA in iBMDMs treated with 30 μM pristanic acid together with indicated concentrations of GW6471 for 24 hours. (C) Immunofluorescence analysis of Pex14 in iBMDMs treated with 30 μM pristanic acid for 24 hours. Green: Pex14, Blue: DAPI (nucleus). (D) Immunoblot analysis of lysates from iBMDMs treated with 30 μM pristanic acid for 24 hours and/or 10 ng/mL LPS for 3 hours. (E) Immunofluorescence analysis of Pex14 in iBMDMs stably expressing Myc-Pex11β with bicistronic GFP expression.

Figure 3.4 (Continued)

Green: GFP, Red: Pex14. (F-H) Real-Time qRT-PCR analysis of *Ifnb* (F), *Rsad2* (G), and *Il1b* mRNA in Pex11β-expressing iBMDMs treated with 10 ng/mL LPS for 3 hours. (I, J) Real-Time qRT-PCR analysis of *Ifnb* (I) and *Rsad2* (J) mRNA in Pex11β-expressing iBMDMs transfected with 1 μg/mL poly (I:C) for 4 hours. Graph data are means ± SEM of three (A and B) or five (F-J) independent experiments. Immunoblot data and micrographs are representative of three independent experiments. Statistical significance was determined by one-way ANOVA and Tukey's multicomparison test. Asterisks indicate the statistical significance between connected two bars. ***$P < 0.001$.

3.4.4. Pristanic acid activates HDAC to stimulate cGAS-STING signaling

Other reported activities of phytanic acid include the activation of HDAC[346]. Interestingly, several studies have found that the HDAC inhibitors such as butyrate and trichostatin A (TSA) not only regulate innate immune responses but also increase the abundance of peroxisomal proteins[347,348]. Therefore, we hypothesized that pristanic acid also has HDAC-regulating activity, thereby modulating innate immune responses. To test this hypothesis, we incubated the nuclear extract from HeLa cells with pristanic acid and measured HDAC activity. As a result, in contrast to HDAC inhibitor TSA that reduced histone deacetylation (Figure 3.5A), pristanic acid and phytanic acid increased the abundance of deacetylated histone in the nuclear extract (Figure 3.5B). Moreover, the co-treatment with TSA abolished the increase in the type I IFN responses by pristanic acid (Figure 3.5C and D). These results therefore suggest the induction of type I IFN responses by pristanic acid is dependent on its HDAC activity.

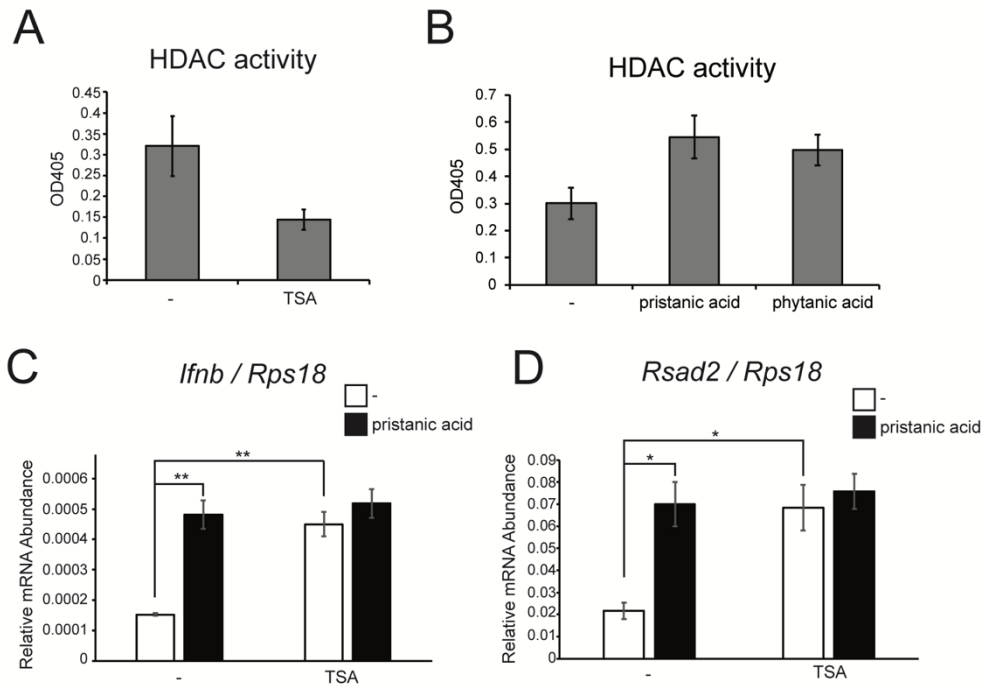

Figure 3.5. Pristanic acid activates HDAC to stimulate cGAS

(A and B) *In vitro* HDAC activity of 30 nM TSA (A), 30 μM pristanic acid, and 100 μM phytanic acid (B). (C and D) Real-Time qRT-PCR analysis of *Ifnb* and *Rsad2* mRNA in iBMDMs treated with 30 μM pristanic acid together with 30 nM TSA. Graph data are means ± SEM of three independent experiments. Statistical significance was determined by one-way ANOVA and Tukey's multicomparison test. Asterisks indicate the statistical significance between connected two bars. $*P < 0.05$; $**P < 0.01$

3.5. Discussion

Despite the similarity of peroxisomes and mitochondria, the roles of peroxisomes in innate immune responses are largely unclear in contrast to mitochondria. By CRISPR/Cas9-mediated disruption of peroxisomal biogenesis, we found that peroxisomes play essential roles in the cytokine responses to both extracellular and intracellular PAMPs. Although it is still possible that the peroxisomal membrane structure or proteins are involved, we found Pex14, the peroxin responsible for peroxisomal protein import, was required for PRR responses, suggesting that the peroxisomal metabolism regulates these responses. Our further analysis revealed that the PTS1-

containing peroxisomal proteins are likely responsible for the immune regulation. Future investigation is needed to screen PTS1-containing genes that regulate these PRR responses. Once the hit genes in the screening are obtained and validated, the roles of the peroxisomal metabolic functions, in which those genes are involved, in the innate immune responses will be further investigated.

Besides genetic manipulation of peroxisomal metabolism, this study also directly examined the roles of branched chain fatty acids as the substrates of peroxisomal FAO in the innate immune response of mouse macrophages. Interestingly, while pristanic acid restricted proinflammatory responses marked by IL-1β synthesis and release, it enhanced type I IFN responses induced by TLR and RLR ligands. Thus, pristanic acid functions not as just a positive or negative regulator of PRR responses, but rather rewires the innate immune profiles of macrophages. Our further analysis revealed the activation of PPARα-cGAS-STING pathway as the responsible mechanism of pristanic acid-triggered immune rewiring, while how PPARα activates cGAS remains elusive. In this study, we also found pristanic acid induces the proliferation of peroxisomes in a cGAS-dependent fashion. Considering the study showing type I IFN promotes mitochondrial FAO[283], it is highly possible that the excessive presence of pristanic acid induce peroxisomal FAO that oxidizes it. This study also found that mitochondrial FAO enhances type I IFN responses[283]. As such, peroxisomal FAO may promote type I IFN responses in a similar manner. Contrary to this speculation, Pex11β-mediated peroxisomal proliferation did not enhance type I IFN responses in our study. Nevertheless, it is still possible that Pex11β-mediated fission only increases the number of peroxisomes but not their protein contents and metabolic functions, which therefore did not test this hypothesis adequately.

We also discovered HDAC promoting activity of pristanic acid, which was required for type I IFN responses. This is consistent with that HDAC inhibitors attenuate PRR responses. Interestingly, cGAS protein itself is acetylated by HDAC, which is required for the signaling[220,221].

Therefore, pristanic acid may also promote direct acetylation of cGAS, which needs future examination. Moreover, it is noteworthy that butyrate, a SCFA that is metabolized by mitochondria, functions as a HDAC inhibitor and inhibit cytokine responses[292]. Altogether, these results highlight the different roles of mitochondrial and peroxisomal FAO in the regulation of innate immune responses.

Overall, this study not only found the essential roles of peroxisomal functions in PRR response but also discovered the unique property of pristanic acid, a peroxisomal FAO substrate, that rewires macrophages from an inflammatory state to an antiviral state. Further investigation into the roles of other substrates and products of peroxisomal metabolism in the innate immune responses are needed to the comprehensive mechanism in which peroxisomes support various PRR signaling. Because peroxisomal dysfunction leads to severe lipotoxicity evidenced by the lethality of peroxisomal disorders that lack effective treatment, this and future studies will untangle the immunopathology of these disorders and therefore lead to the development of therapeutics.

Chapter 4: Discussion

Kenta Mosallanejad[1]

[1]Division of Gastroenterology, Boston Children's Hospital, Harvard Medical School, 300 Longwood Avenue, Boston, MA 02115, USA.

4.1. Overview

In 1989, one year after when was born, Charles Janeway proposed the fundamental model of evolutionarily conserved non-self-pattern recognition in innate immunity, where he termed the receptors “pattern recognition receptors (PRRs)”[349]. Now I am 33 years old, and this model has been filled with many PRRs and pathogen-associated molecular patterns (PAMPs) since then. Now we know that each PRR response is tightly regulated by protein-based signal transductions. We know that these PRRs are also responsible for the detection of damage-associated molecular patterns (DAMPs). We know that these responses have a crosstalk with mitochondrial metabolism. Nevertheless, despite such advances in our understanding, this field is still not full of knowledge but rather full of questions. These questions include: Is the PRR-mediated PAMP or DAMP recognition really the same throughout the evolution? How about the roles of other organelles such as peroxisomes in these responses? Throughout my graduate training, I aimed to answer these questions. In this chapter, I will discuss what I have learned from my thesis work mainly regarding the self-DNA reactivity of cGAS in mitochondria and its diversity in evolution, as well as the roles of peroxisomal fatty acids in innate immunity. The discussion will be extended to what needs to be answered in the future investigations.

4.2. cGAS

4.2.1. Self-DNA reactivity in human cGAS revealed by the C-terminal epitope tags

cGAS responds to microbial DNA and induces STING and downstream signal activation to induce type I IFN responses[350]. As the DNA recognition by cGAS is largely sequence-independent, cGAS is able to react to not only foreign DNA but also host-derived DNA[174,175,184]. Then, how is self-DNA prevented from being sensed by cGAS in normal cells? The answer in the past has been solely the spatial regulation of cGAS – cGAS localizes in the cytosol, where it encounters only foreign DNA but not nuclear or mitochondrial DNA. However, this simple answer has been revised by the recent findings that cGAS is also present in the nucleus, warranting the

additional explanations for the lack of reactivity of nuclear cGAS to chromosomal DNAs[149,197,199,201]. Currently proposed mechanisms of nuclear cGAS inhibition include the binding of nuclear proteins such as histone and BAF to cGAS and DNA, respectively, which competes with cGAS-DNA interaction[202,205-209]. However, how cGAS protein regulates the self-DNA reactivity by its internal domains has not been addressed yet. It was not until two years ago that the possibility of cGAS self-inhibition has been raised, when our group found that the deletion of cGAS N-terminal domain leads to the spontaneous activation of STING pathway[200]. This conclusion contradicted to other studies that had demonstrated the opposite – cGAS N-terminal domain is rather required for the signaling activity[195,199]. Therefore, this possible cGAS self-inhibition needs further examination and validation.

This thesis project not only validated our previous findings on the autoinhibitory mechanism of self-DNA reactivity by cGAS N-terminal domain but also revealed the technical reason why we and others led to the opposite results. N-terminal epitope tags used in other studies completely abolished the activity of human cGAS C-terminal domain (cGASΔN)[195,199], while C-terminal tag used in this work did not. We further found that the addition or deletion of only more than two amino acids interferes cGASΔN activity. Because cGASΔN activity is abolished by the addition of any amino acids, it is suggested that self-DNA reactivity of cGAS is strictly determined by the protein structure. However, it is still possible that cGASΔN requires specific the amino acid residues on the N-terminal end to activate STING pathway. This possibility will be tested in the future by the substitution of the N-terminal amino acids on cGASΔN 160-163 a.a. (PGAS) without altering the length of the protein.

These results need strong attention of the field of molecular biology. Most of the protein functions currently reported are based on the studies using tagged proteins, which often fail to consider the effects of tags on those functions. Now is the time to look again at these studies in the past. We need to be careful about the construct design of the molecules you are interested in

and ask yourself whether the data using it represent the functions of the native proteins. Indeed, our study shows the partial reduction of cGASΔN activity by the C-terminal tags, so we need to keep in mind the possibility that the self-DNA recognition by cGAS is inhibited not only by N-terminal domain but also the C-terminal structure. The structure determinants of C-terminal end of cGAS needs to be examined in the future by adding or deleting different numbers of amino acids.

4.2.2. Mitochondrial localization of cGASΔN

Consistent to the recent report by Zhijian Chen's group[210], this thesis work revealed that the autoinhibition of cGAS by the N-terminal domain is not mediated by interfering with ligand binding or reducing enzymatic activity but rather by preventing mitochondrial localization, in which cGAS reacts to mtDNA. Therefore, it can be said that the self-inhibitory regulation of cGAS protein is to specifically avoid the detection of mitochondrial DNA but not chromosomal DNA. This spatial regulation by a domain of a PRR is unique to cGAS, in contrast to the conventional PRR autoinhibition such as RIG-I, whose C-terminal domain interferes RNA binding[44]. Currently, mtDNA-induced cGAS activation is thought to occur in the cytosol, where mtDNA is released from damaged mitochondria[184]. However, the mitochondrial localization of cGASΔN found in this study raises the possibility of the opposite in some settings – the inhibition of mitochondrial localization by cGAS N-terminal domain is abolished by post-translational modifications including proteolysis, which relocates cGAS to the mitochondria and causes mtDNA-induced inflammation. Human cGAS has been reported to be cleaved by caspase-1 during inflammasome activation at D140 and D157, producing a cGAS fragment that is almost identical to the active form of cGAS deletion mutant (starting at 158A) used in our study[222]. It is therefore expected that the cGAS cleavage at D157 induces the type I IFN responses, although the published study found the opposite – cGAS cleavage by caspase-1 rather restricts cGAS activation upon DNA virus infection. This may be because caspase-1 cleaves cGAS at not only D157 but also at other residues in cGASΔN or other

proteins in cGAS-STING signaling[222]. Future efforts are required to discover the cellular stresses that induces cGAS modifications, if any, releasing cGAS from autoinhibition to induce self-DNA-triggered IFN responses in the mitochondria. Most of the studies in the past have examined the localization of cGAS by either live imaging of N-terminal GFP-tagged construct or immunofluorescence analysis using a commercially available cGAS antibody that detects the N-terminus of cGAS[199,201], which cannot detect mitochondrial localization of cGASΔN. On the other hand, live imaging confocal analysis of C-terminally GFP-tagged cGAS performed in this thesis will allow the future screening of the stimuli that translocates cGAS from the cytosol to the mitochondria.

Also, during this thesis work on cGAS localization, we discovered the limitation of the biochemical analysis – post-lysis DNA binding affects the behavior of cGAS in these assays. These findings are quite important to the field, because cGAS subcellular localization has been largely discussed with the results of the fractionation and other biochemical analyses[199,200]. This thesis revealed that these experiments are able to reflect the binding capacity of cGAS to DNA and potentially other cellular molecules, but not able to capture the cGAS dynamics within cells. This statement should apply to not only cGAS but also other proteins, so we should not rely solely on the biochemical analysis when discussing the subcellular localization of proteins. However, despite these limitations in assessing subcellular localization, membrane flotation assay used in this thesis can be used to study DNA binding ability of cGAS protein. In the future, for example, the development of small molecules that physically dissociate cGAS condensates will use these biochemical analyses for validation.

4.2.3. Diversity of self-DNA reactivity of cGAS in evolution

This thesis work also made another important discovery regarding cGAS self-DNA reactivity. Innate immune signaling pathways are evolutionarily conserved as Janeway originally posited[349], and therefore structurally homologous PRRs are often regarded to operate via the

similar mechanisms. Although the recent studies have challenged this idea in the context of PAMP sensing such as LPS[351], no such studies have been conducted regarding DAMPs. In our study, we found that cGAS reactivity to self-DNA is diverse in mammals, which we classified into three distinct categories (Class 1, 2, and 3). Class 1 cGAS in some non-human primate (NHPs) such as orangutan, gibbon, and marmoset showed the similar property as human cGAS did – the N-terminal domain autoinhibits the otherwise self-DNA-reactive C-terminal enzymatic domain. Class 2 cGAS found in mouse was reactive to self-DNA in the full-length form, but cGAS∆N was inactive in contrast to Class 1 cGAS. Lastly, Class 3 cGAS found in other NHPs such as chimpanzee, rhesus macaques, and white-handed gibbon are inactive to self-DNA regardless of whether it is in the full-length or ∆N form. Although a couple of recent reports have addressed the difference between human and mouse cGAS, this thesis work is the first to my knowledge that has differentiated the PRR responses to DAMPs among mammalian species, especially in NHPs.

Although the reason why the self-DNA reactivity differs among NHPs remains unclear, the results that both Class 1 (orangutan) and Class 3 (chimpanzee) cGAS∆N localizes in the mitochondria and synthesizes cGAMP *in vitro* indicate that this difference is due to the different interaction profiles of these cGAS with the mitochondrial factors rather than the protein intrinsic activity. The possibility is either that Class 1 cGAS is activated by other molecules which does not activate Class 3 cGAS, or that Class 3 cGAS is inhibited by other molecules that does not restrict Class 1 cGAS. Interestingly, the amino acid sequences of cGAS∆N is so highly conserved among mammalian species including NHPs that no single amino acid that differentiates Class 1 and 3 cGAS can be found. Therefore, it is assumed that not the primary but the tertiary protein structures determine the association of Class 1 and 3 cGAS with other cellular molecules. As the activity of nuclear cGAS is regulated by nuclear proteins that inhibit cGAS-DNA binding[202,205-209], it is also possible that cGAS∆N binding to mtDNA is regulated by mitochondrial proteins, which may differ between Class1 and Class 3 cGAS. The mitochondrial proteins that regulate cGAS self-DNA

reactivity wait to be identified in the future studies such as mass spectrometry-based interactome screening or CRISPR-based genetic screening.

It should be highlighted in this work that some of Class 1 cGAS such as gibbon and marmoset are reactive to self-DNA in mouse macrophages but not in human macrophages. These results support the idea that the self-DNA reactivity of cGAS is not solely determined by the cGAS protein itself but also by the interaction with other cellular factors. In the meantime, these results may also challenge the classification of mammalian cGAS made in this study – each Class 3 cGAS may be self-DNA reactive in the NHP cells which it originally belongs to. In the future, I suggest that we derive cell culture from NHPs and induce expression of the species-matched cGAS and cGASΔN to examine the self-DNA reactivity of cGAS in each primate cell type.

Overall, this thesis is the first to discover the diversity of DAMP sensing ability of cGAS in mammals. The physiological reasons for this diversity of self-DNA reactivity in mammals are unclear, but one possibility is that each species developed cGAS function differently under different selective pressures. For example, mice may have developed Class 2 cGAS, which is reactive to self-DNA in the full-length form, because they need to express higher basal level of IFN to respond to any kind of viruses that is abundant in their environment. On the other hand, human and some other primates may have developed Class 1 cGAS to combat specific pathogens around them that possibly cleave cGAS to release cGASΔN. These are only the speculations at this point, but by testing the self-DNA reactivity of cGAS in other mammalian and non-mammalian species such as Xenopus and Zebrafish, we will better understand the relationship between environment and self-DNA reactivity to polish this hypothesis. In this regard, it is of my interest whether self-DNA reactivity differs even in the same species. For example, several cGAS polymorphisms have been reported in human, such as rs610913 that exchanges histidine to proline at position 261 of cGAS[352,353]. These cGAS polymorphisms may alter self-DNA reactivity of cGASΔN, which leads to the diversity of basal IFN expression among different people.

Regardless, the cGAS diversity in mammals discovered in this study is quite important to the field, because the preclinical studies in the drug development are often based on the NHPs such as chimpanzee and rhesus macaques that have Class 3 cGAS, which is different from Class 1 human cGAS.

4.2.4. Synthetic biology-based induction of self-DNA-mediated type I IFN responses

As mentioned above, the post-translational modifications of cGAS that induces mitochondrial localization and subsequent innate immune responses are yet to be identified and are the scope of future studies. In the meantime, this thesis work demonstrates that cGAS can be artificially designed to induce cGAS∆N-based type I IFN responses in a user-defined manner. HCV is an RNA virus that RIG-I recognizes, but it evades RLR responses by NS3/4A protease-mediated cleavage of the adaptor protein MAVS[246]. The cGAS∆N-MAVS transmembrane domain fusion protein used in our study (described as cGAS∆N-OMM) is anchored to the mitochondrial membrane and is released upon the cleavage by the HCV NS3/4A protease. Because the cGAS∆N does not activate downstream signaling when anchored to mitochondria, this cGAS construct is activated only in the presence of NS3/4A protease. Therefore, this engineered "cGAS 2.0" protein takes advantages on the HCV immune evasion mechanism targeting RLR and induces type I IFN responses only in the cells that are infected with the virus. While this study showed the IFN responses induced by this synthetic cGAS in macrophages expressing NS3/4A protease, future studies are needed to validate the antiviral roles of this cGAS construct in hepatocytes and mice during HCV infection by measuring viral titer and cytokine production.

In theory, the strategy to induce IFN responses by designing cGAS constructs can be applied to take advantages of not only microbial proteases but also the proteases in the host cells. As mentioned above, caspase-1 has been reported to cleave cGAS, while whether this cleavage produce signal-activating cGAS∆N remains unclear. However, cGAS can be artificially designed to release cGAS∆N and subsequent IFN responses during cellular stresses that activate

caspases or other proteases. For example, design of a synthetic cGAS construct that releases cGASΔN upon apoptotic caspases such as caspase-3 will convert apoptosis from immunologically silent to immunologically active cell death. As a therapeutic application, adeno-associated virus (AAV)-mediated gene delivery of this cGAS construct can be combined with cancer immunotherapy such as PD-1 blockade antibody to induce IFN responses only in the apoptosis-inducing tumor cells, which would further sensitize the neighboring tumor cells to apoptosis.

Therefore, this thesis study provides not only the new knowledge about the self-DNA reactivity of cGAS and its diversity in mammals but also the unlimited possibilities of the development of therapeutics that induces immune responses during various pathogenesis by using this knowledge.

4.2.5. Future Perspectives

Although this thesis advanced our understanding in the self-DNA reactivity and its evolutionary diversity of cGAS, several important questions remained unanswered. For example, how does cGASΔN induce cell death in THP-1 macrophages? The loss of cell viability in PMA-treated THP-1 cells upon cGASΔN expression was observed both in this thesis and in the previous reports by Barnett *et al*[200]. Because only IFN-inducing mammalian cGASΔN led to cell death, it is possible that IFN induces cell death in differentiated THP-1 cells. Alternatively, it is also possible that signal-inducing cGASΔN causes mitochondrial damages upon detecting mtDNA, which induces apoptosis. These hypotheses will be examined using apoptosis inhibitor along with necroptosis and pyroptosis inhibitor, as well as the treatment with IFNAR-blocking antibody. Moreover, why do some Class 1 cGASΔN, including gibbon and marmoset cGASΔN, induce IFN only in iBMDMs but not in THP-1 cells? These results suggest that there are cell type-specific factors that regulate the self-DNA reactivity of cGAS. In the future, other cell types will be used to examine the signaling activity and localization of cGASΔN in each class to test whether these

differences are due to the species of the cell types. Also, related to this question, why do Class 3 cGASΔN not induce type I IFN while localizing in the mitochondria? Because all cGAS tested induced cGAMP *in vitro*, there may be the cellular factors, probably mitochondrial proteins, that associate with Class 1 and Class 3 cGAS differently. Identifying these molecules will help us understand the mechanism in which cGASΔN synthesizes cGAMP inside the mitochondria. Lastly, how is cGAMP synthesized in the mitochondria released into the cytosol? It is possible that cGASΔN activation by mtDNA induces mitochondrial damages and membrane rupture, which releases cGAMP. Future study will investigate into how self-DNA-reactive cGASΔN affects the mitochondrial integrity and metabolism and how important it is in signal transduction.

4.3. Peroxisomes

4.3.1. The roles of peroxisomal metabolisms in PRR responses

Despite increasing understanding of the roles of mitochondria in the innate immune responses[242,244], including the cGAS activation by self-DNA as described in thesis, much less is known about the roles of peroxisomes. By CRISPR/Cas9-based depletion of genes responsible for peroxisomal assembly, this thesis revealed that peroxisomes are required for various PRR responses in macrophages, including TLR, RLR, and NLRP3 inflammasome. Pex14 depletion reduced these responses as well as Pex19 depletion, indicating that peroxisomal lumen proteins rather than/and peroxisomal membranes are required. This is consistent with the study by Di Cara *et al.* showing positive regulation of antimicrobial responses by peroxisomes[319], while contradicting to the report by Vijayan *et al.* showing anti-inflammatory roles of peroxisomes in macrophages[318]. In our study, cytokine responses are not fully abolished in peroxisome-deficient cells although attenuated. Therefore, it is possible that different metabolic functions of peroxisomes have the opposing effects on the innate immune responses, which are combined when the organelles are depleted.

This study used Pex19-deficient cells and Pex14-deficient cells to study the requirement for peroxisomes themselves and peroxisomal lumen proteins, respectively. As discussed above, both Pex14 KO and Pex19 KO macrophages showed similarly attenuated PRR responses, suggesting the roles of peroxisomal matrix proteins in the innate immune responses. However, this does not rule out the possibility that peroxisomal membrane plays specific roles in these responses. Indeed, our lab has discovered the presence of RLR adaptor MAVS on the peroxisomal membrane, which induces IFN responses upon RLR activation[56]. Although whether proteins in other PRR pathways are on the peroxisomal membrane remains unknown, NLRP3 inflammasome has been reported to assemble on the mitochondria through the association with MAVS, suggesting the possibilities of the formation of inflammasome assembly on the peroxisomal membrane including MAVS[259]. Future research will examine the localization of PRRs and adaptors including NLRP3 on the peroxisomes by immunofluorescence analysis.

Another question remained unanswered is whether PRR responses regulate peroxisomal metabolism. As mitochondrial metabolism is altered during innate immune responses, with an example being the promotion of fatty acid oxidation by type I IFN[283], it is reasonable to hypothesize that peroxisomal metabolism is similarly regulated by PRR signaling. Indeed, LPS has been reported to decrease peroxisomal fatty acid oxidation[354]. In the future, I suggest that the future work needs to measure peroxisomal metabolism substrates and products in macrophages before and after stimulating cells with TLR, RLR, and NLRP3 ligands to test whether the metabolism is regulated by each PRR.

4.3.2. Pristanic acid-induced rewiring of innate immune responses

Given that peroxisomes play significant roles in PRR responses, a question arises regarding the roles of each metabolic function of peroxisomes. Peroxisomes are responsible for the β-oxidation of very long-chain fatty acids (VLCFAs) as well as α-oxidation of branched-chain fatty acids (BCFAs), whose products are transported to the mitochondria for further

oxidization[302,303]. This study specifically aimed to identify the role of peroxisomal α-oxidation of BCFAs in the PRR responses by treating macrophages with the BCFA substrates including phytanic acid and pristanic acid. In contrast to phytanic acid, pristanic acid inhibited proinflammatory cytokine production upon TLR activation. Considering that pristanic acid accumulates in the context of peroxisomal dysfunction which disturbs the oxidization, these results are consistent with the attenuation of PRR responses in peroxisome-deficient cells that is also found in this thesis. Interestingly, however, we also discovered the enhancement of type I IFN responses by pristanic acid. In-depth investigation revealed that cGAS-STING signaling is responsible for pristanic acid-induced IFN production, and PPARα is required for cGAS activation. Because this study only used a PPARα antagonist, these results need to be validated by genetic depletion of PPARα as well. The main consequences of PPARα activation include peroxisomal proliferation[343]. Intriguingly, this thesis study found that pristanic acid increases peroxisomal abundance in a cGAS-dependent manner. Therefore, it is possible that peroxisomal proliferation by PPARα may require cGAS-dependent IFN production. Although Pex11β-induced peroxisomal proliferation does not induce cGAS activation, it is still possible that peroxisomal function rather than just the amount is required for pristanic acid-induced cGAS activation, which needs further investigation using Pex14-deficient macrophages. Alternatively, pristanic acid may proliferate peroxisomes in a cGAS-dependent but IFN-independent manner, which is consistent to the results that LPS, another inducer of type I IFN responses, did not induce catalase production. This possibility can be tested in the future by examining peroxisomal proliferation in the presence of IFNAR-blocking antibody or in STING-S365A cells that lack IRF3-activating function of STING.

This thesis work also revealed that pristanic acid is an activator of HDAC, which was required for cGAS activation. Dai *et al.* have recently shown that the acetylation of cGAS blocks its self-DNA reactivity[220]. Therefore, it is possible that pristanic acid is able to promote not only histone deacetylation but also cGAS deacetylation to induce type I IFN synthesis. Future work is

needed to examine the acetylation status of cGAS by using site-specific cGAS acetylation antibody upon pristanic acid treatment, as well as assess whether acetylation-mimic mutation of cGAS (K384Q/K394Q/ K414Q)[220] abolishes pristanic acid-induced IFN responses.

Phytanic acid and pristanic acid are obtained from dietary intake such as meat and milk fat, and pristanic acid can be also derived as the product of α-oxidation of phytanic acid[339,341,355]. Although these fatty acids are derived from the same food sources and share functions such as PPARα and HDAC activation[341,346], only pristanic acid, but not phytanic acid, rewires innate immune responses. Therefore, it is suggested that pristanic acid exerts other bioactivities that phytanic acid does not and are required for cGAS activation. Moreover, because phytanic acid is converted to pristanic acid by peroxisomal α-oxidation, the lack of type I IFN responses by phytanic acid might be through the inhibition of pristanic acid-induced responses. To test this hypothesis, cells can be treated with both phytanic acid and pristanic acid simultaneously to examine the inhibitory effects of phytanic acid. Moreover, the treatment of peroxisome-deficient cells with these BCFAs will eliminate possible conversion of phytanic acid into pristanic acid by peroxisomal α-oxidation, which allows us to differentiate the roles of these two BCFAs in innate immunity.

4.3.3. Future Perspectives

This thesis revealed that peroxisomes and their metabolisms are required for PRR responses, and pristanic acid as a peroxisomal FAO substrate rewires macrophages to inflammatory state to antiviral state. Nevertheless, many questions have been unanswered in this study and are the subjects of the future investigations, including the roles of other peroxisomal functions than FAO in these responses. Because this thesis revealed that Pex5, not Pex7, was required for TLR4-induced proIL-1β synthesis in macrophages, it is hypothesized that PTS1-containing proteins in peroxisomal matrix are playing significant roles. CRISPR-based screening of PTS1-containing genes will identify the genes and pathways in peroxisomal metabolisms that

regulate PRR responses. Another related question is the contribution of pristanic acid in the effects of entire peroxisomal dysfunction on the innate immune responses. Because other fatty acids including VLCFAs and BCFAs accumulate upon depletion of peroxisomes[304,311,312], future studies need to measure the levels of each fatty acid in peroxisome-deficient cells as well as examine the effects of each fatty acid treatment on the PRR responses.

Moreover, the mechanism of cGAS activation upon pristanic acid is still unclear, especially what type of DNA activates cGAS. One possibility is that pristanic acid exerts genotoxicity through activating HDAC, which leads to the release of nuclear DNA into the cytosol. An alternative hypothesis is that pristanic acid induces peroxisomal proliferation that alters ROS metabolism in both peroxisomes and mitochondria, which in turn damages mitochondria and releases mtDNA into the cytosolic space. To assess the involvement of mitochondrial metabolism in IFN responses, future studies need to measure the mitochondrial ROS and amount of mtDNA in the cytosol of pristanic acid-treated cells. These results will provide important insights into the cooperative roles of peroxisomes and mitochondria in regulating PRR signaling.

Lastly, it is quite important to examine whether the results found in this thesis apply to *in vivo* and clinical settings. Are Pex19- or Pex14-deficient mice, which lack functional peroxisomes, susceptible to viral and bacterial infections? Do the cells derived from patients of peroxisomal biogenesis disorders such as Zellweger's syndrome have reduced PRR responses? In addition to these questions that can be answered in the lab studies, it is interesting to see by observational study whether people with higher dietary intake of pristanic acid have higher basal expression levels of antiviral cytokines.

4.4. Conclusion

In summary, this thesis identified two organelle-associated anti-self-DNA responses. One is the cGAS catalytic domain-induced type I IFN responses in the mitochondria, as described in Chapter 2. This self-DNA reactivity of cGAS is diverse in mammals, which led us to categorize

cGAS into three distinct classes, including Class 1 (such human and orangutan), Class 2 (mouse), and Class 3 (such as chimpanzee) cGAS. The other anti-self-DNA responses, identified in Chapter 3, is induced by pristanic acid, a peroxisomal fatty acid oxidation substrate. As discussed above, these peroxisome-associated IFN responses may also be linked to mitochondria, which would connect these two independent chapters in this thesis. Altogether, this thesis provides novel evidence of the evolutionarily diverse self-DNA-induced immune responses that are tightly regulated not only by protein network but also by metabolic organelles. The roles of these organelles in other DAMPs-induced signaling will be the subjects of the future studies in the field, as well as how diverse they are in evolution. These future investigations will further advance our understanding of the damage-associated innate immune responses and therefore accelerate the development of therapeutics that target these responses.

Appendices – Supplementary Figures and References

Supplementary Figures

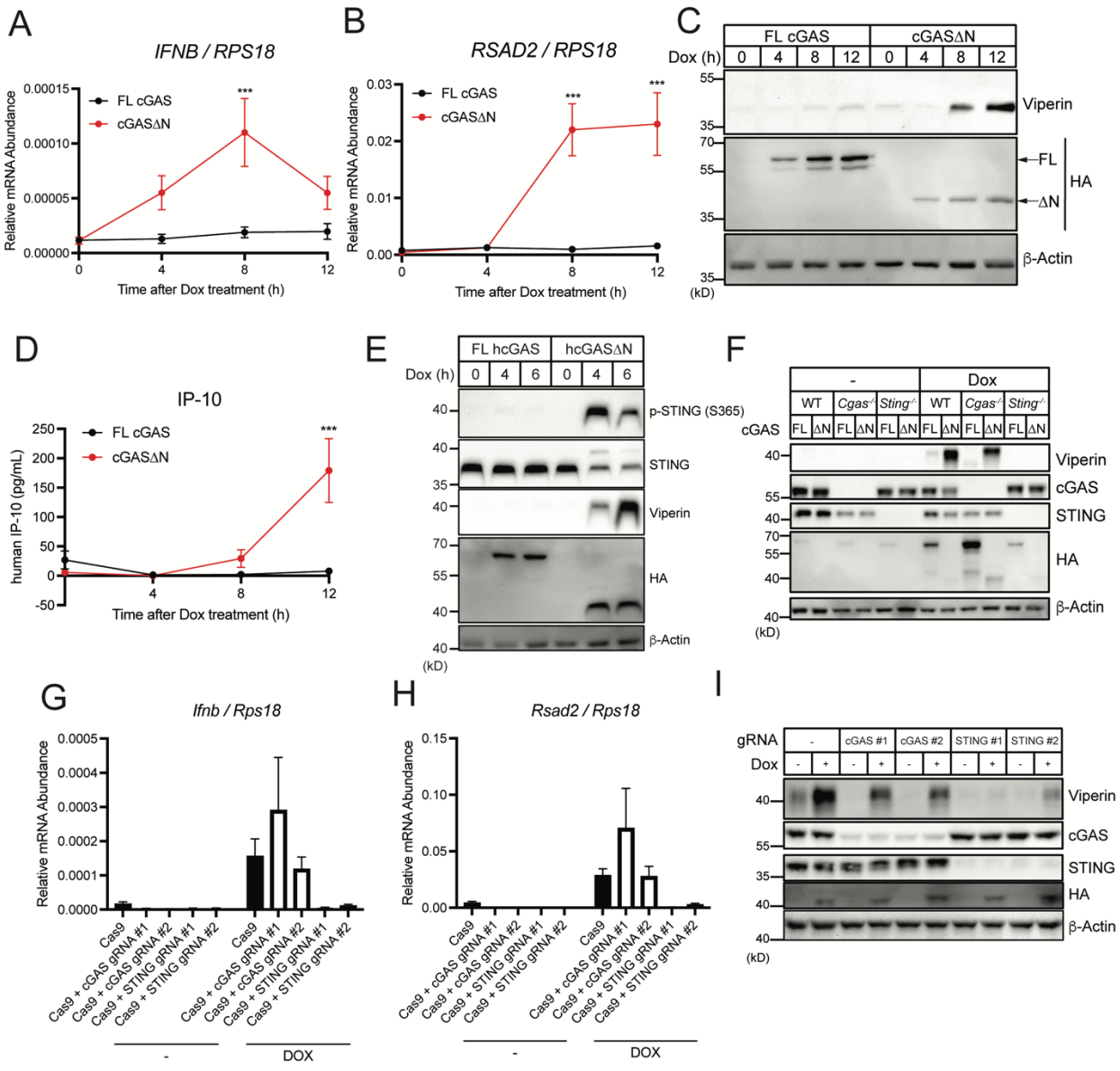

Figure S1. Human cGASΔN induces type I IFN responses in a STING-dependent manner

(A and B) Real-time qRT-PCR analysis of *IFNB* (A) and *RSAD2* (B) mRNAs in normal oral keratinocytes (NOKs). Dox was treated to cells for the induction of FL human cGAS or human cGASΔN, and mRNA expression levels were analyzed at the indicated time points. (C) Immunoblot analysis of NOK cell lysates after the same treatment as in (A) and (B). Arrows in the HA panel indicate FL human cGAS and human cGASΔN. (D) IP-10 ELISA analysis of NOK cell

Figure S1 (Continued)

culture supernatant of the cells in (A) and (B). (E) Immunoblot analysis of lysates from iBMDMs treated with Dox for 4 or 6 hours to induce FL human cGAS or human cGAS∆N expression. (F) Immunoblot analysis of lysates from WT, *Cgas*$^{-/-}$, or *Sting*$^{-/-}$ iBMDMs treated with Dox for 8 hours to induce FL human cGAS or human cGAS∆N expression. (G and H) Real-time qRT-PCR analysis of *Ifnb* (G) and *Rsad2* (H) mRNAs in iBMDMs stably expressing Cas9 and indicated (guide) gRNAs treated with Dox for 8 hours for cGAS expression. (I) Immunoblot analysis of iBMDMs treated with Dox as in (G) and (H). Immunoblot data are the representative from three independent experiments. Graph data are means ± SEM of three (B), four (A), five (G and H), or six (D) independent experiments. Statistical significance was determined by two-way ANOVA and Tukey's multicomparison test. Asterisks indicate the statistical significance between FL hcGAS and hcGAS∆N at each time point (A, B, and D). *$P < 0.05$; **$P < 0.01$; ***$P < 0.001$.

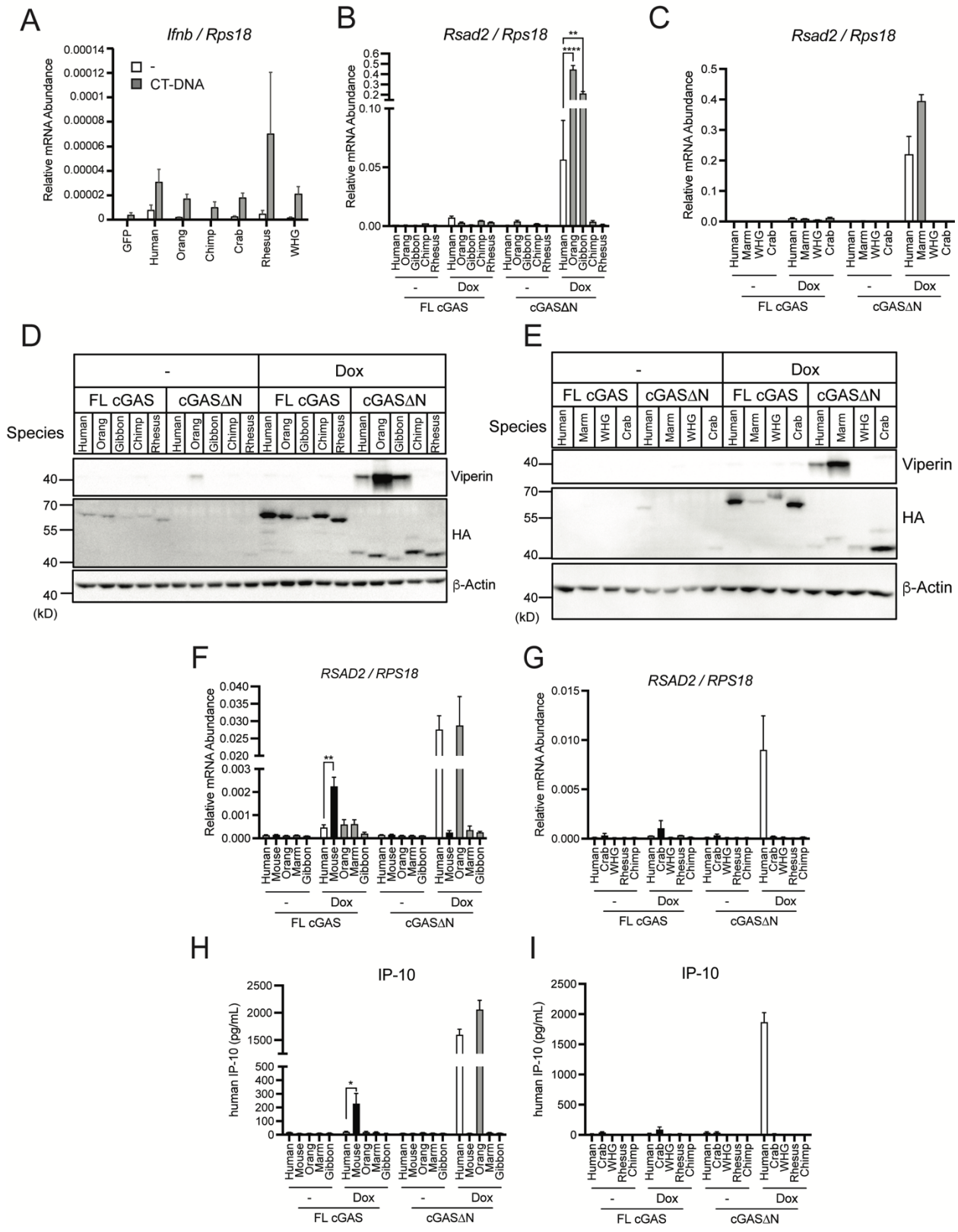
A
Ifnb / Rps18
Relative mRNA Abundance
-
CT-DNA
GFP
Human
Orang
Chimp
Crab
Rhesus
WHG
B
Rsad2 / Rps18
Relative mRNA Abundance
Human
Orang
Gibbon
Chimp
Rhesus
-
Dox
FL cGAS
cGASΔN
C
Rsad2 / Rps18
Relative mRNA Abundance
Human
Marm
WHG
Crab
D
Species
FL cGAS
cGASΔN
Viperin
HA
β-Actin
(kD)
E
F
RSAD2 / RPS18
Relative mRNA Abundance
Mouse
G
RSAD2 / RPS18
H
IP-10
human IP-10 (pg/mL)
I
IP-10

Figure S2. cGAS∆N activities vary across mammalian species

(A) Real-time qRT-PCR analysis of *Ifnb* mRNA in cGAS gRNA-expressing iBMDMs treated with Dox for 8 hours to induce expression of FL cGAS-HA from indicated mammalian species and then transfected with 1 μg/mL CT-DNA for 4 hours. GFP-HA construct was used as a negative control. (B and C) Real-time qRT-PCR analysis of *Rsad2* mRNA in iBMDMs treated with Dox for 8 hours to induce the expression of indicated cGAS. (D and E) Immunoblot analysis of iBMDM lysates treated as in (B) and (C). (F and G) Real-time qRT-PCR analysis of *RSAD2* mRNA in THP-1 cells treated with PMA and Dox for 48 hours to induce the expression of indicated cGAS. (H and I) IP-10 ELISA analysis of the THP-1 culture supernatant in (F) and (G). Immunoblot data are the representative from three independent experiments. Graph data are means ± SEM of three independent experiments. Statistical significance was determined by two-way ANOVA and Tukey's multicomparison test. Asterisks indicate the statistical significance between connected two bars. **P* < 0.05; ***P* < 0.01; ****P* < 0.001.

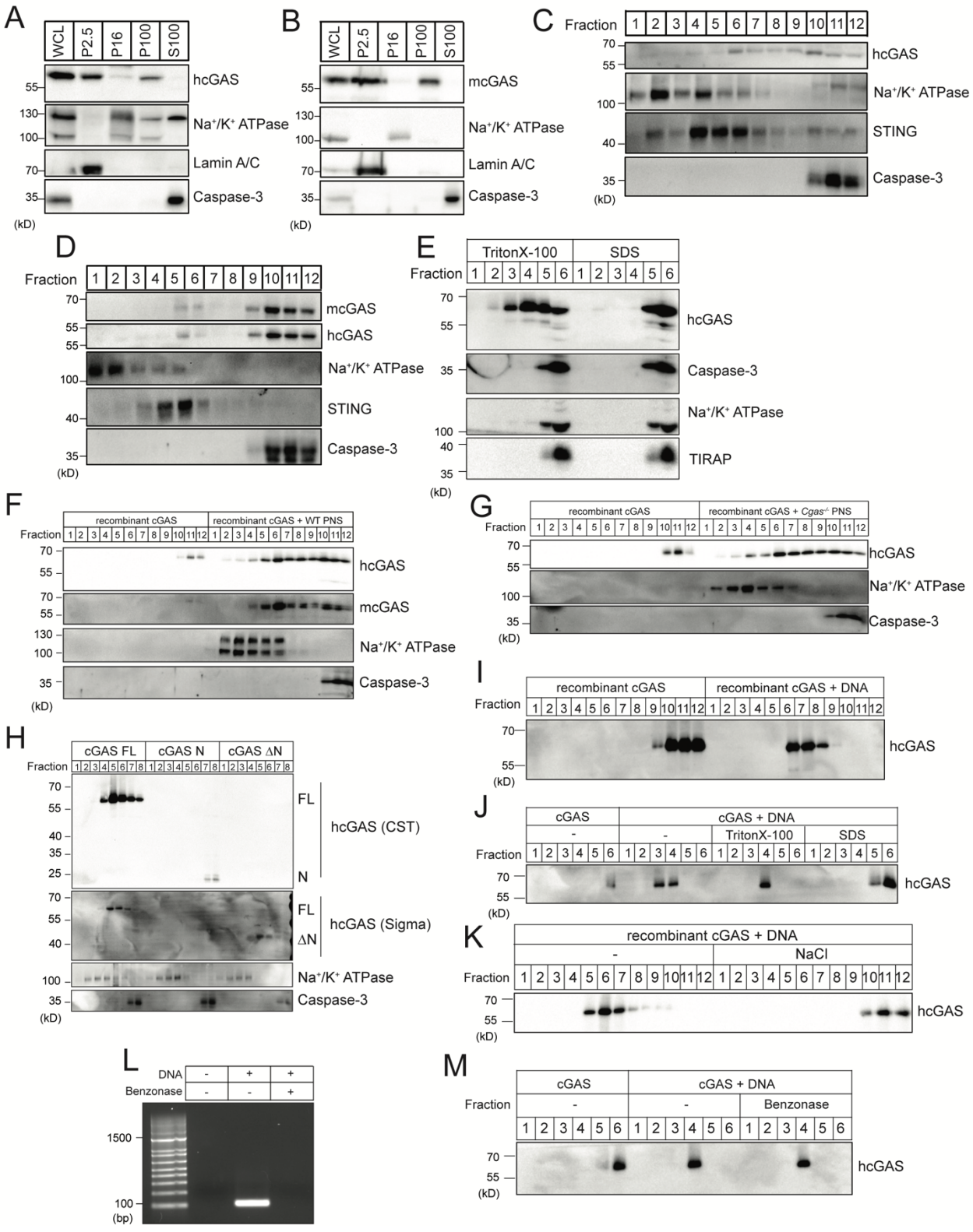
A
WCL
P2.5
P16
P100
S100
hcGAS
Na+/K+ ATPase
Lamin A/C
Caspase-3
(kD)
B
mcGAS
C
Fraction
STING
D
E
TritonX-100
SDS
TIRAP
F
recombinant cGAS
recombinant cGAS + WT PNS
G
recombinant cGAS + Cgas-/- PNS
I
recombinant cGAS + DNA
H
cGAS FL
cGAS N
cGAS ΔN
FL
N
ΔN
hcGAS (CST)
hcGAS (Sigma)
J
cGAS
cGAS + DNA
K
NaCl
L
DNA
Benzonase
1500
100
(bp)
M

Figure S3. cGAS-DNA condensates interfere biochemical analysis of cGAS subcellular localization

(A and B) Subcellular localization of homogenates of THP-1 (A) and iBMDMs (B). (C and D) Membrane flotation assay of post-nuclear supernatants (PNS) from THP-1 (C) and iBMDMs (D). iBMDMs are engineered to stably express FLAG-hcGAS-HA. (E) Membrane flotation assay of PNS from WT iBMDMs in the presence of 1% TritonX-100 or 2% SDS. (F) Membrane flotation assay of recombinant hcGAS protein incubated with PNS from wild type (WT) iBMDMs for 15 minutes. (G) Membrane flotation assay of recombinant hcGAS protein incubated with PNS from $Cgas^{-/-}$ iBMDMs for 15 minutes. (H) Membrane flotation assay of recombinant FL hcGAS, hcGAS 1-160 a.a. (hcGAS N), and hcGAS 157-520 a.a. with K187N/L195R mutation (hcGASΔN) proteins incubated with PNS from WT iBMDMs for 15 minutes. (I) Flotation assay of recombinant hcGAS protein incubated with interferon stimulatory DNA (ISD) for 15 minutes. (J) Flotation assay of recombinant hcGAS protein incubated with ISD for 15 minutes in the presence of 1% TritonX-100 or 2% SDS. (K) Flotation assay of recombinant hcGAS protein incubated with ISD for 15 minutes in the presence of 0.75 M sodium chloride (NaCl). (L) Agarose gel electrophoresis of ISD incubated with 10 U/mL Benzonase for 15 minutes. (M) Flotation assay of recombinant hcGAS protein incubated with ISD for 15 minutes in the presence of 10 U/mL Benzonase. Immunoblot analysis are the representative from three independent experiments.

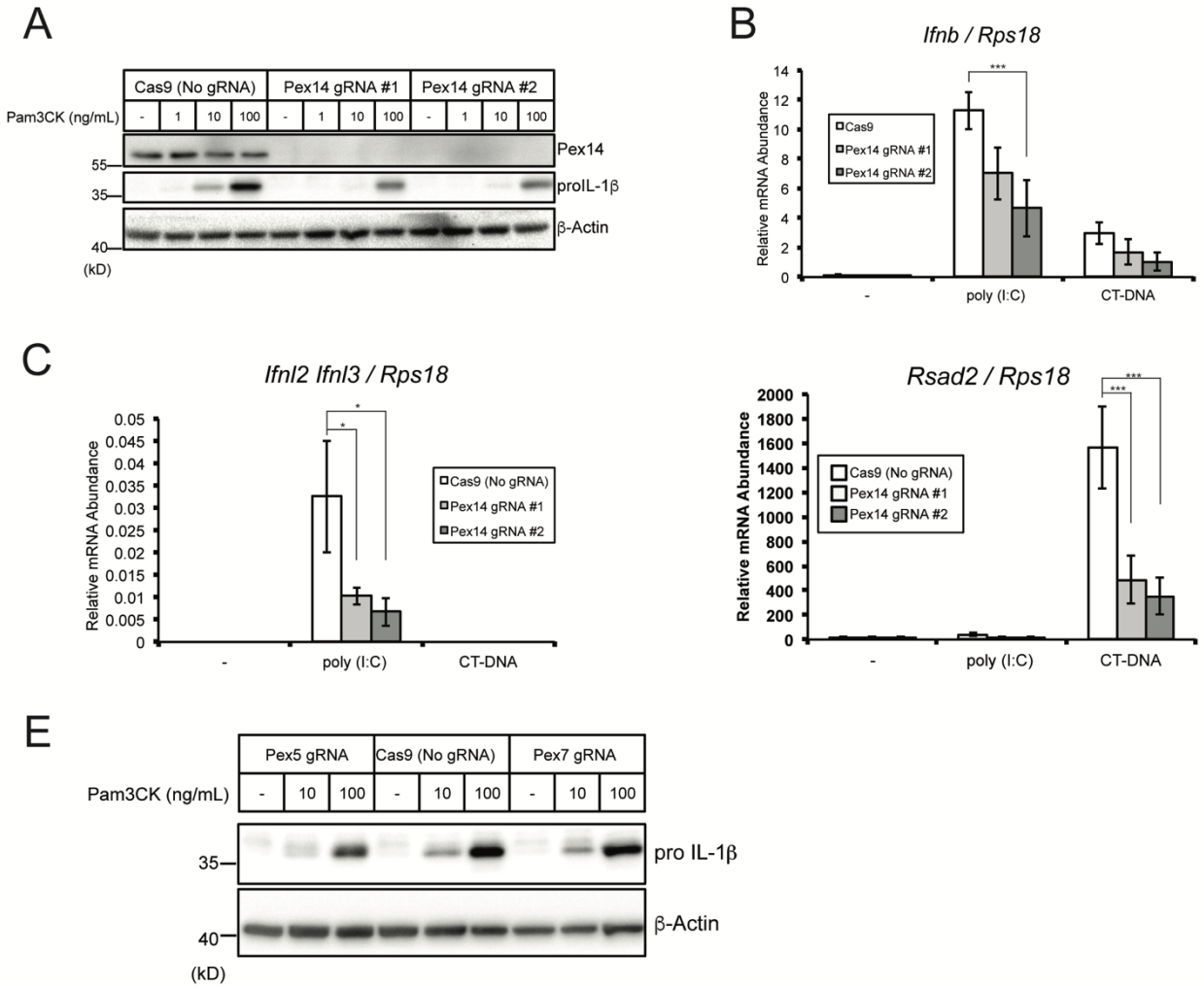

Figure S4. Peroxisomal matrix proteins are required for PRR responses

(A) Immunoblot analysis of lysates from iBMDMs expressing Cas9 and/or *Pex14*-targeting gRNAs. Cells were treated with indicated concentrations of Pam3CK4 for 3 hours. (B-D) Real-Time qRT-PCR analysis of *Ifnb* (B), *Ifnl2/3* (C), and *Rsad2* (D) mRNA in iBMDMs expressing *Pex14*-targeting gRNAs. Cells were transfected with 1 μg/mL poly (I:C) or CT-DNA for 4 hours. (E) Immunoblot analysis of lysates from iBMDMs expressing *Pex5*- or *Pex7*-targeting gRNAs. Cells were treated with indicated concentrations of Pam3CK4 for 3 hours. Immunoblot data are the representative from three independent experiments. Graph data are means ± SEM of three independent experiments.

Figure S4 (Continued)

Asterisks indicate the statistical significance between connected two bars. *P < 0.05; ***P < 0.001.

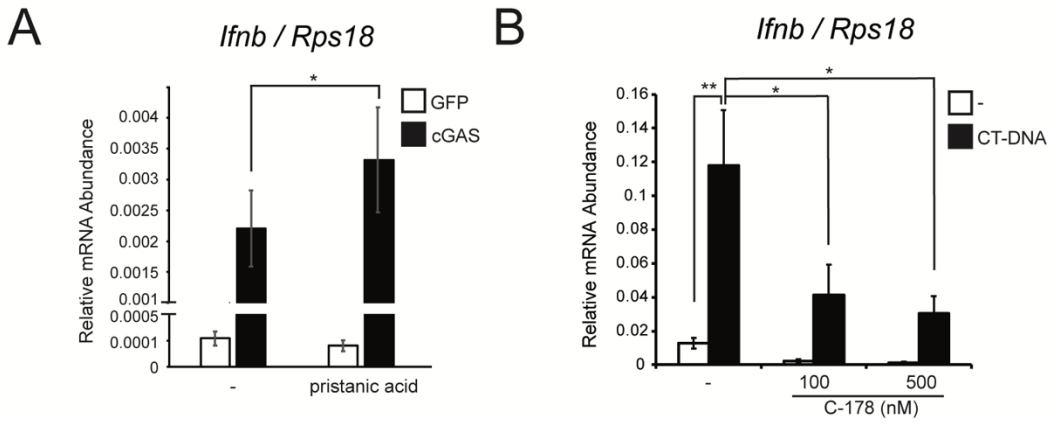

Figure S5. Pristanic acid induces cGAS-STING-dependent IFN responses

(A) Real-Time qRT-PCR analysis of *Ifnb* mRNA in *Cgas*$^{-/-}$ iBMDMs stably expressing GFP or human cGAS. Cells were treated with 30 μM pristanic acid for 24 hours. (B) Real-Time qRT-PCR analysis of *Ifnb* mRNA in iBMDMs treated with indicated concentrations of C-178 for 24 house and transfected with 1 μg/mL CT-DNA for 4 hours. Statistical significance was determined by two-way ANOVA and Tukey's multicomparison test. Asterisks indicate the statistical significance between connected two bars. *P < 0.05; **P < 0.01.

References

1 Janeway, C. A., Jr. & Medzhitov, R. Innate immune recognition. *Annu Rev Immunol* **20**, 197-216, doi:10.1146/annurev.immunol.20.083001.084359 (2002).

2 Takeuchi, O. & Akira, S. Pattern recognition receptors and inflammation. *Cell* **140**, 805-820, doi:10.1016/j.cell.2010.01.022 (2010).

3 Brubaker, S. W., Bonham, K. S., Zanoni, I. & Kagan, J. C. Innate immune pattern recognition: a cell biological perspective. *Annu Rev Immunol* **33**, 257-290, doi:10.1146/annurev-immunol-032414-112240 (2015).

4 Akira, S. & Takeda, K. Toll-like receptor signalling. *Nat Rev Immunol* **4**, 499-511, doi:10.1038/nri1391 (2004).

5 Medzhitov, R., Preston-Hurlburt, P. & Janeway, C. A., Jr. A human homologue of the Drosophila Toll protein signals activation of adaptive immunity. *Nature* **388**, 394-397, doi:10.1038/41131 (1997).

6 Qureshi, S. T. *et al.* Endotoxin-tolerant mice have mutations in Toll-like receptor 4 (Tlr4). *J Exp Med* **189**, 615-625, doi:10.1084/jem.189.4.615 (1999).

7 Poltorak, A. *et al.* Defective LPS signaling in C3H/HeJ and C57BL/10ScCr mice: mutations in Tlr4 gene. *Science* **282**, 2085-2088, doi:10.1126/science.282.5396.2085 (1998).

8 Hoshino, K. *et al.* Cutting edge: Toll-like receptor 4 (TLR4)-deficient mice are hyporesponsive to lipopolysaccharide: evidence for TLR4 as the Lps gene product. *J Immunol* **162**, 3749-3752 (1999).

9 Shimazu, R. *et al.* MD-2, a molecule that confers lipopolysaccharide responsiveness on Toll-like receptor 4. *J Exp Med* **189**, 1777-1782, doi:10.1084/jem.189.11.1777 (1999).

10 Wright, S. D., Ramos, R. A., Tobias, P. S., Ulevitch, R. J. & Mathison, J. C. CD14, a receptor for complexes of lipopolysaccharide (LPS) and LPS binding protein. *Science* **249**, 1431-1433, doi:10.1126/science.1698311 (1990).

11 Fitzgerald, K. A. *et al.* Mal (MyD88-adapter-like) is required for Toll-like receptor-4 signal transduction. *Nature* **413**, 78-83, doi:10.1038/35092578 (2001).

12 Kagan, J. C. & Medzhitov, R. Phosphoinositide-mediated adaptor recruitment controls Toll-like receptor signaling. *Cell* **125**, 943-955, doi:10.1016/j.cell.2006.03.047 (2006).

13 Yamamoto, M. *et al.* Essential role for TIRAP in activation of the signalling cascade shared by TLR2 and TLR4. *Nature* **420**, 324-329, doi:10.1038/nature01182 (2002).

14 Horng, T., Barton, G. M., Flavell, R. A. & Medzhitov, R. The adaptor molecule TIRAP provides signalling specificity for Toll-like receptors. *Nature* **420**, 329-333, doi:10.1038/nature01180 (2002).

15 Motshwene, P. G. *et al.* An oligomeric signaling platform formed by the Toll-like receptor signal transducers MyD88 and IRAK-4. *J Biol Chem* **284**, 25404-25411, doi:10.1074/jbc.M109.022392 (2009).

16 Lin, S. C., Lo, Y. C. & Wu, H. Helical assembly in the MyD88-IRAK4-IRAK2 complex in TLR/IL-1R signalling. *Nature* **465**, 885-890, doi:10.1038/nature09121 (2010).

17 Gay, N. J., Symmons, M. F., Gangloff, M. & Bryant, C. E. Assembly and localization of Toll-like receptor signalling complexes. *Nat Rev Immunol* **14**, 546-558, doi:10.1038/nri3713 (2014).

18 Zanoni, I. *et al.* CD14 controls the LPS-induced endocytosis of Toll-like receptor 4. *Cell* **147**, 868-880, doi:10.1016/j.cell.2011.09.051 (2011).

19 Kagan, J. C. *et al.* TRAM couples endocytosis of Toll-like receptor 4 to the induction of interferon-β. *Nat Immunol* **9**, 361-368, doi:10.1038/ni1569 (2008).

20 Tanimura, N., Saitoh, S., Matsumoto, F., Akashi-Takamura, S. & Miyake, K. Roles for LPS-dependent interaction and relocation of TLR4 and TRAM in TRIF-signaling. *Biochem Biophys Res Commun* **368**, 94-99, doi:10.1016/j.bbrc.2008.01.061 (2008).

21 Fitzgerald, K. A. *et al.* IKKε and TBK1 are essential components of the IRF3 signaling pathway. *Nat Immunol* **4**, 491-496, doi:10.1038/ni921 (2003).

22 Yamamoto, M. *et al.* Role of adaptor TRIF in the MyD88-independent toll-like receptor signaling pathway. *Science* **301**, 640-643, doi:10.1126/science.1087262 (2003).

23 Underhill, D. M., Ozinsky, A., Smith, K. D. & Aderem, A. Toll-like receptor-2 mediates mycobacteria-induced proinflammatory signaling in macrophages. *Proc Natl Acad Sci U S A* **96**, 14459-14463, doi:10.1073/pnas.96.25.14459 (1999).

24 Lien, E. *et al.* Toll-like receptor 2 functions as a pattern recognition receptor for diverse bacterial products. *J Biol Chem* **274**, 33419-33425, doi:10.1074/jbc.274.47.33419 (1999).

25 Ozinsky, A. *et al.* The repertoire for pattern recognition of pathogens by the innate immune system is defined by cooperation between toll-like receptors. *Proc Natl Acad Sci U S A* **97**, 13766-13771, doi:10.1073/pnas.250476497 (2000).

26 Morr, M., Takeuchi, O., Akira, S., Simon, M. M. & Muhlradt, P. F. Differential recognition of structural details of bacterial lipopeptides by toll-like receptors. *Eur J Immunol* **32**, 3337-3347, doi:10.1002/1521-4141(200212)32:12<3337::AID-IMMU3337>3.0.CO;2-# (2002).

27 Takeuchi, O., Hoshino, K. & Akira, S. Cutting edge: TLR2-deficient and MyD88-deficient mice are highly susceptible to Staphylococcus aureus infection. *J Immunol* **165**, 5392-5396, doi:10.4049/jimmunol.165.10.5392 (2000).

28 Takeuchi, O. *et al.* Cutting edge: role of Toll-like receptor 1 in mediating immune response to microbial lipoproteins. *J Immunol* **169**, 10-14, doi:10.4049/jimmunol.169.1.10 (2002).

29 Oshiumi, H., Matsumoto, M., Funami, K., Akazawa, T. & Seya, T. TICAM-1, an adaptor molecule that participates in Toll-like receptor 3-mediated interferon-β induction. *Nat Immunol* **4**, 161-167, doi:10.1038/ni886 (2003).

30 Matsumoto, M. *et al.* Subcellular localization of Toll-like receptor 3 in human dendritic cells. *J Immunol* **171**, 3154-3162, doi:10.4049/jimmunol.171.6.3154 (2003).

31 Alexopoulou, L., Holt, A. C., Medzhitov, R. & Flavell, R. A. Recognition of double-stranded RNA and activation of NF-κB by Toll-like receptor 3. *Nature* **413**, 732-738, doi:10.1038/35099560 (2001).

32 Hoebe, K. *et al.* Identification of Lps2 as a key transducer of MyD88-independent TIR signalling. *Nature* **424**, 743-748, doi:10.1038/nature01889 (2003).

33 Rehwinkel, J. & Gack, M. U. RIG-I-like receptors: their regulation and roles in RNA sensing. *Nat Rev Immunol* **20**, 537-551, doi:10.1038/s41577-020-0288-3 (2020).

34 Yoneyama, M. *et al.* The RNA helicase RIG-I has an essential function in double-stranded RNA-induced innate antiviral responses. *Nat Immunol* **5**, 730-737, doi:10.1038/ni1087 (2004).

35 Yoneyama, M. *et al.* Shared and unique functions of the DExD/H-box helicases RIG-I, MDA5, and LGP2 in antiviral innate immunity. *J Immunol* **175**, 2851-2858, doi:10.4049/jimmunol.175.5.2851 (2005).

36 Kell, A. M. & Gale, M., Jr. RIG-I in RNA virus recognition. *Virology* **479-480**, 110-121, doi:10.1016/j.virol.2015.02.017 (2015).

37 Chow, K. T., Gale, M., Jr. & Loo, Y. M. RIG-I and Other RNA Sensors in Antiviral Immunity. *Annu Rev Immunol* **36**, 667-694, doi:10.1146/annurev-immunol-042617-053309 (2018).

38 Schlee, M. *et al.* Recognition of 5' triphosphate by RIG-I helicase requires short blunt double-stranded RNA as contained in panhandle of negative-strand virus. *Immunity* **31**, 25-34, doi:10.1016/j.immuni.2009.05.008 (2009).

39 Schmidt, A. *et al.* 5'-triphosphate RNA requires base-paired structures to activate antiviral signaling via RIG-I. *Proc Natl Acad Sci U S A* **106**, 12067-12072, doi:10.1073/pnas.0900971106 (2009).

40 Goubau, D. *et al.* Antiviral immunity via RIG-I-mediated recognition of RNA bearing 5'-diphosphates. *Nature* **514**, 372-375, doi:10.1038/nature13590 (2014).

41 Kato, H. *et al.* Length-dependent recognition of double-stranded ribonucleic acids by retinoic acid-inducible gene-I and melanoma differentiation-associated gene 5. *J Exp Med* **205**, 1601-1610, doi:10.1084/jem.20080091 (2008).

42 Kato, H. *et al.* Differential roles of MDA5 and RIG-I helicases in the recognition of RNA viruses. *Nature* **441**, 101-105, doi:10.1038/nature04734 (2006).

43 Pichlmair, A. *et al.* Activation of MDA5 requires higher-order RNA structures generated during virus infection. *J Virol* **83**, 10761-10769, doi:10.1128/JVI.00770-09 (2009).

44 Kowalinski, E. *et al.* Structural basis for the activation of innate immune pattern-recognition receptor RIG-I by viral RNA. *Cell* **147**, 423-435, doi:10.1016/j.cell.2011.09.039 (2011).

45 Oshiumi, H., Matsumoto, M., Hatakeyama, S. & Seya, T. Riplet/RNF135, a RING finger protein, ubiquitinates RIG-I to promote interferon-β induction during the early phase of viral infection. *J Biol Chem* **284**, 807-817, doi:10.1074/jbc.M804259200 (2009).

46 Zeng, W. *et al.* Reconstitution of the RIG-I pathway reveals a signaling role of unanchored polyubiquitin chains in innate immunity. *Cell* **141**, 315-330, doi:10.1016/j.cell.2010.03.029 (2010).

47 Jiang, X. *et al.* Ubiquitin-induced oligomerization of the RNA sensors RIG-I and MDA5 activates antiviral innate immune response. *Immunity* **36**, 959-973, doi:10.1016/j.immuni.2012.03.022 (2012).

48 Patel, J. R. *et al.* ATPase-driven oligomerization of RIG-I on RNA allows optimal activation of type-I interferon. *EMBO Rep* **14**, 780-787, doi:10.1038/embor.2013.102 (2013).

49 Berke, I. C. & Modis, Y. MDA5 cooperatively forms dimers and ATP-sensitive filaments upon binding double-stranded RNA. *EMBO J* **31**, 1714-1726, doi:10.1038/emboj.2012.19 (2012).

50 Peisley, A. *et al.* Cooperative assembly and dynamic disassembly of MDA5 filaments for viral dsRNA recognition. *Proc Natl Acad Sci U S A* **108**, 21010-21015, doi:10.1073/pnas.1113651108 (2011).

51 Seth, R. B., Sun, L., Ea, C. K. & Chen, Z. J. Identification and characterization of MAVS, a mitochondrial antiviral signaling protein that activates NF-κB and IRF 3. *Cell* **122**, 669-682, doi:10.1016/j.cell.2005.08.012 (2005).

52 Xu, L. G. *et al.* VISA is an adapter protein required for virus-triggered IFN-β signaling. *Mol Cell* **19**, 727-740, doi:10.1016/j.molcel.2005.08.014 (2005).

53 Meylan, E. *et al.* Cardif is an adaptor protein in the RIG-I antiviral pathway and is targeted by hepatitis C virus. *Nature* **437**, 1167-1172, doi:10.1038/nature04193 (2005).

54 Kawai, T. *et al.* IPS-1, an adaptor triggering RIG-I- and Mda5-mediated type I interferon induction. *Nat Immunol* **6**, 981-988, doi:10.1038/ni1243 (2005).

55 Horner, S. M., Liu, H. M., Park, H. S., Briley, J. & Gale, M., Jr. Mitochondrial-associated endoplasmic reticulum membranes (MAM) form innate immune synapses and are targeted by hepatitis C virus. *Proc Natl Acad Sci U S A* **108**, 14590-14595, doi:10.1073/pnas.1110133108 (2011).

56 Dixit, E. *et al.* Peroxisomes are signaling platforms for antiviral innate immunity. *Cell* **141**, 668-681, doi:10.1016/j.cell.2010.04.018 (2010).

57 Liu, S. *et al.* MAVS recruits multiple ubiquitin E3 ligases to activate antiviral signaling cascades. *Elife* **2**, e00785, doi:10.7554/eLife.00785 (2013).

58 Thornberry, N. A. *et al.* A novel heterodimeric cysteine protease is required for interleukin-1β processing in monocytes. *Nature* **356**, 768-774, doi:10.1038/356768a0 (1992).

59 Cerretti, D. P. *et al.* Molecular cloning of the interleukin-1β converting enzyme. *Science* **256**, 97-100, doi:10.1126/science.1373520 (1992).

60 Gu, Y. *et al.* Activation of interferon-γ inducing factor mediated by interleukin-1β converting enzyme. *Science* **275**, 206-209, doi:10.1126/science.275.5297.206 (1997).

61 Ghayur, T. *et al.* Caspase-1 processes IFN-γ-inducing factor and regulates LPS-induced IFN-gamma production. *Nature* **386**, 619-623, doi:10.1038/386619a0 (1997).

62 Martinon, F., Burns, K. & Tschopp, J. The inflammasome: a molecular platform triggering activation of inflammatory caspases and processing of proIL-β. *Mol Cell* **10**, 417-426, doi:10.1016/s1097-2765(02)00599-3 (2002).

63 Agostini, L. *et al.* NALP3 forms an IL-1β-processing inflammasome with increased activity in Muckle-Wells autoinflammatory disorder. *Immunity* **20**, 319-325, doi:10.1016/s1074-7613(04)00046-9 (2004).

64 Miao, E. A. *et al.* Cytoplasmic flagellin activates caspase-1 and secretion of interleukin 1β via Ipaf. *Nat Immunol* **7**, 569-575, doi:10.1038/ni1344 (2006).

65 Burckstummer, T. *et al.* An orthogonal proteomic-genomic screen identifies AIM2 as a cytoplasmic DNA sensor for the inflammasome. *Nat Immunol* **10**, 266-272, doi:10.1038/ni.1702 (2009).

66 Hornung, V. *et al.* AIM2 recognizes cytosolic dsDNA and forms a caspase-1-activating inflammasome with ASC. *Nature* **458**, 514-518, doi:10.1038/nature07725 (2009).

67 Fernandes-Alnemri, T., Yu, J. W., Datta, P., Wu, J. & Alnemri, E. S. AIM2 activates the inflammasome and cell death in response to cytoplasmic DNA. *Nature* **458**, 509-513, doi:10.1038/nature07710 (2009).

68 Roberts, T. L. *et al.* HIN-200 proteins regulate caspase activation in response to foreign cytoplasmic DNA. *Science* **323**, 1057-1060, doi:10.1126/science.1169841 (2009).

69 Xu, H. *et al.* Innate immune sensing of bacterial modifications of Rho GTPases by the Pyrin inflammasome. *Nature* **513**, 237-241, doi:10.1038/nature13449 (2014).

70 Broz, P. & Dixit, V. M. Inflammasomes: mechanism of assembly, regulation and signalling. *Nat Rev Immunol* **16**, 407-420, doi:10.1038/nri.2016.58 (2016).

71 Rathinam, V. A. & Fitzgerald, K. A. Inflammasome Complexes: Emerging Mechanisms and Effector Functions. *Cell* **165**, 792-800, doi:10.1016/j.cell.2016.03.046 (2016).

72 Sharma, D. & Kanneganti, T. D. The cell biology of inflammasomes: Mechanisms of inflammasome activation and regulation. *J Cell Biol* **213**, 617-629, doi:10.1083/jcb.201602089 (2016).

73 Mariathasan, S. *et al.* Cryopyrin activates the inflammasome in response to toxins and ATP. *Nature* **440**, 228-232, doi:10.1038/nature04515 (2006).

74 Kanneganti, T. D. *et al.* Bacterial RNA and small antiviral compounds activate caspase-1 through cryopyrin/Nalp3. *Nature* **440**, 233-236, doi:10.1038/nature04517 (2006).

75 Sander, L. E. *et al.* Detection of prokaryotic mRNA signifies microbial viability and promotes immunity. *Nature* **474**, 385-389, doi:10.1038/nature10072 (2011).

76 Kailasan Vanaja, S. *et al.* Bacterial RNA:DNA hybrids are activators of the NLRP3 inflammasome. *Proc Natl Acad Sci U S A* **111**, 7765-7770, doi:10.1073/pnas.1400075111 (2014).

77 Hornung, V. *et al.* Silica crystals and aluminum salts activate the NALP3 inflammasome through phagosomal destabilization. *Nat Immunol* **9**, 847-856, doi:10.1038/ni.1631 (2008).

78 Cassel, S. L. *et al.* The Nalp3 inflammasome is essential for the development of silicosis. *Proc Natl Acad Sci U S A* **105**, 9035-9040, doi:10.1073/pnas.0803933105 (2008).

79 Dostert, C. *et al.* Innate immune activation through Nalp3 inflammasome sensing of asbestos and silica. *Science* **320**, 674-677, doi:10.1126/science.1156995 (2008).

80 Martinon, F., Petrilli, V., Mayor, A., Tardivel, A. & Tschopp, J. Gout-associated uric acid crystals activate the NALP3 inflammasome. *Nature* **440**, 237-241, doi:10.1038/nature04516 (2006).

81 Duewell, P. *et al.* NLRP3 inflammasomes are required for atherogenesis and activated by cholesterol crystals. *Nature* **464**, 1357-1361, doi:10.1038/nature08938 (2010).

82 Manji, G. A. *et al.* PYPAF1, a PYRIN-containing Apaf1-like protein that assembles with ASC and regulates activation of NF-κB. *J Biol Chem* **277**, 11570-11575, doi:10.1074/jbc.M112208200 (2002).

83 Aganna, E. *et al.* Association of mutations in the NALP3/CIAS1/PYPAF1 gene with a broad phenotype including recurrent fever, cold sensitivity, sensorineural deafness, and AA amyloidosis. *Arthritis Rheum* **46**, 2445-2452, doi:10.1002/art.10509 (2002).

84 Hoffman, H. M., Mueller, J. L., Broide, D. H., Wanderer, A. A. & Kolodner, R. D. Mutation of a new gene encoding a putative pyrin-like protein causes familial cold

autoinflammatory syndrome and Muckle-Wells syndrome. *Nat Genet* **29**, 301-305, doi:10.1038/ng756 (2001).

85 Bauernfeind, F. G. *et al.* Cutting edge: NF-κB activating pattern recognition and cytokine receptors license NLRP3 inflammasome activation by regulating NLRP3 expression. *J Immunol* **183**, 787-791, doi:10.4049/jimmunol.0901363 (2009).

86 Swanson, K. V., Deng, M. & Ting, J. P. The NLRP3 inflammasome: molecular activation and regulation to therapeutics. *Nat Rev Immunol* **19**, 477-489, doi:10.1038/s41577-019-0165-0 (2019).

87 Cai, X. *et al.* Prion-like polymerization underlies signal transduction in antiviral immune defense and inflammasome activation. *Cell* **156**, 1207-1222, doi:10.1016/j.cell.2014.01.063 (2014).

88 Lu, A. *et al.* Unified polymerization mechanism for the assembly of ASC-dependent inflammasomes. *Cell* **156**, 1193-1206, doi:10.1016/j.cell.2014.02.008 (2014).

89 He, W. T. *et al.* Gasdermin D is an executor of pyroptosis and required for interleukin-1β secretion. *Cell Res* **25**, 1285-1298, doi:10.1038/cr.2015.139 (2015).

90 Shi, J. *et al.* Cleavage of GSDMD by inflammatory caspases determines pyroptotic cell death. *Nature* **526**, 660-665, doi:10.1038/nature15514 (2015).

91 Ding, J. *et al.* Pore-forming activity and structural autoinhibition of the gasdermin family. *Nature* **535**, 111-116, doi:10.1038/nature18590 (2016).

92 Liu, X. *et al.* Inflammasome-activated gasdermin D causes pyroptosis by forming membrane pores. *Nature* **535**, 153-158, doi:10.1038/nature18629 (2016).

93 Evavold, C. L. *et al.* The Pore-Forming Protein Gasdermin D Regulates Interleukin-1 Secretion from Living Macrophages. *Immunity* **48**, 35-44 e36, doi:10.1016/j.immuni.2017.11.013 (2018).

94 Monteleone, M. *et al.* Interleukin-1β Maturation Triggers Its Relocation to the Plasma Membrane for Gasdermin-D-Dependent and -Independent Secretion. *Cell Rep* **24**, 1425-1433, doi:10.1016/j.celrep.2018.07.027 (2018).

95 Bergsbaken, T., Fink, S. L. & Cookson, B. T. Pyroptosis: host cell death and inflammation. *Nat Rev Microbiol* **7**, 99-109, doi:10.1038/nrmicro2070 (2009).

96 Jin, T. *et al.* Structures of the HIN domain:DNA complexes reveal ligand binding and activation mechanisms of the AIM2 inflammasome and IFI16 receptor. *Immunity* **36**, 561-571, doi:10.1016/j.immuni.2012.02.014 (2012).

97 Jin, T., Perry, A., Smith, P., Jiang, J. & Xiao, T. S. Structure of the absent in melanoma 2 (AIM2) pyrin domain provides insights into the mechanisms of AIM2 autoinhibition and inflammasome assembly. *J Biol Chem* **288**, 13225-13235, doi:10.1074/jbc.M113.468033 (2013).

98 Lu, A. *et al.* Plasticity in PYD assembly revealed by cryo-EM structure of the PYD filament of AIM2. *Cell Discov* **1**, doi:10.1038/celldisc.2015.13 (2015).

99 Morrone, S. R. *et al.* Assembly-driven activation of the AIM2 foreign-dsDNA sensor provides a polymerization template for downstream ASC. *Nat Commun* **6**, 7827, doi:10.1038/ncomms8827 (2015).

100 Briard, B., Place, D. E. & Kanneganti, T. D. DNA Sensing in the Innate Immune Response. *Physiology (Bethesda)* **35**, 112-124, doi:10.1152/physiol.00022.2019 (2020).

101 Sun, L., Wu, J., Du, F., Chen, X. & Chen, Z. J. Cyclic GMP-AMP synthase is a cytosolic DNA sensor that activates the type I interferon pathway. *Science* **339**, 786-791, doi:10.1126/science.1232458 (2013).

102 Kranzusch, P. J., Lee, A. S., Berger, J. M. & Doudna, J. A. Structure of human cGAS reveals a conserved family of second-messenger enzymes in innate immunity. *Cell Rep* **3**, 1362-1368, doi:10.1016/j.celrep.2013.05.008 (2013).

103 Wu, J. *et al.* Cyclic GMP-AMP is an endogenous second messenger in innate immune signaling by cytosolic DNA. *Science* **339**, 826-830, doi:10.1126/science.1229963 (2013).

104 Ishikawa, H. & Barber, G. N. STING is an endoplasmic reticulum adaptor that facilitates innate immune signalling. *Nature* **455**, 674-678, doi:10.1038/nature07317 (2008).

105 Zhang, X. *et al.* Cyclic GMP-AMP containing mixed phosphodiester linkages is an endogenous high-affinity ligand for STING. *Mol Cell* **51**, 226-235, doi:10.1016/j.molcel.2013.05.022 (2013).

106 Ablasser, A. *et al.* cGAS produces a 2'-5'-linked cyclic dinucleotide second messenger that activates STING. *Nature* **498**, 380-384, doi:10.1038/nature12306 (2013).

107 Diner, E. J. *et al.* The innate immune DNA sensor cGAS produces a noncanonical cyclic dinucleotide that activates human STING. *Cell Rep* **3**, 1355-1361, doi:10.1016/j.celrep.2013.05.009 (2013).

108 Gao, P. *et al.* Cyclic [G(2',5')pA(3',5')p] is the metazoan second messenger produced by DNA-activated cyclic GMP-AMP synthase. *Cell* **153**, 1094-1107, doi:10.1016/j.cell.2013.04.046 (2013).

109 Burdette, D. L. *et al.* STING is a direct innate immune sensor of cyclic di-GMP. *Nature* **478**, 515-518, doi:10.1038/nature10429 (2011).

110 Shang, G., Zhang, C., Chen, Z. J., Bai, X. C. & Zhang, X. Cryo-EM structures of STING reveal its mechanism of activation by cyclic GMP-AMP. *Nature* **567**, 389-393, doi:10.1038/s41586-019-0998-5 (2019).

111 Ishikawa, H., Ma, Z. & Barber, G. N. STING regulates intracellular DNA-mediated, type I interferon-dependent innate immunity. *Nature* **461**, 788-792, doi:10.1038/nature08476 (2009).

112 Gui, X. *et al.* Autophagy induction via STING trafficking is a primordial function of the cGAS pathway. *Nature* **567**, 262-266, doi:10.1038/s41586-019-1006-9 (2019).

113 Mukai, K. *et al.* Activation of STING requires palmitoylation at the Golgi. *Nat Commun* **7**, 11932, doi:10.1038/ncomms11932 (2016).

114 Dobbs, N. *et al.* STING Activation by Translocation from the ER Is Associated with Infection and Autoinflammatory Disease. *Cell Host Microbe* **18**, 157-168, doi:10.1016/j.chom.2015.07.001 (2015).

115 Zhao, B. *et al.* A conserved PLPLRT/SD motif of STING mediates the recruitment and activation of TBK1. *Nature* **569**, 718-722, doi:10.1038/s41586-019-1228-x (2019).

116 Zhang, C. *et al.* Structural basis of STING binding with and phosphorylation by TBK1. *Nature* **567**, 394-398, doi:10.1038/s41586-019-1000-2 (2019).

117 Liu, S. *et al.* Phosphorylation of innate immune adaptor proteins MAVS, STING, and TRIF induces IRF3 activation. *Science* **347**, aaa2630, doi:10.1126/science.aaa2630 (2015).

118 Abe, T. & Barber, G. N. Cytosolic-DNA-mediated, STING-dependent proinflammatory gene induction necessitates canonical NF-κB activation through TBK1. *J Virol* **88**, 5328-5341, doi:10.1128/JVI.00037-14 (2014).

119 Schneider, W. M., Chevillotte, M. D. & Rice, C. M. Interferon-stimulated genes: a complex web of host defenses. *Annu Rev Immunol* **32**, 513-545, doi:10.1146/annurev-immunol-032713-120231 (2014).

120 Balka, K. R. *et al.* TBK1 and IKKε Act Redundantly to Mediate STING-Induced NF-κB Responses in Myeloid Cells. *Cell Rep* **31**, 107492, doi:10.1016/j.celrep.2020.03.056 (2020).

121 Yum, S., Li, M., Fang, Y. & Chen, Z. J. TBK1 recruitment to STING activates both IRF3 and NF-κB that mediate immune defense against tumors and viral infections. *Proc Natl Acad Sci U S A* **118**, doi:10.1073/pnas.2100225118 (2021).

122 Yamashiro, L. H. *et al.* Interferon-independent STING signaling promotes resistance to HSV-1 in vivo. *Nat Commun* **11**, 3382, doi:10.1038/s41467-020-17156-x (2020).

123 Wu, J., Dobbs, N., Yang, K. & Yan, N. Interferon-Independent Activities of Mammalian STING Mediate Antiviral Response and Tumor Immune Evasion. *Immunity* **53**, 115-126 e115, doi:10.1016/j.immuni.2020.06.009 (2020).

124 Sharpe, A. H. & Freeman, G. J. The B7-CD28 superfamily. *Nat Rev Immunol* **2**, 116-126, doi:10.1038/nri727 (2002).

125 Li, T. *et al.* TBK1 recruitment to STING mediates autoinflammatory arthritis caused by defective DNA clearance. *J Exp Med* **219**, doi:10.1084/jem.20211539 (2022).

126 Klionsky, D. J. & Emr, S. D. Autophagy as a regulated pathway of cellular degradation. *Science* **290**, 1717-1721, doi:10.1126/science.290.5497.1717 (2000).

127 Shahnazari, S. & Brumell, J. H. Mechanisms and consequences of bacterial targeting by the autophagy pathway. *Curr Opin Microbiol* **14**, 68-75, doi:10.1016/j.mib.2010.11.001 (2011).

128 Schoggins, J. W. *et al.* Pan-viral specificity of IFN-induced genes reveals new roles for cGAS in innate immunity. *Nature* **505**, 691-695, doi:10.1038/nature12862 (2014).

129 Watson, R. O. *et al.* The Cytosolic Sensor cGAS Detects *Mycobacterium tuberculosis* DNA to Induce Type I Interferons and Activate Autophagy. *Cell Host Microbe* **17**, 811-819, doi:10.1016/j.chom.2015.05.004 (2015).

130 Collins, A. C. *et al.* Cyclic GMP-AMP Synthase Is an Innate Immune DNA Sensor for *Mycobacterium tuberculosis*. *Cell Host Microbe* **17**, 820-828, doi:10.1016/j.chom.2015.05.005 (2015).

131 Wassermann, R. *et al. Mycobacterium tuberculosis* Differentially Activates cGAS- and Inflammasome-Dependent Intracellular Immune Responses through ESX-1. *Cell Host Microbe* **17**, 799-810, doi:10.1016/j.chom.2015.05.003 (2015).

132 Liang, Q. *et al.* Crosstalk between the cGAS DNA sensor and Beclin-1 autophagy protein shapes innate antimicrobial immune responses. *Cell Host Microbe* **15**, 228-238, doi:10.1016/j.chom.2014.01.009 (2014).

133 Prabakaran, T. *et al.* Attenuation of cGAS-STING signaling is mediated by a p62/SQSTM1-dependent autophagy pathway activated by TBK1. *EMBO J* **37**, doi:10.15252/embj.201797858 (2018).

134 Gulen, M. F. *et al.* Signalling strength determines proapoptotic functions of STING. *Nat Commun* **8**, 427, doi:10.1038/s41467-017-00573-w (2017).

135 Wu, J. *et al.* STING-mediated disruption of calcium homeostasis chronically activates ER stress and primes T cell death. *J Exp Med* **216**, 867-883, doi:10.1084/jem.20182192 (2019).

136 Warner, J. D. *et al.* STING-associated vasculopathy develops independently of IRF3 in mice. *J Exp Med* **214**, 3279-3292, doi:10.1084/jem.20171351 (2017).

137 Hayman, T. J. *et al.* STING enhances cell death through regulation of reactive oxygen species and DNA damage. *Nat Commun* **12**, 2327, doi:10.1038/s41467-021-22572-8 (2021).

138 Schock, S. N. *et al.* Induction of necroptotic cell death by viral activation of the RIG-I or STING pathway. *Cell Death Differ* **24**, 615-625, doi:10.1038/cdd.2016.153 (2017).

139 Chen, D. *et al.* PUMA amplifies necroptosis signaling by activating cytosolic DNA sensors. *Proc Natl Acad Sci U S A* **115**, 3930-3935, doi:10.1073/pnas.1717190115 (2018).

140 Zhang, X. *et al.* mtDNA-STING pathway promotes necroptosis-dependent enterocyte injury in intestinal ischemia reperfusion. *Cell Death Dis* **11**, 1050, doi:10.1038/s41419-020-03239-6 (2020).

141 Webster, S. J. *et al.* Detection of a microbial metabolite by STING regulates inflammasome activation in response to *Chlamydia trachomatis* infection. *PLoS Pathog* **13**, e1006383, doi:10.1371/journal.ppat.1006383 (2017).

142 Meunier, E. *et al.* Guanylate-binding proteins promote activation of the AIM2 inflammasome during infection with *Francisella novicida*. *Nat Immunol* **16**, 476-484, doi:10.1038/ni.3119 (2015).

143 Gaidt, M. M. *et al.* The DNA Inflammasome in Human Myeloid Cells Is Initiated by a STING-Cell Death Program Upstream of NLRP3. *Cell* **171**, 1110-1124 e1118, doi:10.1016/j.cell.2017.09.039 (2017).

144 Vanaja, S. K., Rathinam, V. A. & Fitzgerald, K. A. Mechanisms of inflammasome activation: recent advances and novel insights. *Trends Cell Biol* **25**, 308-315, doi:10.1016/j.tcb.2014.12.009 (2015).

145 MacMicking, J. D. IFN-inducible GTPases and immunity to intracellular pathogens. *Trends Immunol* **25**, 601-609, doi:10.1016/j.it.2004.08.010 (2004).

146 Burke, T. P. *et al.* Inflammasome-mediated antagonism of type I interferon enhances *Rickettsia* pathogenesis. *Nat Microbiol*, doi:10.1038/s41564-020-0673-5 (2020).

147 Meunier, E. *et al.* Caspase-11 activation requires lysis of pathogen-containing vacuoles by IFN-induced GTPases. *Nature* **509**, 366-370, doi:10.1038/nature13157 (2014).

148 Guirouilh-Barbat, J., Lambert, S., Bertrand, P. & Lopez, B. S. Is homologous recombination really an error-free process? *Front Genet* **5**, 175, doi:10.3389/fgene.2014.00175 (2014).

149 Liu, H. *et al.* Nuclear cGAS suppresses DNA repair and promotes tumorigenesis. *Nature* **563**, 131-136, doi:10.1038/s41586-018-0629-6 (2018).

150 Jiang, H. *et al.* Chromatin-bound cGAS is an inhibitor of DNA repair and hence accelerates genome destabilization and cell death. *EMBO J* **38**, e102718, doi:10.15252/embj.2019102718 (2019).

151 Liu, R. *et al.* Innate immune response orchestrates phosphoribosyl pyrophosphate synthetases to support DNA repair. *Cell Metabolism*, doi:10.1016/j.cmet.2021.07.009 (2021).

152 Campisi, J. Aging, cellular senescence, and cancer. *Annu Rev Physiol* **75**, 685-705, doi:10.1146/annurev-physiol-030212-183653 (2013).

153 Yang, H., Wang, H., Ren, J., Chen, Q. & Chen, Z. J. cGAS is essential for cellular senescence. *Proc Natl Acad Sci U S A* **114**, E4612-E4620, doi:10.1073/pnas.1705499114 (2017).

154 Gluck, S. *et al.* Innate immune sensing of cytosolic chromatin fragments through cGAS promotes senescence. *Nat Cell Biol* **19**, 1061-1070, doi:10.1038/ncb3586 (2017).

155 Dou, Z. *et al.* Cytoplasmic chromatin triggers inflammation in senescence and cancer. *Nature* **550**, 402-406, doi:10.1038/nature24050 (2017).

156 Lam, E., Stein, S. & Falck-Pedersen, E. Adenovirus detection by the cGAS/STING/TBK1 DNA sensing cascade. *J Virol* **88**, 974-981, doi:10.1128/JVI.02702-13 (2014).

157 Garcia-Belmonte, R., Perez-Nunez, D., Pittau, M., Richt, J. A. & Revilla, Y. African Swine Fever Virus Armenia/07 Virulent Strain Controls Interferon Beta Production through the cGAS-STING Pathway. *J Virol* **93**, doi:10.1128/JVI.02298-18 (2019).

158 Lio, C. W. *et al.* cGAS-STING Signaling Regulates Initial Innate Control of Cytomegalovirus Infection. *J Virol* **90**, 7789-7797, doi:10.1128/JVI.01040-16 (2016).

159 Paijo, J. *et al.* cGAS Senses Human Cytomegalovirus and Induces Type I Interferon Responses in Human Monocyte-Derived Cells. *PLoS Pathog* **12**, e1005546, doi:10.1371/journal.ppat.1005546 (2016).

160 Horan, K. A. *et al.* Proteasomal degradation of herpes simplex virus capsids in macrophages releases DNA to the cytosol for recognition by DNA sensors. *J Immunol* **190**, 2311-2319, doi:10.4049/jimmunol.1202749 (2013).

161 Gao, D. *et al.* Cyclic GMP-AMP synthase is an innate immune sensor of HIV and other retroviruses. *Science* **341**, 903-906, doi:10.1126/science.1240933 (2013).

162 Sun, B. *et al.* Dengue virus activates cGAS through the release of mitochondrial DNA. *Sci Rep* **7**, 3594, doi:10.1038/s41598-017-03932-1 (2017).

163 Zhou, C. M. *et al.* Identification of cGAS as an innate immune sensor of extracellular bacterium Pseudomonas aeruginosa. *iScience* **24**, 101928, doi:10.1016/j.isci.2020.101928 (2021).

164 Hansen, K. *et al. Listeria monocytogenes* induces IFNβ expression through an IFI16-, cGAS- and STING-dependent pathway. *EMBO J* **33**, 1654-1666, doi:10.15252/embj.201488029 (2014).

165 Storek, K. M., Gertsvolf, N. A., Ohlson, M. B. & Monack, D. M. cGAS and Ifi204 cooperate to produce type I IFNs in response to *Francisella* infection. *J Immunol* **194**, 3236-3245, doi:10.4049/jimmunol.1402764 (2015).

166 Andrade, W. A. *et al.* Type I Interferon Induction by *Neisseria gonorrhoeae*: Dual Requirement of Cyclic GMP-AMP Synthase and Toll-like Receptor 4. *Cell Rep* **15**, 2438-2448, doi:10.1016/j.celrep.2016.05.030 (2016).

167 Auerbuch, V., Brockstedt, D. G., Meyer-Morse, N., O'Riordan, M. & Portnoy, D. A. Mice lacking the type I interferon receptor are resistant to *Listeria monocytogenes*. *J Exp Med* **200**, 527-533, doi:10.1084/jem.20040976 (2004).

168 Jenal, U., Reinders, A. & Lori, C. Cyclic di-GMP: second messenger extraordinaire. *Nat Rev Microbiol* **15**, 271-284, doi:10.1038/nrmicro.2016.190 (2017).

169 Barker, J. R. *et al.* STING-dependent recognition of cyclic di-AMP mediates type I interferon responses during *Chlamydia trachomatis* infection. *mBio* **4**, e00018-00013, doi:10.1128/mBio.00018-13 (2013).

170 Gallego-Marin, C. *et al.* Cyclic GMP-AMP Synthase Is the Cytosolic Sensor of *Plasmodium falciparum* Genomic DNA and Activates Type I IFN in Malaria. *J Immunol* **200**, 768-774, doi:10.4049/jimmunol.1701048 (2018).

171 Han, F. *et al.* The cGAS-STING signaling pathway contributes to the inflammatory response and autophagy in *Aspergillus fumigatus* keratitis. *Exp Eye Res* **202**, 108366, doi:10.1016/j.exer.2020.108366 (2021).

172 Negrini, S., Gorgoulis, V. G. & Halazonetis, T. D. Genomic instability--an evolving hallmark of cancer. *Nat Rev Mol Cell Biol* **11**, 220-228, doi:10.1038/nrm2858 (2010).

173 Harding, S. M. *et al.* Mitotic progression following DNA damage enables pattern recognition within micronuclei. *Nature* **548**, 466-470, doi:10.1038/nature23470 (2017).

174 Mackenzie, K. J. *et al.* cGAS surveillance of micronuclei links genome instability to innate immunity. *Nature* **548**, 461-465, doi:10.1038/nature23449 (2017).

175 de Oliveira Mann, C. C. & Kranzusch, P. J. cGAS Conducts Micronuclei DNA Surveillance. *Trends Cell Biol* **27**, 697-698, doi:10.1016/j.tcb.2017.08.007 (2017).

176 Flynn, P. J., Koch, P. D. & Mitchison, T. J. Chromatin bridges, not micronuclei, activate cGAS after drug-induced mitotic errors in human cells. *Proc Natl Acad Sci U S A* **118**, doi:10.1073/pnas.2103585118 (2021).

177 Ablasser, A. *et al.* TREX1 deficiency triggers cell-autonomous immunity in a cGAS-dependent manner. *J Immunol* **192**, 5993-5997, doi:10.4049/jimmunol.1400737 (2014).

178 Sato, H. *et al.* Downregulation of mitochondrial biogenesis by virus infection triggers antiviral responses by cyclic GMP-AMP synthase. *PLoS Pathog* **17**, e1009841, doi:10.1371/journal.ppat.1009841 (2021).

179 White, M. J. *et al.* Apoptotic caspases suppress mtDNA-induced STING-mediated type I IFN production. *Cell* **159**, 1549-1562, doi:10.1016/j.cell.2014.11.036 (2014).

180 Rongvaux, A. *et al.* Apoptotic caspases prevent the induction of type I interferons by mitochondrial DNA. *Cell* **159**, 1563-1577, doi:10.1016/j.cell.2014.11.037 (2014).

181 Ning, X. *et al.* Apoptotic Caspases Suppress Type I Interferon Production via the Cleavage of cGAS, MAVS, and IRF3. *Mol Cell* **74**, 19-31 e17, doi:10.1016/j.molcel.2019.02.013 (2019).

182 Willemsen, J. *et al.* TNF leads to mtDNA release and cGAS/STING-dependent interferon responses that support inflammatory arthritis. *Cell Rep* **37**, 109977, doi:10.1016/j.celrep.2021.109977 (2021).

183 Aarreberg, L. D. *et al.* Interleukin-1β Induces mtDNA Release to Activate Innate Immune Signaling via cGAS-STING. *Mol Cell* **74**, 801-815 e806, doi:10.1016/j.molcel.2019.02.038 (2019).

184 West, A. P. *et al.* Mitochondrial DNA stress primes the antiviral innate immune response. *Nature* **520**, 553-557, doi:10.1038/nature14156 (2015).

185 Kawane, K. *et al.* Chronic polyarthritis caused by mammalian DNA that escapes from degradation in macrophages. *Nature* **443**, 998-1002, doi:10.1038/nature05245 (2006).

186 Ahn, J., Gutman, D., Saijo, S. & Barber, G. N. STING manifests self DNA-dependent inflammatory disease. *Proc Natl Acad Sci U S A* **109**, 19386-19391, doi:10.1073/pnas.1215006109 (2012).

187 Brinkmann, V. *et al.* Neutrophil extracellular traps kill bacteria. *Science* **303**, 1532-1535, doi:10.1126/science.1092385 (2004).

188 Apel, F. *et al.* The cytosolic DNA sensor cGAS recognizes neutrophil extracellular traps. *Sci Signal* **14**, doi:10.1126/scisignal.aax7942 (2021).

189 Li, X. *et al.* Cyclic GMP-AMP synthase is activated by double-stranded DNA-induced oligomerization. *Immunity* **39**, 1019-1031, doi:10.1016/j.immuni.2013.10.019 (2013).

190 Zhang, X. *et al.* The cytosolic DNA sensor cGAS forms an oligomeric complex with DNA and undergoes switch-like conformational changes in the activation loop. *Cell Rep* **6**, 421-430, doi:10.1016/j.celrep.2014.01.003 (2014).

191 Civril, F. *et al.* Structural mechanism of cytosolic DNA sensing by cGAS. *Nature* **498**, 332-337, doi:10.1038/nature12305 (2013).

192 Andreeva, L. *et al.* cGAS senses long and HMGB/TFAM-bound U-turn DNA by forming protein-DNA ladders. *Nature* **549**, 394-398, doi:10.1038/nature23890 (2017).

193 Xie, W. *et al.* Human cGAS catalytic domain has an additional DNA-binding interface that enhances enzymatic activity and liquid-phase condensation. *Proc Natl Acad Sci U S A* **116**, 11946-11955, doi:10.1073/pnas.1905013116 (2019).

194 Zhou, W. *et al.* Structure of the Human cGAS-DNA Complex Reveals Enhanced Control of Immune Surveillance. *Cell* **174**, 300-311 e311, doi:10.1016/j.cell.2018.06.026 (2018).

195 Du, M. & Chen, Z. J. DNA-induced liquid phase condensation of cGAS activates innate immune signaling. *Science* **361**, 704-709, doi:10.1126/science.aat1022 (2018).

196 Zhao, Z. *et al.* Mn^{2+} Directly Activates cGAS and Structural Analysis Suggests Mn^{2+} Induces a Noncanonical Catalytic Synthesis of 2'3'-cGAMP. *Cell Rep* **32**, 108053, doi:10.1016/j.celrep.2020.108053 (2020).

197 Orzalli, M. H. *et al.* cGAS-mediated stabilization of IFI16 promotes innate signaling during herpes simplex virus infection. *Proc Natl Acad Sci U S A* **112**, E1773-1781, doi:10.1073/pnas.1424637112 (2015).

198 Sun, H. *et al.* A Nuclear Export Signal Is Required for cGAS to Sense Cytosolic DNA. *Cell Rep* **34**, 108586, doi:10.1016/j.celrep.2020.108586 (2021).

199 Volkman, H. E., Cambier, S., Gray, E. E. & Stetson, D. B. Tight nuclear tethering of cGAS is essential for preventing autoreactivity. *Elife* **8**, doi:10.7554/eLife.47491 (2019).

200 Barnett, K. C. *et al.* Phosphoinositide Interactions Position cGAS at the Plasma Membrane to Ensure Efficient Distinction between Self- and Viral DNA. *Cell* **176**, 1432-1446 e1411, doi:10.1016/j.cell.2019.01.049 (2019).

201 Gentili, M. *et al.* The N-Terminal Domain of cGAS Determines Preferential Association with Centromeric DNA and Innate Immune Activation in the Nucleus. *Cell Rep* **26**, 2377-2393 e2313, doi:10.1016/j.celrep.2019.01.105 (2019).

202 Guey, B. *et al.* BAF restricts cGAS on nuclear DNA to prevent innate immune activation. *Science* **369**, 823-828, doi:10.1126/science.aaw6421 (2020).

203 Lahaye, X. *et al.* NONO Detects the Nuclear HIV Capsid to Promote cGAS-Mediated Innate Immune Activation. *Cell* **175**, 488-501 e422, doi:10.1016/j.cell.2018.08.062 (2018).

204 Zierhut, C. *et al.* The Cytoplasmic DNA Sensor cGAS Promotes Mitotic Cell Death. *Cell* **178**, 302-315 e323, doi:10.1016/j.cell.2019.05.035 (2019).

205 Pathare, G. R. *et al.* Structural mechanism of cGAS inhibition by the nucleosome. *Nature*, doi:10.1038/s41586-020-2750-6 (2020).

206 Michalski, S. *et al.* Structural basis for sequestration and autoinhibition of cGAS by chromatin. *Nature*, doi:10.1038/s41586-020-2748-0 (2020).

207 Zhao, B. *et al.* The Molecular Basis of Tight Nuclear Tethering and Inactivation of cGAS. *Nature*, doi:10.1038/s41586-020-2749-z (2020).

208 Boyer, J. A. *et al.* Structural basis of nucleosome-dependent cGAS inhibition. *Science*, doi:10.1126/science.abd0609 (2020).

209 Kujirai, T. *et al.* Structural basis for the inhibition of cGAS by nucleosomes. *Science*, doi:10.1126/science.abd0237 (2020).

210 Li, T. *et al.* Phosphorylation and chromatin tethering prevent cGAS activation during mitosis. *Science* **371**, doi:10.1126/science.abc5386 (2021).

211 Zhou, W., Mohr, L., Maciejowski, J. & Kranzusch, P. J. cGAS phase separation inhibits TREX1-mediated DNA degradation and enhances cytosolic DNA sensing. *Mol Cell* **81**, 739-755 e737, doi:10.1016/j.molcel.2021.01.024 (2021).

212 Mohr, L. *et al.* ER-directed TREX1 limits cGAS activation at micronuclei. *Mol Cell* **81**, 724-738 e729, doi:10.1016/j.molcel.2020.12.037 (2021).

213 Seo, G. J. *et al.* Akt Kinase-Mediated Checkpoint of cGAS DNA Sensing Pathway. *Cell Rep* **13**, 440-449, doi:10.1016/j.celrep.2015.09.007 (2015).

214 Zhong, L. *et al.* Phosphorylation of cGAS by CDK1 impairs self-DNA sensing in mitosis. *Cell Discovery* **6**, doi:10.1038/s41421-020-0162-2 (2020).

215 Wang, Q. *et al.* The E3 ubiquitin ligase RNF185 facilitates the cGAS-mediated innate immune response. *PLoS Pathog* **13**, e1006264, doi:10.1371/journal.ppat.1006264 (2017).

216 Seo, G. J. *et al.* TRIM56-mediated monoubiquitination of cGAS for cytosolic DNA sensing. *Nat Commun* **9**, 613, doi:10.1038/s41467-018-02936-3 (2018).

217 Hu, M. M. *et al.* Sumoylation Promotes the Stability of the DNA Sensor cGAS and the Adaptor STING to Regulate the Kinetics of Response to DNA Virus. *Immunity* **45**, 555-569, doi:10.1016/j.immuni.2016.08.014 (2016).

218 Chen, M. *et al.* TRIM14 Inhibits cGAS Degradation Mediated by Selective Autophagy Receptor p62 to Promote Innate Immune Responses. *Mol Cell* **64**, 105-119, doi:10.1016/j.molcel.2016.08.025 (2016).

219 Li, C. *et al.* RNF111-facilitated neddylation potentiates cGAS-mediated antiviral innate immune response. *PLoS Pathog* **17**, e1009401, doi:10.1371/journal.ppat.1009401 (2021).

220 Dai, J. *et al.* Acetylation Blocks cGAS Activity and Inhibits Self-DNA-Induced Autoimmunity. *Cell* **176**, 1447-1460 e1414, doi:10.1016/j.cell.2019.01.016 (2019).

221 Song, Z. M. *et al.* KAT5 acetylates cGAS to promote innate immune response to DNA virus. *Proc Natl Acad Sci U S A* **117**, 21568-21575, doi:10.1073/pnas.1922330117 (2020).

222 Wang, Y. *et al.* Inflammasome Activation Triggers Caspase-1-Mediated Cleavage of cGAS to Regulate Responses to DNA Virus Infection. *Immunity* **46**, 393-404, doi:10.1016/j.immuni.2017.02.011 (2017).

223 Liu, Z. S. *et al.* G3BP1 promotes DNA binding and activation of cGAS. *Nat Immunol* **20**, 18-28, doi:10.1038/s41590-018-0262-4 (2019).

224 Zhao, M. *et al.* The stress granule protein G3BP1 promotes pre-condensation of cGAS to allow rapid responses to DNA. *EMBO Rep* **23**, e53166, doi:10.15252/embr.202153166 (2022).

225 Yoh, S. M. *et al.* PQBP1 Is a Proximal Sensor of the cGAS-Dependent Innate Response to HIV-1. *Cell* **161**, 1293-1305, doi:10.1016/j.cell.2015.04.050 (2015).

226 Lian, H. *et al.* ZCCHC3 is a co-sensor of cGAS for dsDNA recognition in innate immune response. *Nat Commun* **9**, 3349, doi:10.1038/s41467-018-05559-w (2018).

227 Jin, M. *et al.* Tau activates microglia via the PQBP1-cGAS-STING pathway to promote brain inflammation. *Nat Commun* **12**, 6565, doi:10.1038/s41467-021-26851-2 (2021).

228 Aguirre, S. *et al.* Dengue virus NS2B protein targets cGAS for degradation and prevents mitochondrial DNA sensing during infection. *Nat Microbiol* **2**, 17037, doi:10.1038/nmicrobiol.2017.37 (2017).

229 Zheng, Y. *et al.* Zika virus elicits inflammation to evade antiviral response by cleaving cGAS via NS1-caspase-1 axis. *EMBO J* **37**, doi:10.15252/embj.201899347 (2018).

230 Meade, N. *et al.* Poxviruses Evade Cytosolic Sensing through Disruption of an mTORC1-mTORC2 Regulatory Circuit. *Cell* **174**, 1143-1157 e1117, doi:10.1016/j.cell.2018.06.053 (2018).

231 Huang, J. *et al.* Herpes Simplex Virus 1 Tegument Protein VP22 Abrogates cGAS/STING-Mediated Antiviral Innate Immunity. *J Virol* **92**, doi:10.1128/JVI.00841-18 (2018).

232 Zhang, J. *et al.* Species-Specific Deamidation of cGAS by Herpes Simplex Virus UL37 Protein Facilitates Viral Replication. *Cell Host Microbe* **24**, 234-248 e235, doi:10.1016/j.chom.2018.07.004 (2018).

233 Huang, Z. F. *et al.* Human Cytomegalovirus Protein UL31 Inhibits DNA Sensing of cGAS to Mediate Immune Evasion. *Cell Host Microbe* **24**, 69-80 e64, doi:10.1016/j.chom.2018.05.007 (2018).

234 Fu, Y. Z. *et al.* Human cytomegalovirus protein UL42 antagonizes cGAS/MITA-mediated innate antiviral response. *PLoS Pathog* **15**, e1007691, doi:10.1371/journal.ppat.1007691 (2019).

235 Biolatti, M. *et al.* Human Cytomegalovirus Tegument Protein pp65 (pUL83) Dampens Type I Interferon Production by Inactivating the DNA Sensor cGAS without Affecting STING. *J Virol* **92**, doi:10.1128/JVI.01774-17 (2018).

236 Wu, J. J. *et al.* Inhibition of cGAS DNA Sensing by a Herpesvirus Virion Protein. *Cell Host Microbe* **18**, 333-344, doi:10.1016/j.chom.2015.07.015 (2015).

237 Zhang, G. *et al.* Cytoplasmic isoforms of Kaposi sarcoma herpesvirus LANA recruit and antagonize the innate immune DNA sensor cGAS. *Proc Natl Acad Sci U S A* **113**, E1034-1043, doi:10.1073/pnas.1516812113 (2016).

238 Hertzog, J. *et al.* Varicella-Zoster Virus ORF9 Is an Antagonist of the DNA Sensor cGAS. *bioRxiv*, doi:10.1101/2020.02.11.943415 (2021).

239 Xu, G. *et al.* Viral tegument proteins restrict cGAS-DNA phase separation to mediate immune evasion. *Mol Cell*, doi:10.1016/j.molcel.2021.05.002 (2021).

240 Kagan, J. C. Signaling organelles of the innate immune system. *Cell* **151**, 1168-1178, doi:10.1016/j.cell.2012.11.011 (2012).

241 Demarquoy, J. & Le Borgne, F. Crosstalk between mitochondria and peroxisomes. *World J Biol Chem* **6**, 301-309, doi:10.4331/wjbc.v6.i4.301 (2015).

242 Mills, E. L., Kelly, B. & O'Neill, L. A. J. Mitochondria are the powerhouses of immunity. *Nat Immunol* **18**, 488-498, doi:10.1038/ni.3704 (2017).

243 Ferreira, A. R., Marques, M., Ramos, B., Kagan, J. C. & Ribeiro, D. Emerging roles of peroxisomes in viral infections. *Trends Cell Biol* **32**, 124-139, doi:10.1016/j.tcb.2021.09.010 (2022).

244 McBride, H. M., Neuspiel, M. & Wasiak, S. Mitochondria: more than just a powerhouse. *Curr Biol* **16**, R551-560, doi:10.1016/j.cub.2006.06.054 (2006).

245 Hou, F. *et al.* MAVS forms functional prion-like aggregates to activate and propagate antiviral innate immune response. *Cell* **146**, 448-461, doi:10.1016/j.cell.2011.06.041 (2011).

246 Li, X. D., Sun, L., Seth, R. B., Pineda, G. & Chen, Z. J. Hepatitis C virus protease NS3/4A cleaves mitochondrial antiviral signaling protein off the mitochondria to evade innate immunity. *Proc Natl Acad Sci U S A* **102**, 17717-17722, doi:10.1073/pnas.0508531102 (2005).

247 Refolo, G., Vescovo, T., Piacentini, M., Fimia, G. M. & Ciccosanti, F. Mitochondrial Interactome: A Focus on Antiviral Signaling Pathways. *Front Cell Dev Biol* **8**, 8, doi:10.3389/fcell.2020.00008 (2020).

248 Moore, C. B. *et al.* NLRX1 is a regulator of mitochondrial antiviral immunity. *Nature* **451**, 573-577, doi:10.1038/nature06501 (2008).

249 Yasukawa, K. *et al.* Mitofusin 2 inhibits mitochondrial antiviral signaling. *Sci Signal* **2**, ra47, doi:10.1126/scisignal.2000287 (2009).

250 Onoguchi, K. *et al.* Virus-infection or 5'ppp-RNA activates antiviral signal through redistribution of IPS-1 mediated by MFN1. *PLoS Pathog* **6**, e1001012, doi:10.1371/journal.ppat.1001012 (2010).

251 Liu, X. Y., Wei, B., Shi, H. X., Shan, Y. F. & Wang, C. Tom70 mediates activation of interferon regulatory factor 3 on mitochondria. *Cell Res* **20**, 994-1011, doi:10.1038/cr.2010.103 (2010).

252 Liu, X. Y., Chen, W., Wei, B., Shan, Y. F. & Wang, C. IFN-induced TPR protein IFIT3 potentiates antiviral signaling by bridging MAVS and TBK1. *J Immunol* **187**, 2559-2568, doi:10.4049/jimmunol.1100963 (2011).

253 Rebsamen, M. *et al.* NLRX1/NOD5 deficiency does not affect MAVS signalling. *Cell Death Differ* **18**, 1387, doi:10.1038/cdd.2011.64 (2011).

254 Arnoult, D. *et al.* An N-terminal addressing sequence targets NLRX1 to the mitochondrial matrix. *J Cell Sci* **122**, 3161-3168, doi:10.1242/jcs.051193 (2009).

255 Koshiba, T., Yasukawa, K., Yanagi, Y. & Kawabata, S. Mitochondrial membrane potential is required for MAVS-mediated antiviral signaling. *Sci Signal* **4**, ra7, doi:10.1126/scisignal.2001147 (2011).

256 Castanier, C., Garcin, D., Vazquez, A. & Arnoult, D. Mitochondrial dynamics regulate the RIG-I-like receptor antiviral pathway. *EMBO Rep* **11**, 133-138, doi:10.1038/embor.2009.258 (2010).

257 Buskiewicz, I. A. *et al.* Reactive oxygen species induce virus-independent MAVS oligomerization in systemic lupus erythematosus. *Sci Signal* **9**, ra115, doi:10.1126/scisignal.aaf1933 (2016).

258 Zhou, R., Yazdi, A. S., Menu, P. & Tschopp, J. A role for mitochondria in NLRP3 inflammasome activation. *Nature* **469**, 221-225, doi:10.1038/nature09663 (2011).

259 Subramanian, N., Natarajan, K., Clatworthy, M. R., Wang, Z. & Germain, R. N. The adaptor MAVS promotes NLRP3 mitochondrial localization and inflammasome activation. *Cell* **153**, 348-361, doi:10.1016/j.cell.2013.02.054 (2013).

260 Iyer, S. S. *et al.* Mitochondrial cardiolipin is required for Nlrp3 inflammasome activation. *Immunity* **39**, 311-323, doi:10.1016/j.immuni.2013.08.001 (2013).

261 Gross, C. J. *et al.* K^+ Efflux-Independent NLRP3 Inflammasome Activation by Small Molecules Targeting Mitochondria. *Immunity* **45**, 761-773, doi:10.1016/j.immuni.2016.08.010 (2016).

262 Park, S. *et al.* The mitochondrial antiviral protein MAVS associates with NLRP3 and regulates its inflammasome activity. *J Immunol* **191**, 4358-4366, doi:10.4049/jimmunol.1301170 (2013).

263 Nakahira, K. *et al.* Autophagy proteins regulate innate immune responses by inhibiting the release of mitochondrial DNA mediated by the NALP3 inflammasome. *Nat Immunol* **12**, 222-230, doi:10.1038/ni.1980 (2011).

264 West, A. P. & Shadel, G. S. Mitochondrial DNA in innate immune responses and inflammatory pathology. *Nat Rev Immunol* **17**, 363-375, doi:10.1038/nri.2017.21 (2017).

265 Shimada, K. *et al.* Oxidized mitochondrial DNA activates the NLRP3 inflammasome during apoptosis. *Immunity* **36**, 401-414, doi:10.1016/j.immuni.2012.01.009 (2012).

266 Jabir, M. S. *et al.* Mitochondrial damage contributes to Pseudomonas aeruginosa activation of the inflammasome and is downregulated by autophagy. *Autophagy* **11**, 166-182, doi:10.4161/15548627.2014.981915 (2015).

267 Bicci, I., Calabrese, C., Golder, Z. J., Gomez-Duran, A. & Chinnery, P. F. Single-molecule mitochondrial DNA sequencing shows no evidence of CpG methylation in human cells and tissues. *Nucleic Acids Res* **49**, 12757-12768, doi:10.1093/nar/gkab1179 (2021).

268 Patil, V. *et al.* Human mitochondrial DNA is extensively methylated in a non-CpG context. *Nucleic Acids Res* **47**, 10072-10085, doi:10.1093/nar/gkz762 (2019).

269 Zhang, Q., Itagaki, K. & Hauser, C. J. Mitochondrial DNA is released by shock and activates neutrophils via p38 map kinase. *Shock* **34**, 55-59, doi:10.1097/SHK.0b013e3181cd8c08 (2010).

270 Zhang, Q. *et al.* Circulating mitochondrial DAMPs cause inflammatory responses to injury. *Nature* **464**, 104-107, doi:10.1038/nature08780 (2010).

271 Rodriguez-Prados, J. C. *et al.* Substrate fate in activated macrophages: a comparison between innate, classic, and alternative activation. *J Immunol* **185**, 605-614, doi:10.4049/jimmunol.0901698 (2010).

272 Krawczyk, C. M. *et al.* Toll-like receptor-induced changes in glycolytic metabolism regulate dendritic cell activation. *Blood* **115**, 4742-4749, doi:10.1182/blood-2009-10-249540 (2010).

273 Williams, N. C. & O'Neill, L. A. J. A Role for the Krebs Cycle Intermediate Citrate in Metabolic Reprogramming in Innate Immunity and Inflammation. *Front Immunol* **9**, 141, doi:10.3389/fimmu.2018.00141 (2018).

274 Selak, M. A. *et al.* Succinate links TCA cycle dysfunction to oncogenesis by inhibiting HIF-alpha prolyl hydroxylase. *Cancer Cell* **7**, 77-85, doi:10.1016/j.ccr.2004.11.022 (2005).

275 Tannahill, G. M. *et al.* Succinate is an inflammatory signal that induces IL-1β through HIF-1alpha. *Nature* **496**, 238-242, doi:10.1038/nature11986 (2013).

276 Mills, E. L. *et al.* Succinate Dehydrogenase Supports Metabolic Repurposing of Mitochondria to Drive Inflammatory Macrophages. *Cell* **167**, 457-470 e413, doi:10.1016/j.cell.2016.08.064 (2016).

277 Jha, A. K. *et al.* Network integration of parallel metabolic and transcriptional data reveals metabolic modules that regulate macrophage polarization. *Immunity* **42**, 419-430, doi:10.1016/j.immuni.2015.02.005 (2015).

278 Lampropoulou, V. *et al.* Itaconate Links Inhibition of Succinate Dehydrogenase with Macrophage Metabolic Remodeling and Regulation of Inflammation. *Cell Metab* **24**, 158-166, doi:10.1016/j.cmet.2016.06.004 (2016).

279 Chouchani, E. T. *et al.* Ischaemic accumulation of succinate controls reperfusion injury through mitochondrial ROS. *Nature* **515**, 431-435, doi:10.1038/nature13909 (2014).

280 Chen, L. L. *et al.* Itaconate inhibits TET DNA dioxygenases to dampen inflammatory responses. *Nat Cell Biol* **24**, 353-363, doi:10.1038/s41556-022-00853-8 (2022).

281 Vats, D. *et al.* Oxidative metabolism and PGC-1β attenuate macrophage-mediated inflammation. *Cell Metab* **4**, 13-24, doi:10.1016/j.cmet.2006.05.011 (2006).

282 Batista-Gonzalez, A., Vidal, R., Criollo, A. & Carreno, L. J. New Insights on the Role of Lipid Metabolism in the Metabolic Reprogramming of Macrophages. *Front Immunol* **10**, 2993, doi:10.3389/fimmu.2019.02993 (2019).

283 Wu, D. *et al.* Type 1 Interferons Induce Changes in Core Metabolism that Are Critical for Immune Function. *Immunity* **44**, 1325-1336, doi:10.1016/j.immuni.2016.06.006 (2016).

284 Correa-Oliveira, R., Fachi, J. L., Vieira, A., Sato, F. T. & Vinolo, M. A. Regulation of immune cell function by short-chain fatty acids. *Clin Transl Immunology* **5**, e73, doi:10.1038/cti.2016.17 (2016).

285 Li, M. *et al.* Pro- and anti-inflammatory effects of short chain fatty acids on immune and endothelial cells. *Eur J Pharmacol* **831**, 52-59, doi:10.1016/j.ejphar.2018.05.003 (2018).

286 Sam, Q. H. *et al.* The Divergent Immunomodulatory Effects of Short Chain Fatty Acids and Medium Chain Fatty Acids. *Int J Mol Sci* **22**, doi:10.3390/ijms22126453 (2021).

287 Hidalgo, M. A., Carretta, M. D. & Burgos, R. A. Long Chain Fatty Acids as Modulators of Immune Cells Function: Contribution of FFA1 and FFA4 Receptors. *Front Physiol* **12**, 668330, doi:10.3389/fphys.2021.668330 (2021).

288 Kim, M. H., Kang, S. G., Park, J. H., Yanagisawa, M. & Kim, C. H. Short-chain fatty acids activate GPR41 and GPR43 on intestinal epithelial cells to promote inflammatory responses in mice. *Gastroenterology* **145**, 396-406 e391-310, doi:10.1053/j.gastro.2013.04.056 (2013).

289 Bhatt, B. *et al.* Gpr109a Limits Microbiota-Induced IL-23 Production To Constrain ILC3-Mediated Colonic Inflammation. *J Immunol* **200**, 2905-2914, doi:10.4049/jimmunol.1701625 (2018).

290 Thangaraju, M. *et al.* GPR109A is a G-protein-coupled receptor for the bacterial fermentation product butyrate and functions as a tumor suppressor in colon. *Cancer Res* **69**, 2826-2832, doi:10.1158/0008-5472.CAN-08-4466 (2009).

291 Singh, N. *et al.* Activation of Gpr109a, receptor for niacin and the commensal metabolite butyrate, suppresses colonic inflammation and carcinogenesis. *Immunity* **40**, 128-139, doi:10.1016/j.immuni.2013.12.007 (2014).

292 Chang, P. V., Hao, L., Offermanns, S. & Medzhitov, R. The microbial metabolite butyrate regulates intestinal macrophage function via histone deacetylase inhibition. *Proc Natl Acad Sci U S A* **111**, 2247-2252, doi:10.1073/pnas.1322269111 (2014).

293 Youm, Y. H. *et al.* The ketone metabolite β-hydroxybutyrate blocks NLRP3 inflammasome-mediated inflammatory disease. *Nat Med* **21**, 263-269, doi:10.1038/nm.3804 (2015).

294 Luzardo-Ocampo, I., Loarca-Pina, G. & Gonzalez de Mejia, E. Gallic and butyric acids modulated NLRP3 inflammasome markers in a co-culture model of intestinal inflammation. *Food Chem Toxicol* **146**, 111835, doi:10.1016/j.fct.2020.111835 (2020).

295 Tzeng, H. T., Chyuan, I. T. & Chen, W. Y. Shaping of Innate Immune Response by Fatty Acid Metabolite Palmitate. *Cells* **8**, doi:10.3390/cells8121633 (2019).

296 Lancaster, G. I. *et al.* Evidence that TLR4 Is Not a Receptor for Saturated Fatty Acids but Mediates Lipid-Induced Inflammation by Reprogramming Macrophage Metabolism. *Cell Metab* **27**, 1096-1110 e1095, doi:10.1016/j.cmet.2018.03.014 (2018).

297 Mogilenko, D. A. *et al.* Metabolic and Innate Immune Cues Merge into a Specific Inflammatory Response via the UPR. *Cell* **178**, 263, doi:10.1016/j.cell.2019.06.017 (2019).

298 Weber, K. & Schilling, J. D. Lysosomes integrate metabolic-inflammatory cross-talk in primary macrophage inflammasome activation. *J Biol Chem* **289**, 9158-9171, doi:10.1074/jbc.M113.531202 (2014).

299 Wen, H. *et al.* Fatty acid-induced NLRP3-ASC inflammasome activation interferes with insulin signaling. *Nat Immunol* **12**, 408-415, doi:10.1038/ni.2022 (2011).

300 Karasawa, T. *et al.* Saturated Fatty Acids Undergo Intracellular Crystallization and Activate the NLRP3 Inflammasome in Macrophages. *Arterioscler Thromb Vasc Biol* **38**, 744-756, doi:10.1161/ATVBAHA.117.310581 (2018).

301 Waterham, H. R., Ferdinandusse, S. & Wanders, R. J. Human disorders of peroxisome metabolism and biogenesis. *Biochim Biophys Acta* **1863**, 922-933, doi:10.1016/j.bbamcr.2015.11.015 (2016).

302 He, A., Dean, J. M. & Lodhi, I. J. Peroxisomes as cellular adaptors to metabolic and environmental stress. *Trends Cell Biol* **31**, 656-670, doi:10.1016/j.tcb.2021.02.005 (2021).

303 Kim, J. A. Peroxisome Metabolism in Cancer. *Cells* **9**, doi:10.3390/cells9071692 (2020).

304 Wanders, R. J., Klouwer, F. C., Ferdinandusse, S., Waterham, H. R. & Poll-The, B. T. Clinical and Laboratory Diagnosis of Peroxisomal Disorders. *Methods Mol Biol* **1595**, 329-342, doi:10.1007/978-1-4939-6937-1_30 (2017).

305 Farre, J. C., Mahalingam, S. S., Proietto, M. & Subramani, S. Peroxisome biogenesis, membrane contact sites, and quality control. *EMBO Rep* **20**, doi:10.15252/embr.201846864 (2019).

306 Koch, J. *et al.* PEX11 family members are membrane elongation factors that coordinate peroxisome proliferation and maintenance. *J Cell Sci* **123**, 3389-3400, doi:10.1242/jcs.064907 (2010).

307 Gatto, G. J., Jr., Geisbrecht, B. V., Gould, S. J. & Berg, J. M. Peroxisomal targeting signal-1 recognition by the TPR domains of human PEX5. *Nat Struct Biol* **7**, 1091-1095, doi:10.1038/81930 (2000).

308 Braverman, N. *et al.* Human PEX7 encodes the peroxisomal PTS2 receptor and is responsible for rhizomelic chondrodysplasia punctata. *Nat Genet* **15**, 369-376, doi:10.1038/ng0497-369 (1997).

309 Ma, C., Schumann, U., Rayapuram, N. & Subramani, S. The peroxisomal matrix import of Pex8p requires only PTS receptors and Pex14p. *Mol Biol Cell* **20**, 3680-3689, doi:10.1091/mbc.E09-01-0037 (2009).

310 Montilla-Martinez, M. *et al.* Distinct Pores for Peroxisomal Import of PTS1 and PTS2 Proteins. *Cell Rep* **13**, 2126-2134, doi:10.1016/j.celrep.2015.11.016 (2015).

311 Fujiki, Y. *et al.* Recent insights into peroxisome biogenesis and associated diseases. *J Cell Sci* **133**, doi:10.1242/jcs.236943 (2020).

312 Honsho, M., Okumoto, K., Tamura, S. & Fujiki, Y. Peroxisome Biogenesis Disorders. *Adv Exp Med Biol* **1299**, 45-54, doi:10.1007/978-3-030-60204-8_4 (2020).

313 Sugiura, A., Mattie, S., Prudent, J. & McBride, H. M. Newly born peroxisomes are a hybrid of mitochondrial and ER-derived pre-peroxisomes. *Nature* **542**, 251-254, doi:10.1038/nature21375 (2017).

314 Gandre-Babbe, S. & van der Bliek, A. M. The novel tail-anchored membrane protein Mff controls mitochondrial and peroxisomal fission in mammalian cells. *Mol Biol Cell* **19**, 2402-2412, doi:10.1091/mbc.E07-12-1287 (2008).

315 Koch, A., Yoon, Y., Bonekamp, N. A., McNiven, M. A. & Schrader, M. A role for Fis1 in both mitochondrial and peroxisomal fission in mammalian cells. *Mol Biol Cell* **16**, 5077-5086, doi:10.1091/mbc.e05-02-0159 (2005).

316 Odendall, C. *et al.* Diverse intracellular pathogens activate type III interferon expression from peroxisomes. *Nat Immunol* **15**, 717-726, doi:10.1038/ni.2915 (2014).

317 Bender, S. *et al.* Activation of Type I and III Interferon Response by Mitochondrial and Peroxisomal MAVS and Inhibition by Hepatitis C Virus. *PLoS Pathog* **11**, e1005264, doi:10.1371/journal.ppat.1005264 (2015).

318 Vijayan, V. *et al.* A New Immunomodulatory Role for Peroxisomes in Macrophages Activated by the TLR4 Ligand Lipopolysaccharide. *J Immunol* **198**, 2414-2425, doi:10.4049/jimmunol.1601596 (2017).

319 Di Cara, F., Sheshachalam, A., Braverman, N. E., Rachubinski, R. A. & Simmonds, A. J. Peroxisome-Mediated Metabolism Is Required for Immune Response to Microbial Infection. *Immunity* **47**, 93-106 e107, doi:10.1016/j.immuni.2017.06.016 (2017).

320 Decout, A., Katz, J. D., Venkatraman, S. & Ablasser, A. The cGAS-STING pathway as a therapeutic target in inflammatory diseases. *Nat Rev Immunol*, doi:10.1038/s41577-021-00524-z (2021).

321 Luecke, S. *et al.* cGAS is activated by DNA in a length-dependent manner. *EMBO Rep* **18**, 1707-1715, doi:10.15252/embr.201744017 (2017).

322 Tao, J. *et al.* Nonspecific DNA Binding of cGAS N Terminus Promotes cGAS Activation. *J Immunol* **198**, 3627-3636, doi:10.4049/jimmunol.1601909 (2017).

323 Robinson, K. S. *et al.* Enteroviral 3C protease activates the human NLRP1 inflammasome in airway epithelia. *Science* **370**, doi:10.1126/science.aay2002 (2020).

324 Chavarria-Smith, J. & Vance, R. E. Direct proteolytic cleavage of NLRP1B is necessary and sufficient for inflammasome activation by anthrax lethal factor. *PLoS Pathog* **9**, e1003452, doi:10.1371/journal.ppat.1003452 (2013).

325 Hellmich, K. A. *et al.* Anthrax lethal factor cleaves mouse nlrp1b in both toxin-sensitive and toxin-resistant macrophages. *PLoS One* **7**, e49741, doi:10.1371/journal.pone.0049741 (2012).

326 Levinsohn, J. L. *et al.* Anthrax lethal factor cleavage of Nlrp1 is required for activation of the inflammasome. *PLoS Pathog* **8**, e1002638, doi:10.1371/journal.ppat.1002638 (2012).

327 Hancks, D. C., Hartley, M. K., Hagan, C., Clark, N. L. & Elde, N. C. Overlapping Patterns of Rapid Evolution in the Nucleic Acid Sensors cGAS and OAS1 Suggest a Common Mechanism of Pathogen Antagonism and Escape. *PLoS Genet* **11**, e1005203, doi:10.1371/journal.pgen.1005203 (2015).

328 Stewart, S. A. *et al.* Lentivirus-delivered stable gene silencing by RNAi in primary cells. *RNA* **9**, 493-501, doi:10.1261/rna.2192803 (2003).

329 Campeau, E. *et al.* A versatile viral system for expression and depletion of proteins in mammalian cells. *PLoS One* **4**, e6529, doi:10.1371/journal.pone.0006529 (2009).

330 Kranzusch, P. J. *et al.* Structure-guided reprogramming of human cGAS dinucleotide linkage specificity. *Cell* **158**, 1011-1021, doi:10.1016/j.cell.2014.07.028 (2014).

331 Stetson, D. B. & Medzhitov, R. Recognition of cytosolic DNA activates an IRF3-dependent innate immune response. *Immunity* **24**, 93-103, doi:10.1016/j.immuni.2005.12.003 (2006).

332 Wu, X. *et al.* Molecular evolutionary and structural analysis of the cytosolic DNA sensor cGAS and STING. *Nucleic Acids Res* **42**, 8243-8257, doi:10.1093/nar/gku569 (2014).

333 Daniels, R. W., Rossano, A. J., Macleod, G. T. & Ganetzky, B. Expression of multiple transgenes from a single construct using viral 2A peptides in Drosophila. *PLoS One* **9**, e100637, doi:10.1371/journal.pone.0100637 (2014).

334 Ahier, A. & Jarriault, S. Simultaneous expression of multiple proteins under a single promoter in Caenorhabditis elegans via a versatile 2A-based toolkit. *Genetics* **196**, 605-613, doi:10.1534/genetics.113.160846 (2014).

335 Lopes Fischer, N., Naseer, N., Shin, S. & Brodsky, I. E. Effector-triggered immunity and pathogen sensing in metazoans. *Nat Microbiol* **5**, 14-26, doi:10.1038/s41564-019-0623-2 (2020).

336 Kufer, T. A., Creagh, E. M. & Bryant, C. E. Guardians of the Cell: Effector-Triggered Immunity Steers Mammalian Immune Defense. *Trends Immunol* **40**, 939-951, doi:10.1016/j.it.2019.08.001 (2019).

337 Kawai, T. & Akira, S. The role of pattern-recognition receptors in innate immunity: update on Toll-like receptors. *Nat Immunol* **11**, 373-384, doi:10.1038/ni.1863 (2010).

338 Sacksteder, K. A. *et al.* PEX19 binds multiple peroxisomal membrane proteins, is predominantly cytoplasmic, and is required for peroxisome membrane synthesis. *J Cell Biol* **148**, 931-944 (2000).

339 Zomer, A. W., van der Saag, P. T. & Poll-The, B. T. Phytanic and pristanic acid are naturally occuring ligands. *Adv Exp Med Biol* **544**, 247-254 (2003).

340 Haag, S. M. *et al.* Targeting STING with covalent small-molecule inhibitors. *Nature* **559**, 269-273, doi:10.1038/s41586-018-0287-8 (2018).

341 Zomer, A. W. *et al.* Pristanic acid and phytanic acid: naturally occurring ligands for the nuclear receptor peroxisome proliferator-activated receptor alpha. *J Lipid Res* **41**, 1801-1807 (2000).

342 Issemann, I. & Green, S. Activation of a member of the steroid hormone receptor superfamily by peroxisome proliferators. *Nature* **347**, 645-650, doi:10.1038/347645a0 (1990).

343 Poulsen, L., Siersbaek, M. & Mandrup, S. PPARs: fatty acid sensors controlling metabolism. *Semin Cell Dev Biol* **23**, 631-639, doi:10.1016/j.semcdb.2012.01.003 (2012).

344 Li, X. & Gould, S. J. PEX11 promotes peroxisome division independently of peroxisome metabolism. *J Cell Biol* **156**, 643-651, doi:10.1083/jcb.200112028 (2002).

345 Schrader, M. *et al.* Expression of PEX11β mediates peroxisome proliferation in the absence of extracellular stimuli. *J Biol Chem* **273**, 29607-29614, doi:10.1074/jbc.273.45.29607 (1998).

346 Nagai, K. Phytanic acid induces Neuro2a cell death via histone deacetylase activation and mitochondrial dysfunction. *Neurotoxicol Teratol* **48**, 33-39, doi:10.1016/j.ntt.2015.01.006 (2015).

347 Weng, H., Endo, K., Li, J., Kito, N. & Iwai, N. Induction of peroxisomes by butyrate-producing probiotics. *PLoS One* **10**, e0117851, doi:10.1371/journal.pone.0117851 (2015).

348 Gondcaille, C. *et al.* Phenylbutyrate up-regulates the adrenoleukodystrophy-related gene as a nonclassical peroxisome proliferator. *J Cell Biol* **169**, 93-104, doi:10.1083/jcb.200501036 (2005).

349 Janeway, C. A., Jr. Approaching the asymptote? Evolution and revolution in immunology. *Cold Spring Harb Symp Quant Biol* **54 Pt 1**, 1-13, doi:10.1101/sqb.1989.054.01.003 (1989).

350 Mosallanejad, K. & Kagan, J. C. Control of innate immunity by the cGAS-STING pathway. *Immunol Cell Biol*, doi:10.1111/imcb.12555 (2022).

351 Devant, P., Cao, A. & Kagan, J. C. Evolution-inspired redesign of the LPS receptor caspase-4 into an interleukin-1β converting enzyme. *Sci Immunol* **6**, doi:10.1126/sciimmunol.abh3567 (2021).

352 Genomes Project, C. *et al.* A global reference for human genetic variation. *Nature* **526**, 68-74, doi:10.1038/nature15393 (2015).

353 Kazmierski, J. *et al.* A base-line cellular antiviral state is maintained by cGAS and its most frequent naturally occurring variant rs610913. *bioRxiv*, 2021.2008.2024.457532, doi:10.1101/2021.08.24.457532 (2021).

354 Feingold, K. R., Wang, Y., Moser, A., Shigenaga, J. K. & Grunfeld, C. LPS decreases fatty acid oxidation and nuclear hormone receptors in the kidney. *J Lipid Res* **49**, 2179-2187, doi:10.1194/jlr.M800233-JLR200 (2008).

355 Verhoeven, N. M. & Jakobs, C. Human metabolism of phytanic acid and pristanic acid. *Prog Lipid Res* **40**, 453-466 (2001).